The geotectonic setting, age and mineral deposit inventory of global layered intrusions

W.D. Smith, W.D. Maier

PII: S0012-8252(21)00237-3

DOI: https://doi.org/10.1016/j.earscirev.2021.103736

Reference: EARTH 103736

To appear in: *Earth-Science Reviews*

Received date: 18 January 2021

Revised date: 27 June 2021

Accepted date: 4 July 2021

Please cite this article as: W.D. Smith and W.D. Maier, The geotectonic setting, age and mineral deposit inventory of global layered intrusions, *Earth-Science Reviews* (2018), https://doi.org/10.1016/j.earscirev.2021.103736

The geotectonic setting, age and mineral deposit inventory of global layered intrusions

W.D. Smith[*,1] smithwd1@cardiff.ac.uk and W.D. Maier[1]

[1]School of Earth and Environmental Sciences, Cardiff University, United Kingdom

[*]Corresponding author.

Abstract

In the present paper, we have compiled data on 565 layered and differentiated igneous intrusions globally, documenting their (i) location, (ii) age, (iii) size, (iv) geotectonic setting, (v) putative parent magma(s), (vi) crystallisation sequence, and (vii) mineral deposits. Most studied intrusions occur in Russia (98), Australia (72), Canada (52), Finland (37), South Africa (38), China (33), and Brazil (31). Notable clusters of: (i) Archaean intrusions (~ 15%) include those of the McFaulds Lake Area (commonly known as the Ring of Fire, Canada), Pilbara and Yilgarn cratons (Australia), and Barberton (South Africa); (ii) Proterozoic intrusions (~ 56%) include those of the Giles Event and Halls Creek Orogen (Australia), Kaapvaal craton and its margin (South Africa and Botswana), Kola and Karelia cratons (Finland and Russia), and Midcontinent Rift (Canada and USA); and (iii) Phanerozoic intrusions (~ 29%) include those of eastern Greenland, the Central Asian Orogenic Belt (China and Mongolia) and Emeishan large igneous province (China). Throughout geological time, the occurrence of many layered intrusions correlate broadly with the amalgamation and break-up of supercontinents, yet the size and mineral inventory of intrusions shows no obvious secular changes.

In our compilation, 337 intrusions possess one or more types of mineral occurrences, including: (i) 107 with stratiform PGE reef-style mineralisation, (ii) 138 with Ni-Cu-(PGE) contact-style mineralisation, (iii) 74 with stratiform Fe-Ti-V-(P) horizons, and (iv) ≥ 35 with chromitite seams. Sill-like or chonolithic differentiated intrusions present in extensional tectonic settings and spanning geological time are most prospective for Ni-Cu-(PGE) mineralisation. In contrast, PGE reef-style deposits are most prevalent in larger, commonly lopolithic intrusions that are generally > 1 Ga in age (~ 75%). Stratiform Fe-Ti-V-(P) horizons are most common in the

central and upper portions of larger layered intrusions, occurring in the Archaean and Phanerozoic. Approximately 80% of intrusions with chromitite seams are older than 1 Ga and > 50% of them also contain PGE reefs.

Based on the distribution of layered intrusions in relatively well explored terranes (*e.g.*, Finland, South Africa, Western Australia), we propose that many layered intrusions remain to be discovered on Earth, particularly in poorly explored and relatively inaccessible regions of Africa, Australia, Russia, Greenland, Antarctica, South America, and northern Canada.

Keywords

layered intrusions, igneous petrology, mineralisation, ore deposit, compilation

1. Introduction

Layered intrusions represent igneous bodies composed of stratified layers, made apparent through variations in (i) mineralogy (*e.g.*, mineral modes, grain sizes, and preferential weathering and alteration), and (ii) chemical composition of the rock or its constituent minerals. Following the pioneering works of Cameron and Emerson (1959), Hess and Smith (1960), Jackson (1960), and Wager and Brown (1968), numerous studies have focussed on the origin of the layering (see Naslund and McBirney 1996, and Namur *et al.* 2015 for comprehensive reviews). Amongst the earliest widely accepted concepts was that of gravitational fractionation, whereby liquidus crystals settle from the evolving magma and accumulate on the temporary floor of the magma chamber (Darwin 1844; Bowen 1915; Wager and Brown 1968; Morse 1969). However, the discovery of hundreds of layered igneous bodies during the last 50 years has revealed types of layering that cannot be explained by gravitational settling alone.

Namur *et al.* (2015) have classified layer-forming processes into dynamic and non-dynamic processes (Table 1). The former category includes syn-magmatic, hydrodynamic, and late- to post-magmatic processes, whereas non-dynamic processes refer to fluctuations in intensive parameters (*e.g.*, temperature, pressure, and oxygen fugacity) that govern the liquid line of descent of a silicate magma. Under certain circumstances, dynamic and non-dynamic processes can cause the formation of monomineralic cumulate layers composed predominantly of minerals that normally crystallise along cotectics (*e.g.*, chromitite, magnetitite, anorthosite).

In addition to being natural laboratories for studies on igneous processes, layered intrusions host a wide range of important mineral deposits. Among the most studied are PGE reef-style deposits (*e.g.*, UG2 and Merensky reefs of the Bushveld Complex, JM reef of the Stillwater Complex, and the Main sulphide zone of the Great Dyke), commonly with Ni and Cu as significant by-products. Additional important ore types include massive seams or disseminated layers of chromite and titanomagnetite. The chromite seams usually occur in the unevolved portions of the intrusions whereas Fe-Ti-V oxide seams and layers typically occur in the more evolved portions of layered intrusions. Both types of oxide seams tend to show remarkable lateral consistency and commonly share knife-sharp contacts with the underlying and overlying silicate host rocks. Other important types of ore deposits associated with layered intrusions include rare earth elements (REEs), Zr, and Nb, hosted by alkaline layered intrusions (*e.g.*, Ilimaussaq, Thor Lake, Bokan, Khibina) or in mineralised pegmatites in their roof rocks (Dostal 2016), and platinum placers associated with zoned Ural-Alaskan intrusions (Hinnelberg & Loney 1995; Tolstykh et al. 2005).

In the present study, we have compiled data on 565 layered intrusions, documenting their (i) location, (ii) size, (iii) age, (iv) setting, (v) putative parent magma(s), (vi) crystallisation sequence, and (vii) mineral deposits. Our database includes intrusions of tholeiitic, calc-alkaline, and alkaline lineage, emplaced in intra-continental, arc, and collisional settings that show clearly defined modal and cryptic layering of ultramafic, mafic, and/or felsic minerals. We do not include oceanic intrusions formed at spreading ridges although the styles and origin of layering in these clearly show many commonalities to continental intrusions (*e.g.*, Bedard 2015). Finally, we also do not discuss intrusions of the granitic family although we are conscious that some of these can be layered (*i.e.*, syenites; Parsons 1987). Based on our data, we review the distribution of the intrusions in space and time and evaluate concepts of igneous layering and ore genesis.

2. Liquids, Cumulates, and Layers

Our understanding of the formation of layered intrusions is built on the idea that liquidus crystals precipitated from a silicate magma and accumulated, through processes such as gravitational settling or *in situ* crystallisation, on the temporary magma chamber floor. The cumulus minerals are typically embedded in a matrix of crystallised (trapped) liquid and cumulus theory acknowledges the existence of relatively liquid-poor and crystal-poor portions of an evolving magma chamber. Because the term “cumulate” has genetic connotations (it implies that crystals have accumulated) it has not been immune from criticism (see Boudreau

2019). Prior to further discussion, it is thus important to briefly outline common terminology for components of such systems and their genetic connotations.

The ratio of cumulus minerals to the crystallisation products of the trapped liquid (*i.e.,* cumulus crystal rims and/or oikocrysts) is generally used to distinguish between adcumulates (> 95% cumulus minerals), orthocumulates (95-85% cumulus minerals), and mesocumulates (85-75% cumulus minerals; Wager *et al.* 1960). Primocrysts are liquidus crystals, whereas oikocrysts and chadacrysts constitute the enclosing and enclosed crystals, respectively, in a poikilitic rock. The origin of oikocrysts and chadacrysts remains debated, with various authors proposing crystallisation of intercumulus liquid (Wager *et al.* 1960), turbulent mechanical sedimentation (Barnes *et al.* 2016), infiltration metasomatism (Maier *et al.* 2021), and peritectic reaction between melt and crystals near solidification fronts (Barnes *et al.* 2021).

Cumulates may also contain crystals that did not precipitate from the same parent magma, including (i) xenocrysts (*i.e.,* crystals inherited through assimilation) and (ii) antecrysts (*i.e.,* crystals inherited from a genetically related antecedent magma). Finally, more exotic types of cumulates include: (i) heteradcumulates, which are poikilitic adcumulates that are composed entirely of oikocrysts and chadacrysts (Barnes *et al.* 2016) and (ii) crescumulates, which refer to the spinifex type texture of allochthonous primocrysts in a metastable environment (Wager and Brown 1968).

Common terms found in many petrological models of layered intrusions are “liquid”, “mush”, and “slurry”. In fluid mechanics, a liquid refers to an incompressible substance that can flow independently of pressure. The term liquid thus includes crystal-bearing liquids (*i.e.,* liquids entraining a cargo of phenocrysts). A slurry refers to a crystal-liquid mixture that is only able to flow under pressure (*i.e.,* a Bingham fluid), whereas a mush is a partially molten rock consisting of a continuous solid framework, within which trapped liquids may percolate and convect (Marsh 2013; Cashman *et al.* 2017). Much debate in recent years (see Holness *et al.* 2019 for a current review) has focussed on the nature of trans-crustal magma systems. Some authors propose that these systems are predominantly composed of mush (*e.g.,* Marsh 1996; 2006; Christopher *et al.* 2015; Cashman *et al.* 2017; Sparks and Cashman 2017; Edmonds *et al.* 2019; Lissenberg *et al.* 2019), whereas others propose that these systems consist predominantly of liquids that fractionate *in situ* (*e.g.,* Jackson 1960; Campbell 1978; Marsh 1996; Latypov 2003; Latypov *et al.* 2013). Proponents of a mush-rich trans-crustal network draw on (i) the absence of geophysical evidence for liquid-rich chambers beneath active volcanos (Hill *et al.* 2009; Kiser *et al.* 2016; Cashman *et al.* 2017; Magee *et al.* 2018), (ii) the diversity and complexity of erupted crystal cargo

(Ginibre *et al.* 2002; Berlo *et al.* 2007; Kilgour *et al.*, 2014; Cashman and Blundy 2013), and (iii) the contradictory residence times of phenocrysts and melts as determined by radiometric dating, diffusion rates and numerical modelling (Morgan *et al.* 2004; Costa *et al.* 2010; Cooper 2015). On the other hand, the presence of liquid-rich systems is supported by the (i) progressive inward crystallisation of layered intrusions (*e.g.*, Skaergaard; McBirney and Noyes 1979), (ii) fractionation of liquids as recorded by compositional zonation of liquidus crystals (Loomis 1983), (iii) the disruption of accumulated crystals by processes such as scouring or slumping (Morse 1969), and (iv) the presence of unevolved chilled margins and fine grained to aphyric sills in the floor of some intrusions (*e.g.*, Bushveld; Barnes *et al*. 2010; Wilson 2012; Maier *et al*. 2016a).

Igneous layering is characterised by sheet-like units that are mineralogically, texturally, and (or) compositionally distinct. Where these show regular and repetitive grading from unevolved to evolved compositions, they are termed Cyclic Units (Eales *et al.* 1986). By convention, layered intrusions comprise multiple cyclic units, whereas layered sills/dykes comprise only one cyclic unit (Namur *et al.* 2015). In the present study, we have referred to these types of intrusions collectively as 'layered intrusions'. Individual layers are generally distinguished and characterised by their variation in mineralogy (*e.g.*, monomineralic, meso-, melano-, and leucocratic), grain size, shape (*e.g.*, planer, lenticular, convolute, colloform, lenses/pods, and seams), or mineral composition, which in part monitors their lateral continuity. A sequence of individual layers can be characterised by their lithological and compositional variability (*e.g.*, modal, graded, or cryptic layering), regularity (*e.g.*, cyclic, rhythmic, and chomb), contacts (*e.g.*, sharp, irregular/wavy, gradational, convolute, and unconformable), and continuity (*e.g.*, continuous, discontinuous, intermittent, truncated, and bifurcated).

It is now widely accepted that a single process cannot account for the layering present in most known layered igneous intrusions. Layering processes can operate at any time during the solidification of the intrusions. These mechanisms may be independent (*e.g.*, crystal settling and metasomatism) or dependent (*i.e.*, tectonism and density currents) of one another, occurring either contemporaneously, consecutively, or consequently. The implication is that rocks may record several superimposed layer-forming processes that require detailed holistic studies to be disentangle. Namur *et al.* (2015) have proposed a useful classification of layer-forming processes into dynamic (*i.e.*, magmatic and mechanical processes) and non-dynamic (*i.e.*, intensive parameters) processes.

Dynamic layer-forming processes refer to the physical movement or migration of liquid, crystals, and mush within an active magma chamber. Major dynamic layer-forming processes include mechanical sedimentation and sorting of liquidus phases (*e.g.*, Wadsworth 1961; Goode 1976; Irvine 1987; Namur *et al.* 2011; Holness *et*

al. 2012), chamber replenishment and magma mixing (*e.g.*, Hoatson and Keays 1989; Harney *et al.* 1990; Eales *et al.*, 1990; Karykowski *et al.* 2017a), convection-related processes (*e.g.*, Kogarko and Khapaev 1987; Wilson *et al.* 1987, Naslund *et al.* 1991; Holness *et al.* 2017), magma currents or flow segregation (*e.g.*, Irvine 1987; Gorring and Naslund 1995; Irvine *et al.* 1998; Maier *et al.* 2013a), liquid immiscibility (*e.g.*, McBirney and Nakamura 1974; Namur *et al.* 2012), contact metamorphism (*e.g.*, Naslund 1986), and metasomatism (*e.g.*, Irvine 1980; McBirney 1987; Boudreau 1988; Sonnenthal 1990; Boudreau & McCallum 1992; Nicholson and Mathez 1991; Mathez 1995; Holness *et al.* 2007; Mathez and Kinzler 2017; Maier *et al.* 2021; Marsh *et al.* 2021).

Non-dynamic layer-forming processes generally refer to fluctuations in intensive parameters within an evolving magma chamber. An intensive parameter is one which operates independently of systems scale, *i.e.*, they operate similarly in small and large layered intrusions. The primary layer-forming intensive parameters include temperature (T), pressure (p), composition (X), oxygen fugacity (fO_2) and viscosity (η). In addition to fluctuations in intensive parameters (*e.g.*, Ferguson and Pulvertaft 1963; Ryder 1984; Pang *et al.* 2009), non-dynamic layer-forming processes also refer to self-organising processes operating in a cumulate pile or mush, or in the sub-solidus state of cumulates. Such processes include fluctuations in crystal nucleation rates (*e.g.*, Hawkes 1967; Wager and Brown 1968; McBirney and Noyes 1979; Duchesne and Charlier 2005), constitutional zone refining during fluid/vapour flux along a geochemical potential gradient (*e.g.*, McBirney 1987; Bruegmann *et al.* 1989), and Ostwald Ripening (*e.g.*, Boudreau 1987; McBirney *et al.* 1990; Boudreau and McBirney 1997; Higgins 2002).

A range of syn-magmatic processes have been proposed to be responsible for disturbing or enhancing primary igneous layering. The most important examples include: (i) the indentation of igneous layers by dislodged autoliths (*e.g.*, Skaergaard, Irvine *et al.* 1998; Bolangir and Laramie anorthosite complexes, Dobmeier 2006; Scoates *et al.* 2010); (ii) scouring of layers by crystal slurries cascading along the top of the cumulate pile (*e.g.*, Bushveld Complex, Maier *et al.* 2013a); (iii) break-up of layers due to chamber instabilities (*e.g.*, Boulder Bed of the Bushveld Complex, Jones 1976); (iv) thermochemical and/or thermomechanical erosion of igneous layers by magma influx (*e.g.*, potholes of the Merensky Reef, Eales *et al.* 1988; Carr *et al.* 1999, Latypov *et al.* 2013); and (v) o of the most dynamic environments may apply to oceanic spreading centres, where layering of gabbroic protoliths may be caused by ut-of-sequence emplacement of sills (*e.g.*, Bushveld Complex; Mungall *et al.* 2016; Abernethy 2020, Scoates et al. 2021). One ductile shear at near-solidus temperatures. This resulted in

tectonic repetition of layers characterised by relatively low trapped melt fractions interpreted through tectonically induced expulsion of pore melt (Bedard, 2015).

3. Layered intrusions in space and time

3.1. Introduction

Layered igneous intrusions have been identified in every continent on Earth (Fig. 1) and their existence has been hypothesised on the Moon and Mars (McEnroe *et al.* 2004; Francis, 2011; Elardo *et al.* 2012). The greatest density of terrestrial intrusions occurs within stabilised Archaean cratons, particularly the Kaapvaal (*e.g.*, Bushveld, Uitkomst, Stella, Molopo Farms, Trompsburg), Zimbabwe (*e.g.*, Great Dyke), Pilbara (*e.g.*, Munni Munni), Yilgarn (*e.g.*, Windimurra, Jimberlana), Nain (*e.g.*, Kiglapait, Fishanaesset, Ilimaussaq), Superior (*e.g.*, Duluth, Sudbury, Coldwell, Ring of Fire), Wyoming (Stillwater), Kola (*e.g.*, Monchegorsk, Fedorova Tundra, Imandra) and Karelia (*e.g.*, Kemi, Penikat, Portimo, Koillismaa) cratons. The dilated margins of cratonic blocks appear to be equally favourable, *e.g.*, the Brasilia Belt of the Amazonia craton (hosting the Cana Brava, Niquelândia, and Barro Alto intrusions), the Halls Creek Orogen of the Kimberly craton (*e.g.*, Hart, Savannah, Panton), the Kibaran Fold Belt of the Tanzania craton (*e.g.*, Kabanga, Musongati, Kapalagulu), the Kotalahti Belt of the Karelia craton (*e.g.*, Kotalahti, Pyttky, Laukunkangas), the Central Asian Orogenic Belt (*e.g.*, Heishan, Huangshandong, Tulargen, Xiaotong) and the Giles event of the Musgrave province, Australia (*e.g.*, Wingellina Hills, Kalka, Mantamaru). There are relatively few intrusions that show no obvious connection with Archaean cratons or their periphery, examples being the Chilas Complex of Pakistan and the Beja and Aguablanca intrusions of Portugal and Spain.

Layered intrusions occur throughout geological time, from the Archaean (including the ~ 3123 Ma Nuasahi intrusion, India and the ~ 3033 Ma Stella intrusion, South Africa) to the Cenozoic (including the ~ 55-45 Ma east Greenland intrusions, *e.g.*, Kruuse Fjord, Skaergaard, and Lilloise). There is no clear correlation between age and size; giant intrusions occur from the Archean, *e.g.*, the ~ 2.8 Ga Windimurra intrusion, Australia, to the Phanerozoic, *e.g.*, the ~ 0.18 Ga Dufek intrusion, Antarctica. Amongst the intrusions compiled in this study, 11.0% occur in the Archaean, 25.2% in the Proterozoic and 41.0% in the Phanerozoic (Fig. 2; 22.8% are unconstrained). As noted by Maier and Groves (2011), the ages of many layered intrusions correlate broadly with the amalgamation and break-up of supercontinents. Intrusions temporally associated with amalgamation may include those at ~ 2.5-2.4 Ga (Kola and Karelia cratons, Great Dyke), ~ 2.0-1.8 Ga (Kaapvaal and Superior

cratons), ~ 1.2-1.0 Ga (Midcontinent Rift), and 0.3-0.25 Ga (China and New Zealand). The trigger for magmatism may have been (i) slab-rollback and consequent lithospheric extension, (ii) trans-tensional rift zones during oblique collision, or (iii) sub-continental lithospheric mantle (SCLM) delamination in response to enhanced subduction (Maier and Groves 2011). Other intrusions appear to be temporally related to supercontinent dismemberment likely formed in response to mantle plume activity (*e.g.,* Ernst and Buchan 1997; Ernst 2014), In the following chapters, selected intrusions from all continents are discussed in more detail.

3.2. Africa

Africa hosts 104 layered intrusions (18.5% of the compilation), ranging in age from ~ 3454 to 126 Ma, in size from 0.15 to > 65,000 km^2, and in thickness from 0.1 to 12 km (Fig. 3). The distribution of the intrusions is highly biased towards southern Africa, with another important cluster in the Kibaran fold belt of Tanzania-Burundi. The reason likely relates to exposure, access, and infrastructure and thus, exploration history. While small-scale mining did take place in the pre-colonial era (*e.g.,* for Cu at Okiep, South Africa; Cawthorn and Meyer 1993; Clifford and Barton 2012), the bulk of mining and exploration activity commenced in the 20th century, in the relatively well-exposed and accessible Kaapvaal and Zimbabwe cratons. Exploration opportunities remain significant in these regions (*e.g.,* the recently discovered Flatreef and Waterberg deposits of the northern lobe of the Bushveld Complex, Kinnaird *et al.* 2017; Huthmann *et al.* 2018; Grobler *et al.* 2019), but additional future discoveries will likely be made elsewhere in Africa, notably the Congo, Tanzania, and West African cratons and their peripheries.

Africa's (and the world's) most important layered intrusion is the Bushveld Complex of South Africa. It is the largest known layered intrusion on Earth (> 100,000 km^2, Hayes *et al.* 2017) by an order of magnitude, for reasons that remain unclear. The remarkable size of the complex suggests that its emplacement must also have exerted a significant impact on global atmospheric conditions. This idea is possibly supported by the correlation of the Bushveld emplacement (~ 2054.4 ± 1.3 Ma; Scoates and Wall 2015) with the end of the Lomagundi-Jatuli event (~ 2058 ± 6 Ma; Melezhik *et al.* 2007) and the onset of the Shunga event (~ 2050 Ma; Hannah *et al.* 2008; Ernst 2014). Abernethy (2020) estimated that the emplacement of the northern limb of the Bushveld Complex into the Transvaal dolomites may have caused the release of at least 1,213 Gt of CO_2 into the Precambrian atmosphere. This estimate is likely highly conservative as it does not consider the potential contribution of the extensive sill complex in the floor of the intrusion, across the entire Bushveld Complex.

The complex displays an extremely diverse range of layering, including transgressive features such as potholes (Eales *et al.* 1988; Kruger 1994; Carr *et al.* 1999; Latypov *et al.* 2013), pipes (Scoon and Mitchell 1994; 2004; Reid and Basson 2002) and diatremes (Boorman *et al.* 2003). It is also one of few intrusions for which the parent magmas have been well constrained, based on fine-grained basaltic sills in the floor of the intrusion (Davies *et al.* 1980; Sharpe 1981; Barnes *et al.* 2010) and magnesian basaltic and komatiitic chilled margins (Wilson 2012; Maier *et al.* 2017). These data suggest that the complex formed from a komatiitic parent magma that assimilated upper crust during its ascent and emplacement. Numerous petrogenetic models have been proposed to explain the layering (see recent reviews by Maier *et al.* 2013a; Cawthorn 2015; Smith *et al.* 2020). Thus, the Bushveld Complex is arguably one of the most important natural laboratories in the study of layered intrusions.

The Bushveld hosts the diverse range of ore deposit types, amongst them the world's most important PGE, Cr and V deposits (*e.g.*, Merensky Reef, Platreef, Flatreef, UG2 and LG6 chromitites, Main Magnetite Layer; Barnes and Maier 2002; McDonald *et al.* 2005; Naldrett *et al.* 2009; Junge *et al.* 2014; Oberthür *et al.* 2016; Grobler *et al.* 2019). The PGE deposits have been exploited for nearly a century since the discovery of Pt by Hans Merensky and his associates in 1924. The Bushveld event also led to the formation of: (i) Ni-Cu in chonolithic satellite intrusions (*e.g.*, Uitkomst; Gauert *et al.* 1995; De Waal *et al.* 2001; Yudovskaya *et al.* 2015; Maier *et al.* 2018a; DA); (ii) polymetallic Sn-W granite-related mineralisation (McNaughton *et al.* 1993; Mutele *et al.* 2017); (iii) andalusite deposits in the metamorphic aureole (Hammerbeck 1986); (iv) building stones such as the Impala Black and African Red granites (Pivko 2004); (v) hydrothermal fluorite deposits (*e.g.*, Warmbaths and Vergenoeg, Pringle 1986; Gotti *et al.* 2004); and (vi) hydrothermal gold mineralisation in the floor rocks to the complex (*e.g.*, Witwatersberg and Sabie-Pilgrim's Rest goldfields; Frimmel *et al.* 2005; Killick and Scheepers 2005).

The Bushveld Complex is part of the Bushveld LIP (Rajesh *et al.* 2013) that also includes other notable intrusions such as Uitkomst and the Molopo Farms Complex (MFC). The Uitkomst intrusion is a tubular layered body that hosts one of South Africa's largest Ni-Cu-PGE deposits (407 Mt at 0.35% Ni, 0.13% Cu, 0.63 g/t PGE) and Cr (6.23 Mt at 33.47% Cr_2O_3), named Nkomati (Gauert *et al.* 1995; Maier *et al.* 2018a). Recent geochronological work yielded an age of 2057.64 ± 0.69 Ma, showing that the intrusion formed part of the Bushveld event (Maier *et al.* 2018a). The Molopo Farms Complex (MFC) of Botswana is an extremely poorly exposed, large layered intrusion (~ 13,000 km^2) that has a similar Sr isotope signature, mineral composition, and age (~ 2054 ± 5 Ma) as the neighbouring Bushveld Complex (Prendergast 2012; Kaavera *et al.* 2020). Despite

these commonalities, the two complexes appear to be separate intrusive suites (Skryzalin *et al.* 2016). The MFC comprises a 1.3-km-thick lower ultramafic sequence (harzburgite and pyroxenite) overlain by a 1.5-km-thick mafic sequence (gabbro and norite), (Willhelm *et al.* 1988) thought to derive from a parent magma similar in composition to the B1 magma for the Bushveld Complex (Barnes *et al.* 2010; Kaavera *et al.* 2018). No economic PGE reefs have been intersected in the MFC, but low-grade PGE mineralisation (~ 1.1 ppm Pt+Pd at 1 m) has been identified in the basal ultramafic portion of the Tubane Section (Kaavera *et al.* 2020)

Other notable layered intrusions in South Africa include the Stella and Trompsburg intrusions. The Stella intrusion in the Kraaipan greenstone belt is one of the oldest layered intrusions on Earth (~ 3033.5 ± 0.3 Ma). It has been poorly studied since the intrusion has a limited exposure (~ 12 km^2; Maier *et al.,* 2003a). The bulk of the intrusion consists of gabbro, which is overlain by magnetite-rich gabbro and titanomagnetitites that host PGE enrichments of up to 15 ppm over 1 m (Maier *et al.* 2003a). Trompsburg is a large, lopolithic layered intrusion (~ 2,500 km^2; ~ 1915.2 ± 5.6 Ma; Maré and Cole 2006) identified by a gravimetric survey conducted by Transvaal Orangia Limited in 1946 (Maier *et al.* 2003b). Several boreholes drilled in the 1950s intersected mostly gabbro and troctolite, but also anorthosite with up to 19 magnetitite layers containing up to 1.82% V_2O_5.

One of the greatest densities of layered intrusions (> 18 identified bodies) occurs in the Barberton greenstone belt (Anhaeusser 1983; 2006). This raises the question as to why other greenstone belts have much fewer intrusions. Some of the Barberton intrusions could be cumulate portions of lava flows. Distinguishing these from intrusive cumulates is not straightforward (*e.g.,* Mouri *et al.* 2013), and some lava flow cumulates have been shown to reach a thickness of several 100s of metres (*e.g.,* Mt Keith, Fiorentini *et al.* 2010). Alternatively, lava flows in other greenstone belts could have been misidentified and instead represent intrusions.

In terms of economic importance, the Great Dyke of Zimbabwe (~ 2575 ± 0.7 Ma) is the second most significant layered intrusion in Africa. The intrusion forms a ~ 550 km long elongated body that ranges from 4 to 11 km in width (Wilson 1982; 1991). It likely represents the upper portion of a dyke that transitioned upwards into a sill complex (Podmore and Wilson 1987). Based on mineral chemistry, the composition of the parent magmas was high-Mg basalt (~ 15-16 wt.% MgO; Wilson 1982). Prendergast (1991) and Maier *et al.* (2015a) presented field evidence documenting a highly irregular contact between the ultramafic and mafic portions of the intrusion which they interpreted to result from granular flow of cumulate slurries. The Great Dyke is one of few layered intrusions where it was possible to conduct detailed studies of compositional variation relative to

distance from the putative feeder zones (*i.e.*, the axis of the intrusion, Prendergast 1991). This revealed systematic variation in PGE ratios and total PGE concentrations, with the latter systematically elevated in the axial facies (Wilson and Tredoux 1990).

The Archaean Monts de Cristal intrusion of Gabon (~ 2765 ± 11 Ma) consists of several bodies thought to represent a tectonically dismembered layered intrusion spaced over 100 km (Maier *et al.* 2015b). The intrusion consists predominantly of orthopyroxenite, with subordinate norite and gabbro. The parent magma is proposed to be a basalt with ~ 10 wt.% MgO. Most of the rocks display elevated Pt levels (10-150 ppb) at low Pd contents (mostly < 10 ppb), resulting in high Pt/Pd > 10. The elevated Pt contents in the rocks and soils caused some interest amongst exploration companies, but no PGE reefs were found. Instead, the Pt enrichments were interpreted to reflect the precipitation of primary Pt-As phases from the magma (Maier *et al.* 2015b; Barnes *et al.* 2016).

Much of the giant Kunene Complex of Namibia-Angola (~ 18,000 km^2; ~ 1371 ± 2.5 Ma) consists of > 20 massif-type anorthosite plutons (Ashwal and Twist 1994), which are associated with the ~ 1.3 Ga Kunene-Kibaran LIP (Ernst *et al.* 2013). However, in the Namibian portion there is a ~ 16-km-thick layered troctolite body (called the Zebra Mountain lobe; ~ 2,500 km^2), possibly resulting from multiple sill injection (Drueppel *et al.* 2007; Maier *et al.*, 2013b). The Zebra lobe has numerous, mostly relatively small (< 10 km^2) mafic-ultramafic satellite bodies, some of which host Ni-Cu-PGE mineralisation (*e.g.*, Ohamaremba troctolite and Ombuku peridotite) and chromitite (Ombuku; Maier *et al.* 2013b).

Intrusions of the Kabanga-Musongati-Kapalagulu mafic-ultramafic belt were emplaced during the ~ 1.3 Ga Victoria event of the Kunene-Kibaran LIP that extends for ~ 500 km from Uganda to Lake Tanganyika (Deblond 1994; Tack *et al.* 1994; Makitie *et al.* 2014). The intrusions include Ni-Cu mineralised chonoliths (Kabanga) and reef-style and contact-style PGE-Ni-Cu mineralisation (Kapalagulu and Musongati; Maier *et al.* 2010; Wilhelmij *et al.* 2016; Evans 2017; Prendergast 2021). In addition, there is a titanomagnetite deposit at Rutovu and a large Ni laterite deposit at Musongati (Maier *et al.*, 2010).

Compared to southern and central Africa, relatively few layered intrusions are reported from northern Africa. The best known and largest is the ~202 Ma Freetown intrusion, Liberia, which belongs to the Central Atlantic Magmatic Province (CAMP or CA-LIP) and consists of interlayered ultramafic and gabbroic rocks (*e.g.*, Chalokwu 2001; Bowles *et al.* 2017; Callegaro *et al.* 2017). Exposure is relatively poor and much of the body extends into the Atlantic Ocean. Thus, the economic potential of the intrusion remains poorly defined.

Several gabbroic layered intrusions occur in the Western Ethiopian Shield, the largest of which is the Bikilal-Ghimbi gabbro (~ 846 ± 7.6 Ma; Woldemichael *et al.* 2010) which underlies an area of ~ 350 km^2 (Woldemichael and Kimura 2008). Despite comprising a relatively homogeneous olivine gabbro core, the margins of the intrusion show rhythmic layering of leucogabbro, hornblende gabbro, and hornblendite. The Bikilal intrusion hosts one of Africa's largest igneous phosphate deposits (~ 181 at 3.5% P_2O_5) in two horizons of apatite-bearing hornblende gabbro (Ghebre 2010).

Several Neoproterozoic post-collisional layered mafic-ultramafic intrusions are documented in the Arabian-Nubian Shield of Egypt (*e.g.*, Motaghairat, Imleih, Korab Kansi, and Shahira; Khedr *et al.* 2020 and references therein). Most of the intrusions comprise ~ 10% ultramafic cumulates overlain by layered olivine gabbro, troctolite, gabbro, and hornblende gabbro derived from a tholeiitic to calc-alkaline parent magma (Abdel Halim *et al.* 2016; Khedr *et al.* 2020). The Korab Kansi intrusion differs from the other intrusions since it is host to economic Fe-Ti-V oxide mineralisation within its upper gabbroic interval. It is hypothesised that partial melting of metasomatized mantle produced Fe- and Ti-rich ferropicritic melts leading to the formation of oxide deposits (Khedr *et al.* 2020).

3.3. Asia (including eastern Russia)

Our compilation includes approximately 111 layered intrusions (19.8% of the total) from Asia (including those of eastern Russia), ranging in age from 3123 to 22 Ma, in surface area from 0.025 to 12,000 km^2, and in thickness from 0.06 to 11 km (Fig. 4). The majority of known Asian layered intrusions occur in China and Russia. The Chinese intrusions form several important clusters of relatively small PGE- and Fe-Ti-V-bearing bodies, including in the Emeishan large igneous province (LIP), the Tarim LIP, and the Central Asian Orogenic Belt (CAOB). Important clusters in Russia include the Noril'sk-Talnakh intrusions of the Siberian traps LIP and intrusions of the Urals Belt.

The largest layered intrusion in Asia is the Chilas intrusion of the Kohistan terrane of Pakistan (~ 12,000 km^2), for which little information is available. It is a relatively young intrusion (~ 85.73 ± 0.15 Ma) that comprises mainly olivine- and plagioclase-dominated cumulates overlain by gabbronorite, gabbro, and subordinate anorthosite (Mikoshiba *et al.* 1999; Takahashi *et al.* 2007). No economic mineralisation has been identified in the Chilas intrusion, but PGE enrichments (< 3 ppm Pt+Pd in grab samples) have been reported in

peridotitic cumulates of the Jijal layered complex, which forms an arcuate layered intrusion occurring just south of the Chilas intrusion (Miller *et al.* 1991).

The economically most important intrusions of Asia are relatively small and are associated with LIPs. In the Siberian LIP, economically highly important layered sills occur in the Noril'sk region, notably the Noril'sk 1, Talnakh, and Kharaelakh intrusions that host the Ni-Cu-PGE deposits of the Talnakh-Oktyabrsk and Noril'sk-Talnakh ore junctions (Naldrett *et al.* 1992; Arndt 2011). These layered tabular intrusions have thicknesses up to 360 m and lengths up to 20 km (Malitch *et al.* 2010). The Kharaelakh intrusion has been described as the single most valuable ore deposit ever discovered, consisting primarily of olivine gabbro with subordinate wehrlite and troctolite that contains a ~ 30-m-thick massive sulphide orebody that strikes for up to 20 km (Yakubchuk and Nikishin 2004). Ore formation in these layered sills is still highly debated, yet the earliest petrogenetic models proposed by Russian geologists in the 1950's, involving emplacement of highly sulphidic magmas resulting from assimilation of evaporite appear to be still the most widely supported (Grinenko 1985). A discussion of the ore-forming processes is beyond the scope of the present contribution, but an update of the latest research can be consulted in the 2020 special issue of Economic Geology on the Noril'sk ore district (*e.g.*, Barnes *et al.* 2020) and a revised model for the formation of the Noril'sk ores is detailed in Yao and Mungall (2021).

Numerous small, layered intrusions hosting Ni-Cu-sulphide (*e.g.*, Limahe, Zhubu, Erhongwa, Huangshandong), PGE- (*e.g.*, Jinbaoshan, Aryi, Xinjie) and Fe-Ti-V ores (*e.g.*, Taihe, Baima, Hongge, Panzhihua) are located in the Permian-aged Emeishan LIP of south China (see Wang *et al.* 2018). Many Ni-Cu-sulphide-bearing intrusions in the CAOB have no regular layering (*e.g.*, Niubiziliang, Kalatongke, Tianyu, Hulu, Heishanxia), yet several display modal layering of plagioclase and pyroxene in their central and upper parts (*e.g.*, Erghonwa, Huangshandong, Sun *et al.* 2013a; 2013b). The giant Fe-Ti-V deposits of the Panzhihua (1333 Mt at 33% Fe, 12% TiO_2, and ~ 0.3% V_2O_5; ~ 263 ± 3 Ma), Baima (1497 Mt at 26% Fe, 7% TiO_2, and ~ 0.21% V_2O_5; ~ 262 ± 2 Ma), and Hongge (4572 Mt at 27% Fe, 11% TiO_2, and ~ 0.24% V_2O_5; ~ 259 ± 3 Ma) intrusions rival those of the Bushveld in size. The deposits are also notable in that the titanomagnetitite layers occur in the central and lower portions of the intrusions and the total volume of Fe-Ti oxides far exceeds what could have accumulated from the magma if the intrusions were closed systems. Thus, their petrogenesis has been explained by a combination of emplacement of Fe- and Ti-enriched magmas that had undergone pre-emplacement fractionation of magnesian silicates in a deep-seated magma chamber, followed by gravity settling and sorting of the Fe-Ti oxides (Zhang *et al.* 2012a; Song *et al.* 2013; Luan *et al.* 2014; She *et al.* 2015).

Other economically important, yet relatively small layered intrusions occur in the Central Asian Orogenic Belt of northwest China, which, together with the Finnish Ni belt and the Kabanga-Musongati-Kapalagulu belt, is amongst the most important examples of orogenic Ni-Cu sulphide deposits. The intrusions primarily consist of peridotitic cumulates overlain by pyroxenite, gabbro, and diorite, with Ni-Cu sulphide ores being typically hosted in peridotite and pyroxenite at the base of the intrusions (Li *et al.* 2012; Su *et al.* 2014; Mao *et al.* 2014). The intrusions tend to be relatively PGE depleted (Cu/Pd > 10,000), which has been interpretated to represent equilibration of the magmas with sulphide prior to final emplacement, possibly in a deep-crustal staging chamber (Sun *et al.* 2013a; Xie *et al.* 2014) or magma derivation from the SCLM (Song *et al.* 2011; Xie *et al.* 2014). Several similar-sized Ni-Cu-sulphide-bearing intrusions occur in the Mongolian CAOB (*e.g.*, Nomgon, Dulaan, Oortsog), but are generally more geochemically evolved than the Chinese intrusions, *i.e.*, have thinner and more irregular ultramafic cumulate units (Mao *et al.* 2018).

The Yoko-Dovyren intrusion (~ 728.4 ± 3.4 Ma) of Siberia is amongst the best studied layered intrusions in Asia (Ariskin *et al.* 2016; 2018; 2020; Kislov and Khudyakova 2020). This intrusion is linked with the East Siberian metallogenic (PGE-Cu-Ni) metallogenic province (Polyakov *et al.* 2013), which is part of the ~ 720 Ma Irkutsk LIP (Ernst *et al.* 2016). It consists of a basal peridotite that is interlayered with, and contaminated by country rock carbonates, overlain by layered troctolite, anorthosite and gabbro. The intrusion is 3-4 km thick and hosts disseminated to net-textured Ni-Cu sulphides at its base (*e.g.*, Ariskin *et al.* 2016; 2018) and reef-style PGE deposits in its central and upper portion (Orsoev 2019; Ariskin *et al.* 2020).

Eastern Siberia and the Urals belt host numerous Ural-Alaskan-type zoned intrusions which may contain important placer deposits of Pt, including those of the Nizhny-Tagil Complex and the Koryak-Kamchatka Belt (Tolstykh *et al.* 2004; 2015). The intrusions consist predominantly of lherzolite and have been interpreted as ophiolitic sequences (Savelieva *et al.* 1997) or exhumed sub-continental lithospheric mantle (Zaccarini *et al.* 2002; Tessalina *et al.* 2007). The PGM placers are considered to have formed via erosion and weathering of primary Pt-Fe alloys, Os-Ir-Ru alloys and minerals of the laurite-erlichmanite series hosted in chromite lodes (O'Driscoll and Gonzalez-Jimenez 2016).

India hosts one of the oldest known layered intrusions on Earth, namely the Nuasahi intrusion (~ 3123 ± 7 Ma) of the Singhbhum craton (Samal *et al.* 2021). Nuasahi is relatively small (~ 1.5 km^2) and comprises chromitiferous ultramafic cumulates overlain by layered gabbroic units, with subordinate pyroxenite, anorthosite, and magnetitite (Augé *et al.* 2003; Khatun *et al.* 2014). Chromite lodes (Durga, Laxmi 1, and Laxmi

2) occur amongst the basal peridotitic cumulates, whereas a sulphide-rich breccia zone occurs at the contact between pyroxenite and gabbro in the centre of the intrusion (Augé *et al.* 2003; Mondal and Zhou 2010). In addition, a 1-2-m-thick massive magnetite layer occurs in the upper gabbroic portion (Mohanty and Paul 2008). The intrusion is thought to derive from an S-undersaturated boninitic magma derived from second-stage melting of a depleted metasomatized mantle (Mondal and Zhou 2010; Khatun *et al.* 2014). Other notable intrusions in India are those of the Eastern Ghats Belt (Chimalpahad and Pangidi-Kondapallae complexes). These are medium-sized intrusions (~ 150 km^2) that comprise chromitiferous ultramafic cumulates overlain by gabbro, leucogabbro, and anorthosite (Leelanandam 1997; Dharma Rao *et al.* 2011).

3.4. Europe (including western Russia)

Europe contributes 140 layered intrusions (24.9% of the compilation) to our compilation, ranging in age from 2846 to 1.1 Ma, in extent from 0.005 to 1,500 km^2, and in thickness from 0.004 to 15 km (Fig. 5). The greatest density of layered intrusions is found in the Fennoscandian Shield of Finland and Russia, referred to as "Europe's Treasure Chest" by Maier and Hanski (2017) and including the Archean Kola and Karelia cratons. Many of the intrusions host PGE (*e.g.*, Penikat, Portimo, Koillismaa, Fedorova-Pana), Ni-Cu (*e.g.*, Kevitsa, Sakatti, Kotalahti, Monchegorsk), Cr (*e.g.*, Kemi, Monchegorsk, Koitelainen, Akanvaara), and Fe-Ti-V (*e.g.*, Koillismaa, Koivusaarenneva, Otanmäki, Kaunajärvi, Koitelainen, Akanvaara). Other notable intrusions are those of the North Atlantic LIP in Scotland (*e.g.*, Rum, Cuillin, Aradnamurchin) and the orogenic Ni-Cu-sulphide-bearing layered intrusions in Southern Spain and Portugal (*e.g.*, Aguablanca and Beja).

Many of the most mineralised layered intrusions of the 2.44 Ga Fennoscandian Shield occur in the Tornio-Näränkävaara Belt, which comprises the intrusions of the Portimo and Koillismaa complexes, as well as the Penikat and Kemi intrusions. These intrusions are related to the ~ 2.44 Ga Baltic LIP, which has been linked with the Matachewan LIP of the southern Superior craton (Ernst and Jowitt 2013). The ~ 30 km^2 lopolithic Kemi intrusion (~ 2430 ± 4 Ma) is particularly interesting because it hosts at a chromitite interval that widens from a few cm at the margins to > 100m in the centre of the lopolith (Alapieti *et al.* 1989). The layer hosts ~ 50 Mt of chromite ore (~ 26% Cr_2O_3), constituting one of the world's largest chromite deposits. Few other layered intrusions have their centres exposed, raising the possibility that thick oxide (and perhaps sulphide) layers of the style found at Kemi remain to be discovered elsewhere. Just east of Kemi is the ~ 50 km^2 Penikat intrusion (~ 2430 ± 5 Ma) that comprises five megacyclic units consisting predominantly of norite, gabbro, and

gabbronorite, with subordinate olivine pyroxenite, chromitites, and leucogabbro (Halkoaho 1990a,b; Huhtelin et al. 1990; Maier *et al.* 2018b). Penikat hosts at least six PGE reef-style horizons, several of which contain up to 10 ppm Pd+Pt+Au over approximately 1 m thickness. Furthermore, Penikat contains highly PGE-enriched pothole structures, analogous to those of the Bushveld and Stillwater intrusions. The Portimo (Iljina and Hanski 2005; Iljina *et al.* 2015) and Koillismaa (~ 2426 ± 5 Ma; Karinen 2010) complexes also host PGE and, in the case of Koillismaaa, disseminated titanomagnetite intervals that are enriched in vanadium (*i.e.*, Mustavaara deposit). Both intrusions comprise several tectonically dismembered layered bodies (a few km^2 to up to 100 km^2) (Iljina *et al.* 2015). Koillismaa appears to be connected to Näränkävaara via a deep, dyke- or conduit-like peridotite body that has recently been intersected by drilling (Järvinen *et al.* 2020).

The Koitelainen and Akanvaara intrusions are notable because they contain thick intervals of PGE- and V-rich magnetite gabbro and a chromitite layer of unusually low Mg# in their upper portions. (Mutanen and Huhma 2001; Hanski *et al.* 2001). The 2.06 Ga Otanmäki complex consists of several, relatively small (~ 20 km^2), differentiated layered intrusions that contain thick Fe-Ti-V ore lenses (~ 2-200 m in length and 3-50 m in thickness with a resource of ~ 30 Mt at ~ 34% Fe, 8% TiO_2, and 0.26% V_2O_5) (Mäkisalo, 2019). The 16 km^2 Kevitsa intrusion (~ 2058 ± 4 Ma) hosts Finland's largest Ni deposit. Some of the sulphides are extremely Ni-rich (Yang *et al.* 2013; Luolavirta *et al.* 2018), possibly resulting from assimilation of Ni-rich komatiite by the basaltic parent magma (Yang *et al.* 2013). Lastly, several tectonised layered intrusions (or magma conduits) occur in the 1.88 Ga Kotalahti and Vammala Ni belts of southern Finland, which produced a total of 45 Mt at 0.7% Ni (Peltonen 1995; Makkonen 2015). The intrusions were emplaced into an orogenic setting, analogous to the intrusions in the Appalachians and the CAOB.

Pilgujärvi is the largest (~ 3 km in length and 700 m in thickness) differentiated intrusion in the ferropicritic Pechenga greenstone belt of the ~ 1.98 Ga Pechanga-Onega LIP (*e.g.*, Lubnina *et al.* 2016) and also the largest sill complex of the Kola peninsula, NW Russia (Hanski *et al.* 1990; Hanski 1992). Hanski *et al.* suggested that the incompatible and isotopic geochemistry of the ferropicritic units is consistent with derivation from the partial melting of a mantle plume, yet derivation from metasomatized SCLM could not be excluded. The intrusions host Europe's largest Ni deposits constituted by disseminated to massive Ni-Cu sulphides concentrated near the base of the sills (Barnes *et al*. 2001; Maier and Hanski 2017).

The 550 km^2 Monchegorsk Complex (~ 2054 ± 2 Ma) comprises the ultramafic-mafic Monchepluton (~ 65 km^2) and the largely gabbroic to anorthositic Main Ridge intrusion (485 km^2). This economically important

Complex comprises dunite-hosted Cr seams (Chashchin *et al.* 1999), marginal contact-style PGE-Cu mineralisation (Grokhovskaya *et al.* 2003; Karykowski *et al.* 2018a), massive Ni-Cu sulphide veins (Bekker *et al.* 2016; Karykowski *et al.* 2018a), PGE reef deposits (Sopcha and Vuruchuaivench; Grokhovskaya *et al.* 2000; Karykowski *et al.* 2018b), and Fe-Ti-V mineralisation in the Gabbro-10 massif (Pripachkin *et al.* 2020). The 2.45 Ga lopolithic Burakovsky complex is among the largest layered intrusion in Europe (~ 700 km^2). It has a thickness ranging from 2-8 km (Bailly *et al.* 2011) and contains PGE-rich chromitites (12-40% Cr_2O_3 and < 0.4 g/t Pt+Pt at 3-4 m) located at several stratigraphic positions in the central and lower portions of the intrusion (Sharkov *et al.* 1995). No economic Ni-Cu sulphides have been discovered to date.

Amongst the most intensely studied intrusions in Europe is the Rum intrusion (~ 60.5 ± 0.08 Ma) of the North Atlantic Igneous Province (NAIP or NA-LIP, which also includes mafic-ultramafic complexes of Cuillin and Centre 3), which is located in the Inner Hebrides of Scotland. The intrusion is relatively small (~ 25 km^2) but exceptionally well exposed (~ 600 m thick). As a result, it has been highly influential in our understanding of the formation of igneous layering, including the development of the 'cumulus theory' (Wager *et al.* 1960), providing evidence for layering in response to out-of-sequence emplacement of sills (Bédard *et al.* 1988), evidence for infiltration metasomatism, in the form of the Wavy Horizon (Holness *et al.* 2007), and the formation of enigmatic finger structures (Butcher *et al.* 1985). The latter are found along the contacts between peridotite and troctolite layers, or between different types of peridotites (granular and poikilitic). The fingers cut across layering, laminae, and lamination without any disruption of planar structures. Butcher *et al.* (1985) suggest that the fingers formed through replacement of troctolite by peridotite, achieved by pore magma from the peridotite migrating into the overlying troctolite, in response to compaction. The pore magma resorbed plagioclase but crystallized olivine and pyroxene. The intrusion also contains PGE-rich chromitite stringers (~ 2.5 g/t PGE at 3 m; Butcher *et al.* 1999; Upton *et al*. 2002; O'Driscoll *et al*. 2009; 2010; Hepworth *et al*. 2020).

The Aguablanca (~ 10 km^2; ~ 341 ± 1.5 Ma) and Beja (~ 265 km^2; ~ 342 ± 9 Ma) layered intrusions in the Ossa Morena Zone of southern Spain and Portugal, respectively, are of the syn-orogenic type (Pina *et al.* 2006; Jesus *et al.* 2016). The Ni-Cu-PGE mineralisation at Aguablanca occurs as disseminated sulphides within sub-vertical magmatic breccia (~ 16 Mt at 0.66% Ni, 0.46% Cu, and 0.47 g/t Pt+Pd; Pina *et al.* 2010). In contrast, sub-economic Fe-Ti-V oxide aggregates (up to 10% TiO_2 and 0.99 V_2O_5) and disseminated Ni-Cu sulphides are reported in the lower olivine gabbro and pyroxenite of the Beja layered sequence (Jesus *et al.* 2003; 2005).

3.5. North America and Greenland

Our compilation contains 85 layered intrusions (15.1% of the compilation) from North America, ranging in age from 3811 to 48 Ma, in extent from 0.1 to 5,000 km^2, and in thickness from 0.06 to 8.4 km (Fig. 6).

The economically most important igneous body in North America is the ~ 1.85 Ga Sudbury igneous complex (~ 1,650 km^2). It is seemingly unique amongst igneous complexes in that it represents a differentiated crustal melt sheet that formed in response to a meteorite impact (the bolide is estimated to have been ~ 10 km in diameter; Grieve 1994; Lightfoot 2016). Flash melting of the crust occurred during decompression and crustal rebound milliseconds after the impact, which produced a voluminous melt sheet below the fall-back breccia (see Lightfoot 2016 and references therein). The melt sheet differentiated into norite and leuconorite (~ 40% of the intrusion) overlain by granophyre (~ 60% of the intrusion). The complex hosts some of the world's largest and most intensely studied Ni-Cu-(PGE) deposits (total resource of 1,643 Mt at 1.66% Ni and 0.88% Cu), the origin of which has been heavily debated since its discovery in 1883 during the construction of the Canadian Pacific Railway (Lesher and Thurston 2002). The currently favoured explanation for ore formation is that the bolide struck crust that contained magmatic proto-ores, possibly located in members of the Nipissing mafic suite or layered intrusions of the East Bull Lake suite (James *et al.* 2002; Darling *et al.* 2010). The molten sulphides became further metal enriched during equilibration with the vigorously convecting superheated melt-sheet (Lightfoot 2016). After deposition along the base of the melt-sheet, the sulphide melt underwent fractionation, during which Cu-(PGE)-rich sulphides infiltrated for several 100s of metres into the brecciated basement rocks (Rousell *et al.* 2003).

The ~ 2.7 Ga Stillwater Complex of Montana is a ~ 6.5-km-thick intrusion which, from base to top, is characterised by: (i) a 60-400-m-thick basal series consisting of orthopyroxenite and norite, (ii) an 840-2000-m-thick ultramafic series that comprises > 20 cyclic units of olivine-orthopyroxene cumulates, and (iii) a ~1900-4500-m-thick banded series that comprises norite, gabbronorite, troctolite, and anorthosite (Hess 1939; McCallum 1996; Barnes *et al.* 2020). The Earth's thickest anorthosite layers (up to 600 m) occur in the Middle Banded Series (Haskin and Salpas 1992). Much of the intrusion is poorly exposed and its true extent is likely > 1,500 km^2. Several stratiform chromitites (named A to K from the bottom upwards) occur in the peridotite zone of the ultramafic series. They were discovered during the first world war, but not exploited until the second world war. In contrast, stratiform PGE reefs (notably the JM Howland Reef) were not discovered until the 1970s and are now actively mined at the East Boulder and Stillwater mines (Zientek *et al.* 2002; Keays *et al.* 2012;

Jenkins *et al.* 2020). The Stillwater Complex has also been an important laboratory for theories of reactive porous flow and infiltration metasomatism (see Boudreau 2019 and references therein).

The largest layered Complex of North America is Duluth (~ 5,000 km^2), which comprises a suite of troctolitic to anorthositic intrusions (*e.g.*, South Kawishiwi, Partridge River, and Bald Eagle) associated with the ~ 1.1 Ga Keweenawan LIP of the Midcontinent Rift of the USA and Ontario (Weiblen and Morey 1980; Miller and Ripley 1996; Ernst and Jowitt 2013; Woodruff *et al.* 2020). Despite hosting 4,400 Mt of contact-style Ni-Cu ore, the low metal grades (~ 0.2% Ni and 0.6% Cu) make the deposits currently sub-economic. The magmatic sulphides formed in response to extensive assimilation of sulphidic pelitic rocks of the Virginia Formation (Thériault and Barnes 1998). The Midcontinent Rift contains several other mineralised mafic-ultramafic layered intrusions, including Lac des Iles (Barnes and Gomwe 2011), Sonju Lake (Maes *et al.* 2007), Eagle and Eagle East (Ding *et al.* 2012), Coldwell (Good *et al.* 2017), and Tamarack (Tarkhovic *et al.* 2015).

The ~ 1.27 Ga Muskox intrusion, hosted among the Mackenzie dyke swarm (*e.g.*, Barager *et al.* 1996) of northern Canada, is a relatively large (~ 125 x 11 x 8 km), funnel-shaped body that consists of a keel-shaped feeder dyke, an eastern and western marginal zone, a layered sequence of 25 cyclic units of dunite-peridotite-pyroxenite-gabbro, and a granophyric roof zone (Irvine 1980; Barnes and Francis 1995; Day *et al.* 2008). Muskox was an early case study for the model of magmatic infiltration metasomatism and double-diffusive convection proposed by Irvine (1980). Reef-style chromite horizons with disseminated sulphides are documented amongst the olivine-orthopyroxene cumulates of the layered series yet have too low metal grades to be economic (Barnes and Francis 1995).

The most recent notable discovery of layered intrusions in North America comprises the so-called ~ 2.7-2.6 Ga 'Ring of fire' or 'McFaulds Lake Area', which represents a mineralised greenstone belt containing several strongly tectonised layered intrusions that are host to significant Cr (*e.g.*, Double Eagle), Fe-Ti-V (*e.g.*, Black Thor, Highbank Lake, and Blackbird), and Ni-Cu sulphide (*e.g.*, Eagle's Nest; Mungall *et al.* 2010) mineralisation (see Bleeker and Houlé 2020 and references therein). The chromite-rich layers attain a thickness of several 10s of metres (Houlé *et al.* 2020). The Cr contents of the Ring of Fire chromites are relatively high indicating a komatiitic lineage of the parent magmas (Houlé *et al.* 2020). Other greenstone belt-hosted intrusions in Canada include those of the Abitibi Belt, *e.g.*, Bell River and Dore Lake. The latter contains economically important Fe-Ti-V deposits, whereas Bell River has PGE-(Cu) occurrences (Ebay and Dotcom; Munoz Taborda 2010; Mathieu 2019). Several important volcanogenic massive sulphide (VMS) deposits occur in the vicinity of

magmatic rocks of the Bell River Complex, leading previous workers to suggest that the heat flux from the Bell River Complex drove the circulation of hydrothermal fluids responsible for VMS mineralisation (Maier *et al.* 1996).

Canada also hosts some of the world's largest anorthositic massifs (*e.g.*, Sept Iles, Grader, Michikamau, Tigalak, Bridges, Newark Island, Hettasch, and Kiglapait; Emslie 1965; Morse 1969; Wiebe and Wild 1983; Charlier *et al.* 2008; Ashwal 2013), which occur from southern Québec to northern Labrador (*i.e.*, the Grenville and Nain provinces). While most of the large massifs are not noticeably layered, there are numerous intrusions that are. Perhaps most studied is the ~ 1.3 Ga largely troctolitic (~ 84%) Kiglapait intrusion (~ 560 km^2), which displays spectacular layering on various scales (see Morse 2015 and references therein). The plumbing systems to some of the Nain layered intrusions host important Ni-Cu sulphide deposits, notably at Voisey's Bay (~ 125 Mt at 1.66% Ni and 0.88% Cu; Li *et al.* 2000; Naldrett *et al.* 2000)

The ~ 0.56 Ga Sept Iles intrusion of the Central Iapetus Magmatic Province (CIMP; Higgins and van Breemen 1998; Ernst and Bell 2010) is a large (~ 5,000 km^2) layered body that is characterised by a massif-type anorthositic upper portion that is underlain by a well-layered troctolitic-gabbroic portion (Higgins 1991; 2005). Sept Iles hosts a potentially economic resource of Fe-Ti-V-P, in the form of twenty-four ~ 1-m-thick Fe-Ti oxide layers and a ~ 200-m-thick layer of apatite-rich gabbro (Cimon 1998; Namur *et al.* 2012).

Layered intrusions of the Grenville Province have been studied by Sappin *et al.* (2009; 2011) notably in the Portneuf-Mauricie Domain. The intrusions are mostly relatively small (< 50 km^2) and may host Ni-Cu sulphides (*e.g.*, at Lac Édouard and Kennedy) and vanadiferous titanomagnetite (at Lac Fabien, Maier 2021).

Several notable layered intrusions occur on the east coast of Greenland, the most iconic of which being the ~ 0.55 Ga Skaergaard intrusion of the NA-LIP (~ 70 km^2). This is arguably the birthplace of modern academic studies on igneous petrology and layered intrusions (Wager and Brown 1968), due to spectacular exposure and preservation. Features that are particularly noteworthy include: (i) comb layering along the margins of the intrusion (McBirney and Noyes 1979), (ii) rhythmic layering in the marginal border group (Conrad and Naslund 1989), (iii) deformation of layering by dislodged roof fragments (Irvine *et al.* 1998), (iv) trough layering that may reflect magmatic granular flow (Vukmanovic *et al.* 2018), (v) an evolved Sandwich Horizon that represents the boundary between the Upper Border Series and the rocks that formed through magmatic sedimentation (McBirney 1996), and (vi) Pd-Au-Cu-rich and Ni-Pt-poor sulphide mineralisation of

the Platinova Reef, which may represent the best example of sulphide upgrading via dissolution (Anderson *et al.* 1998; Godel *et al.* 2014; Holwell ad Keays 2014; Nielsen *et al.* 2015; Mungall *et al.* 2020).

In addition, Greenland hosts several layered alkaline intrusions in the Gardar Province. The most studied is the ~ 1.13 Ga Ilimaussaq intrusion (~ 136 km^2; ~ 1160 ± 2.3 Ma) that comprises a series of augite syenite and nepheline syenite (Ferguson 1964; Marks and Markl 2001), the origin of which remains debated (see Marks 2015). Layered alkaline intrusions comprise relatively exotic rock types, including lujavrite, kakortokite, naujaite, (Na)-foyaite, and pulaskite, which are described in detail by Sørensen (2006) and Marks (2015). The formation of these unusual rock assemblages is thought to reflect the low silica and water activity of the parent magmas, allowing extremely differentiated melts to become enriched in alkalis, halogens, and high-field-strength elements (Marks 2015).

3.6. Oceania and Antarctica

Oceania hosts 86 layered intrusions in our compilation (15.3% of the total), ranging in age from 3016 to 90 Ma, extent from 0.16 to 6,600 km^2, and thickness from 0.1 to 11 km (Fig. 7). Several large layered intrusions occur in the Yilgarn and Pilbara cratons of western Australia. Other important clusters of intrusions occur in the Halls Creek Orogen located along the eastern margin of the Kimberley craton, and in the Musgrave province of central Australia (namely the intrusions of the Giles event). Few layered intrusions are reported from Antarctica, the most important being the Dufek intrusion.

One of the largest and economically most important layered intrusions of Australia is the ~ 2.8 Ga Windimurra (2,500 km^2) intrusion, which is located in the Yilgarn craton together with the adjacent Narndee, Barramdi, Yalgowra, and Youanmi intrusions (Ivanic *et al.* 2010). Windimurra comprises a thick (< 11 km) sequence of mafic-ultramafic rocks displaying > 100-m-thick megacyclic units that exhibit modal fractionation as well as several compositional reversals interpreted to reflect multiple magma replenishment (Ahmat 1986; Ivanic *et al.* 2010). The intrusion hosts economically important magnetitites at the base of its upper gabbronoritic zone (~ 210 Mt at 0.5% V_2O_5) and is considered prospective for PGE- and Cr-rich layers in its mafic-ultramafic lower zone (Ivanic *et al.* 2010; Langford *et al.* 2020). Fe-Ti-V mineralisation has also been identified in the neighbouring Barrambie (~ 40 Mt at 15% TiO_2 and 0.78% V_2O_5) and Younami intrusions (185 Mt at 0.33% V_2O_5; Ivanic *et al.* 2010).

Other mafic-ultramafic layered intrusions of the Yilgarn craton include the ~ 2.4 Ga Jimberlana and Nova-Bollinger intrusions. The Jimberlana intrusion is part of the Widgiemooltha swarm/LIP (*e.g.,* Pirajno and Hoatson 2012; Ernst *et al.* 2019) and hosts several macro-rhythmic ultramafic layers in its lower portion, each of which display basal whole-rock and mineral compositional reversals as well as sulphide accumulation at their base (Campbell 1977; Keays and Campbell 1981). The model of *in situ* crystallisation of cumulates (Campbell 1977) was largely developed at Jimberlana and subsequently applied by the author to Bushveld and Stillwater. The recently discovered Nova-Bollinger intrusive suite belongs to the ~ 1.3-1.2 Ma Recherche Supersuite (Bennett *et al.* 2014; Maier *et al.* 2016b, that is located within the Albany Fraser orogen along the southern margin of the Yilgarn craton. It hosts a significant Ni-Cu deposit (13.1 Mt at 2.0% Ni and 0.8% Cu; Barnes *et al.* 2020) formed in response to extensive replacement of country rocks during high-grade metamorphism, analogous to Savannah (Barnes *et al.* 2020; Le Vaillant *et al.* 2020). The Nova discovery triggered a boom in exploration along the margins of the Yilgarn craton, contributing to the discovery of several now discoveries (eg Plato, Octagonal, Chalice).

The largest cluster of layered intrusions (> 20 bodies; 1s of km^2 to > 3000 km^2) in Australia belongs to the ~ 1.09-1.04 Ga Giles Event of the Warakurna LIP in the Musgrave Province of central Australia (Pirajno and Hoatson 2012). Amongst the intrusions are well-known bodies such as the PGE mineralised Wingellina Hills (Ballhaus and Glikson 1989) and the Ni-Cu mineralised Nebo Babel in Western Australia (392 Mt at 0.3% Ni and 0.33% Cu; Seat *et al.* 2007), as well as Kalka, Ewarara and Gosse Pile in South Australia (Goode 1970; 1977; Goode and Moore 1975). Mamamaru is one of the largest intrusions on the planet (~ 3,400 km^2), preserved in the form of three distinct fragments named Jameson, Blackstone and Bell Rock, all of which contain vanadiferous titanomagnetite layers, locally with elevated PGE and apatite (Maier *et al.* 2015, Karykowski et al. 2017b). Other notable intrusions of the Giles event include the Cu-Au enriched Halleys intrusion, as well as Pirntirri Mulari, Cavenagh Range, Morgan Range, and Saturn (Maier *et al.* 2015c). The Giles Event is of considerable petrological interest because although much of the rifting, intrusion emplacement, and uplift occurred between ~ 1078-1075 Ma, magmatism lasted for > 50 million years, which led Smithies *et al.* (2015) to propose that magmatism was the result of plate-driven rather than plume-driven magmatism.

Other important clusters of intrusions occur along the western margin of the Pilbara craton, including Dingo, Sherlock, Andover, Radio Hill, and, most notably, the ~2.9Ga Munni Munni Complex. Munni Munni is a large (~ 225 km^2) and thick (> 5.5 km) layered body, comparable in igneous stratigraphy to the Great Dyke of Zimbabwe (Barnes and Hoatson 1994). Both contain so-called offset PGE reefs (Great Dyke: Prendergast and

Keays 1989; Munni Munni: Barnes 1993), which are characterised by a ~ 5 m offset between peak PGE grades from peak S, Ni, and Cu values.

Another economically important intrusion is the ~ 1.84 Ga Savannah (formerly Sally Malay) intrusion (~ 2 km^2) that comprises five (Savannah, Savannah North, Subchamber-D, Dave Hill, and Wilson's Creek) layered bodies (Hoatson and Blake 2000; Le Vaillant *et al.* 2020) hosted in the Halls Creek Orogen along the eastern margin of the Kimberly craton. This intrusion is interesting in that it is one of few known mineralised intrusions of bladed dyke morphology (*e.g.*, Eagle's Nest of Ontario and the Expo Intrusive Suite of Cape Smith; Barnes and Mungall 2018).

An unusual layered intrusion in central Australia is the ~ 1.13 Ga Mordor alkaline igneous complex (~ 35 km^2) that is composed of a coarse-grained syenite (~ 60% of the complex) enveloping a mafic-ultramafic layered intrusion (~ 40% of the complex; Barnes *et al.* 2008). The latter consists predominantly of phlogopite-rich pyroxenites and syenites with subordinate pyroxenites and wehrlites thought to have crystallised from a hydrous alkalic magma of lamprophyric affinity (Langworthy and Black 1978; Barnes *et al.* 2008). Stratiform PGE reef-style mineralisation in the ultramafic portions has been described in detail by Barnes *et al.* (2008) whereas blebby Cu-(Au-PGE-Ni) sulphides in mafic syenites (or 'shonkinite') are described in detail in Holwell and Blanks (2020). The latter authors proposed that the metals are derived from the SCLM, analogous to the model for the Okiep intrusions of South Africa (Maier *et al*. 2012).

New Zealand hosts several arc-related Triassic layered intrusions (*e.g.*, Riwaka, Otu, Pahia, Greenhills, Knobs, and Lone Stag) that tend to contain amphibole as a primary cumulate phase and thus appear to have crystallised from a relatively hydrous basaltic magma (~ 11-13 wt.% MgO) of calc-alkaline affinity (Spandler *et al.* 2005). The Riwaka Complex consists of out-of-sequence intrusive sheets characterised by sharp and cross-cutting boundaries, with subordinate evidence for crystal accumulation and modal layering (Turnbull *et al.* 2017). The intrusion contains Ni-Cu-PGE sulphides that occur predominantly in hornblende-bearing clinopyroxenite (2.2% Ni, 2.1% Cu, and 1 g/t PGE from grab samples; Turnbull *et al.* 2017). Localised enrichments in PGE have also been reported in the lower units of the Greenhills (Spandler *et al.* 2000) and Pahia (Ashley *et al.* 2012) intrusions. Spandler *et al.* (2000) proposed that the PGM in the basal dunite at Greenhills precipitated directly from a low-K island-arc tholeiite. Several placer PGE deposits (*e.g.*, Orepuki) are proximal to the Greenhills and Pahia intrusions (Spandler *et al.* 2000; Ashley *et al.* 2012) suggesting the PGM likely derived from the intrusions and that further PGE reefs may be discovered in the area.

Only few layered intrusions have been reported in Antarctica, the largest of which being the ~ 1.8 Ga Dufek intrusion (> 6,600 km^2) of the Ferrar Province (Ford 1983; Kistler *et al.* 2000; Ferris *et al.* 2003). Discovered in 1957, the ~ 7-8-km-thick Dufek intrusion consists of sub-horizontal and alternating layers (~ few mm to 10s of metres in thickness) of gabbro, gabbronorite, anorthosite, titanomagnetite gabbronorite, gabbroanorthosite, and pyroxenite (Semenov *et al.* 2014). Despite its size, no economic Ni, Cu, PGE, Ti, V, and Cr concentrations are known (Ford 1983). Other intrusions belonging to the Karoo LIP are much (*e.g.*, Muran and Utpostane).

3.7. South America

South America has 37 known layered intrusions (6.4% of the compilation) ranging in age from 3100 to 501 Ma, extent from 0.55 to 800 km^2, and thickness from 0.1 to 5 km (Fig. 8). The relative paucity of intrusions is likely related to lack of exposure and access in the Amazonian and other cratons and the relatively recent onset of systematic academic study of these systems, from the early 1970s. Among the most studied intrusions are Niquelândia and neighbouring intrusions (*e.g.*, Cana Brava and Barro Alto), as well as Rio Jacaré, Mirabela and Palestina in eastern Brazil, and Rincón del Tigre in Bolivia.

Niquelândia is the largest (~ 800 km^2; ~ 765 ± 8 Ma) of three layered igneous complexes (the others being Cana Brava and Barro Alto) exposed in the Neoproterozoic Brasilia Belt (Ferreira Filho *et al.* 1994; 1995; Pimentel *et al.* 2004). The intrusion is unusual since it represents two layered complexes that have been tectonically juxtaposed along a major shear zone: the ~ 1.25 Ga Upper Layered Series (interlayered leucotroctolite, anorthosite, gabbro, and pyroxenite) and the ~ 0.79 Ga Lower Layered Series (cyclic dunite, harzburgite, websterite, and gabbronorite; Pimentel *et al.* 2004). Layered peridotites in the lower series host cm-scale chromite layers that are enriched in PGE (Garuti *et al.* 2012). Moreover, Garuti *et al.* (2012) report on the occurrence of secondary PGM that re-precipitated during post-magmatic serpentinization and lateritic weathering.

The ~ 2.1 Ga Jacurici Complex (~ 3.5 km^2) is a heavily metamorphosed layered intrusion located in the São Francisco craton and contains the largest chromite deposit in Brazil (~ 4.5 Mt at 30-40% Cr_2O_3; Marques *et al.* 2017; Friedrich *et al.* 2020). The main chromite seam is 5-8 m thick, which is remarkable in view of the relatively modest thickness of the intrusion (~ 300 m). It has been proposed that chromite crystallised from a high-MgO parent magma in response to contamination with country rock marble and calc-silicate. Chromite was further concentrated by granular flow (Marques *et al.* 2017).

Three further examples of economically important layered intrusions are Rio Jacaré (~ 84 km^2; ~ 2640 ± 5 Ma), Mirabela (~ 7 km^2; ~ 2065 Ma), and Luanga (~ 21 km^2; ~ 2763 ± 6 Ma). Rio Jacaré contains three < 23-m-thick V-rich magnetite bodies, one of which being located in pyroxenite of the lower portion of the intrusion (Gulçari A; 0.08 Mt at 2.2% V_2O_5 and 1.6% TiO_2) and two in layered gabbros of the upper portion (Gulçari B and Novo Amparo; Sá *et al.* 2005). These magnetite bodies also show elevated Pt (160 ppb), and Pd (120 ppb) contents, hosted in disseminated sulphides, bismuthides, and antimonides that are interpreted to have co-precipitated with Fe-Ti oxides (Sá *et al.* 2005; Barkov *et al.* 2015). The funnel-shaped Mirabela intrusion comprises a lower ultramafic zone of dunite, harzburgite, and pyroxenite (~800 m thick) and an upper mafic zone of gabbronorite and norite (> 1 km thick; Barnes *et al.* 2011; Knight *et al.* 2011; Ferreira Filho *et al.* 2013). Disseminated sulphides with unusually high Ni tenors (~15-25%) are located at the contact between the ultramafic and mafic zones (Barnes *et al.* 2011). Luanga is one of several layered intrusions (others include Lago Grande and Vermelho) hosted in the Carajás greenstone belt, eastern Amazonia craton (Mansur and Ferreira Filho 2016). The medium-sized intrusion (~ 21 km^2) comprises an ~ 800-m-thick ultramafic zone of serpentinised peridotite, a ~ 750-m-thick transition zone of orthopyroxenite, norite, harzburgite and several < 60-cm-thick chromitites, and a ~ 2-km-thick mafic zone comprised largely of noritic rocks (Mansur and Ferreira Filho 2016). Several PGE-rich mineralised horizons are documented in the transition zone, including the so-called sulphide zone (142 Mt at 0.11% Ni and 1.24 g/t Pt+Pd+Au), which represents a 10-50-m-thick interval of disseminated sulphide located at the top of the ultramafic zone (Mansur *et al.* 2020).

The ~ 1.1 Ga Rincón del Tigre intrusion, part of the Rincón del Tigre-Huanchaca LIP of Bolivia, is a relatively large (~ 720 km^2) and thick (~ 4.6 km^2) layered sill that is surrounded by several smaller mafic-ultramafic bodies (Teixeira *et al.* 2015; Choudhary *et al.* 2019). A geophysical survey delineated a significant gravitational anomaly to the north of the intrusion, which is interpreted to represent a feeder conduit (Litherland *et al.* 1986). Although no economic mineralisation has been identified, an 80-185-m-thick zone of sub-economic disseminated sulphides has been recorded in gabbro and magnetite gabbro of the upper portion of the intrusion (Prendergast 2000; Teixeira *et al.* 2015).

4. Intrusion size and morphology

The average surface area of layered intrusions in our compilation is ~ 444 km^2, but in almost all cases the original size and morphology of intrusions is obscured by late- to post-magmatic subsidence, tectonism, and/or

erosion, to the point where intrusions may be fragmented into several blocks (*e.g.*, Mantamaru, Australia; Portimo and Koillismaaa, Finland; Monts de Cristal, Gabon). In this compilation, the surface area (km^2) of known intrusions ranges from the giant Bushveld Complex (> 100.000 km^2) to numerous small intrusions measuring < 1 km^2. Some of the largest layered intrusions are annotated in Figure 1, which in addition to the Bushveld Complex, include Molopo Farms in Botswana (~ 13,000 km^2), Chilas in Pakistan (~ 12,000 km^2), Dufek in Antarctica (> 6,600 km^2), Duluth in Canada (~ 5,000 km^2), and Sept Iles in Canada (~ 5,000 km^2).

The stratigraphic thickness of intrusions ranges from a few 10s of meters to 12 km (Kabye of Benin, Jijal of Pakistan, and Windimurra of Australia being amongst the thickest). Again, deformation and incomplete exposure make determining the original thickness of intrusions challenging. Cawthorn *et al.* (2018) proposed that large layered intrusions appear to be capped at a thickness of ~ 10 km (*i.e.*, a third to a quarter of the continental crust) and that their growth adheres to a lengthening-dominated regime, whereby their length/thickness ratio (*L*/*T*) increases with increasing volume.

The Skaergaard intrusion of Greenland is an example of a layered intrusion for which a putatively broadly representative cross section and stratigraphy can be deduced from outcrop exposure (McBirney 1996). Another example is Kemi, which has been exposed by drilling, revealing a remarkable thickening of chromitite seams from the margins to the centre (Alapieti *et al.* 1989). However, the upper contact of Kemi is defined by an erosional unconformity, so its most evolved portion is missing.

The size distribution of the layered intrusions adheres to an exponential function (Fig. 9), analogous to some ore deposit classes, *e.g.*, gold (Berlein *et al.* 2006; Groves and Bierlein 2007). The unusually large size of the Bushveld Complex could be related to an unusually large mantle plume (referred to as the 'Bushveld superplume'; Fiorentini *et al.* 2020 and references therein). Alternatively, the large size could result from magma emplacement into the sub-horizontal Transvaal sedimentary basin, including into and above one of the world's largest dolomite platforms. Emplacement caused crustal subsidence accompanied by syn-magmatic devolatilization and volume reduction of the sediments (Wallmach *et al.* 1989), potentially facilitating progression and expansion of sills. Most other intrusions face a more severe 'space problem' requiring displacement (*i.e.*, uplift and lateral compression), removal (*i.e.*, ejection in impact craters), and/or ingestion (*i.e.*, assimilation and stoping) of crustal rocks during the emplacement of the magma (O'Hara 1998).

5. Composition of parent magma(s)

Magmas parental to layered intrusions include komatiite (*e.g.*, Bushveld, Bravo and other intrusions in the Raglan belt, intrusions in the Barberton greenstone belt), magnesian basalt (*e.g.*, Great Dyke, Penikat, Koitelainen, Akanvaara), picrite (*e.g.*, Pilgujärvi, Yoko-Dovyren), tholeiite (*e.g.*, Windimurra, Chilas, Kap Edvard Holm), (ferro)basalt (*e.g.*, Kabye, Sept Iles, Fongen-Hyllingen, Panzhihua), and alkali basalt (*e.g.*, Coldwell, Mordor). Mantle sources considered include the asthenosphere (*e.g.*, Koitelainen and Akanvaara, Hanski *et al*. 2001) and the SCLM (e.g., CAOB intrusions, Zhang *et al.* 2011; Zhang *et al.* 2012b). The geochemical signals of SCLM and crustally contaminated asthenospheric magma are difficult to distinguish, and thus for some intrusions (*e.g.*, Bushveld Complex), both have been suggested (Maier *et al*. 2000, Maier and Barnes 2004, Maier *et al.* 2016a). Knowing the composition of the parent magma to layered intrusions is important as it may provide constraints on tectonic setting and prospectivity. For example, if the parent magma is relatively S-rich (and thus close to saturation in sulphide melt) PGE reefs may be expected at stratigraphically lower portions of intrusions than if the parent magma is S-poor. If the magma is relatively PGE poor (possibly due to small degree mantle melting, or equilibration of the magma with sulphide melt during crustal ascent, or because the magmatism is early Archean in age), economic PGE reefs are unlikely. If the magma is relatively evolved, it is unlikely to be prospective for chromite (but see the Akanvaara and Koitelainen chromitites hosted by relatively evolved rocks; Mutanen 1997). The nature of the parent magma may be assessed through: (i) the composition of fine-grained chilled margins (*e.g.*, Bushveld Complex, Wilson 2012; Maier *et al.* 2016a), (ii) the composition of comagmatic extrusive rocks, sills, or dykes (*e.g.*, Bushveld Complex; Barnes *et al.* 2010), (iii) reverse modelling of cumulate rocks (*e.g.*, Godel *et al.* 2011; Tanner *et al.* 2014; Yang *et al.* 2019), and/or (iv) calculation of the average composition of the intrusion through addition of all layers (*e.g.*, Akanvaara; Mutanen 1997).

6. Ore deposits of layered intrusions

The bulk of the world's PGE resources are extracted from stratiform mineralised horizons (known as 'reefs') typically located near the transition from mafic to ultramafic rocks of layered intrusions (Naldrett 2004; Maier 2005; Mungall and Naldrett 2008; Godel 2015). In addition, layered mafic-ultramafic intrusions can host economically important concentrations of base metal sulphides (Ni-Cu-Co), typically but not exclusively near the basal contact, chromite (Cr-V), typically in the lower portion of intrusions, vanadiferous titanomagnetite and ilmenite (Fe-Ti-V) and/or phosphates (P) in the upper portion, whereas layered alkaline intrusions (such as those

in the Gardar Province) can be host to significant REE-HFSE resources (Schönenberger *et al.* 2008; Marks *et al.* 2011). Moreover, some intrusions host non-magmatic resources, including (i) Ni laterites (*e.g.*, Kapalagulu, Musongati, Wingellina Hills), (ii) asbestos in serpentinised ultramafic cumulates (*e.g.*, many of the intrusions in the Barberton greenstone belt), (iii) andalusite in metamorphic aureoles (*e.g.*, Bushveld Complex at Thabazimbi and Lydenburg), and (iv) building stone (*e.g.*, Bushveld Black Granite).

In the following sections, we briefly outline the petrogenesis of important ore deposits present in layered intrusions. The global and temporal distribution of layered igneous intrusions are presented in Figures 10 to 17. For a more in-depth discussion, the reader is referred to reviews by Naldrett (2004), Maier (2005), and Godel (2015).

6.1. PGE reefs

Prior to the discovery of PGE reefs in layered igneous intrusions (Merensky Reef of the Bushveld Complex in 1924 and JM reef of Stillwater in 1974), the world's PGE production was sourced from placer deposits associated with Ural-Alaskan-type intrusions (Tolstykh *et al.* 2005). Today, PGE are mined as the principal product in just four layered intrusions (Bushveld Complex, Great Dyke, Stillwater, and Lac des Iles). Most of the remainder of global PGE production comes from numerous Ni-Cu mines where the PGE are by-products (notably Noril'sk-Talnakh in Siberia which supplies the bulk of global Pd). In view of the importance of PGE in autocatalysts and hydrogen fuel cells, amongst other uses, this dependency on relatively few sources makes the PGE critical metals (*e.g.*, European Union).

In the Earth's mantle, Pd and Cu are predominantly concentrated in trace sulphides and will be liberated once all the sulphides have been dissolved, requiring a minimum of 15-20% partial melting (Naldrett 2004; Arndt *et al.* 2005; Barnes and Lightfoot 2005). The fact that Pd/Pt and Pd/IPGE ratios in mantle-derived magmas are much higher than in chondrites indicates that IPGE and Pt are more compatible than Pd during asthenospheric melting, likely due to sequestration with spinel and metal alloys (*e.g.*, Barnes *et al.* 2015). This is reflected in the complementary composition of SCLM derived xenoliths which have average Pd/Pt and Pd/IPGE < 1 (Pearson *et al.* 2004). Bushveld magmas appear to be somewhat of an anomality, in that they have lower Pd/Pt (~ 0.7) than most other magmas (Barnes *et al.* 2015). It has been suggested that this is the result of melting of SCLM (Maier and Barnes 2004, Mungall and Brenan 2014), but the komatiitic chilled margin of the complex

also shows elevated Pt/Pd yet cannot be modelled by SCLM melting as it has too low SiO_2 and K_2O (Maier *et al.* 2016a).

Experimental data have shown that the sulphide melt solubility of basalt is inversely correlated with pressure (Mavrogenes and O'Neill 1999). As a result, basaltic melts are typically undersaturated in sulphide melt during emplacement in the upper crust. For a basaltic magma to attain saturation in sulphide melt it must be compositionally modified through processes such as fractional crystallisation, magma mixing, and/or crustal contamination (*e.g.*, Keays and Lightfoot 2010; Ripley and Li 2013). Once saturation in sulphide melt has been attained, the melt may segregate and interact with the silicate magma, where the mass ratio of these two phases is denoted as the *R* factor (Campbell and Naldrett 1979). The chalcophile elements, and particularly the PGE have extremely high partition coefficients with regard to the sulphide melt (possibly > 10^6, Mungall and Brenan 2014) and hence, systems with high *R* factors (high ratios of silicate:sulphide melt) are favourable for the formation of PGE-rich deposits. Lastly, to create an economically important PGE reef, PGE-enriched sulphide droplets must concentrate into a narrow horizon, such that they can be effectively mined at a low stripping ratio.

Most PGE reefs show little evidence for contamination. For example, S isotopes are in the mantle range at most Bushveld reefs (Sharman *et al.* 2013), Great Dyke (Maier *et al.* 2015) and Stillwater (Ripley *et al.* 2017). Some of the earliest models for the formation of PGE reefs invoke the gravitational settling of sulphide melt that exsolved in response to the mixing of resident magma with a relatively more primitive, replenishing magma (Campbell *et al.* 1983; Eales *et al.* 1990). The turbulence associated with replenishment resulted in high *R* factors and thus, PGE-enriched sulphides. However, Li and Ripley (2005) showed that magma mixing can only trigger sulphide melt saturation if the mixing partners are nearly saturated in sulphide melt. This likely makes the model of magma mixing inappropriate for the Bushveld PGE reefs as Bushveld parent melts are strongly sulphide undersaturated (Barnes *et al.* 2010). Alternatively, sulphide melt saturation could have been achieved by fractionation. This model is consistent with the location of most PGE reefs near the transition from ultramafic to mafic rocks. Some PGE reefs occur in the upper portions of intrusions (*e.g.*, Stella, Koitelainen and Akanvaara, Skaergaard), implying that the parent magmas were initially highly undersaturated in sulphide melt, or that sulphide melt saturation was delayed, perhaps due to Fe enrichment of the magma (Ripley and Li 2003) or high oxygen fugacity favouring S speciation as sulphate (Jugo 2009). However, if sulphide melt saturation were triggered by fractionation the question arises why the sulphides are typically concentrated near the ultramafic base of cyclic units. As a possible solution, Maier *et al.* (2013a) suggested that sulphide- (and

chromite-rich) layers may form by hydrodynamic sorting, kinetic sieving and percolation of dense sulphide melt in a mobilised crystal slurry.

Several authors have proposed that layered intrusions may represent stacks of out-of-sequence sills and that PGE reefs may derive from the emplacement of sulphide-bearing and/or PGE-enriched magmas onto (or into) a pre-existing cumulate pile (Lee and Butcher 1990; Scoon and Teigler 1994; Manyeruke *et al.* 2005; Mitchell and Scoon 2007; Mungall *et al.* 2016).

Some studies have suggested that PGE in the reefs were transported by volatiles (*e.g.*, Schiffries 1982; Ballhaus and Stumpfl 1986). Boudreau *et al.* (1986) showed that PGE reefs at the Bushveld and Stillwater complexes are spatially associated with chloroapatite and Cl-bearing phlogopite. They hypothesised that PGE were transported as chloride complexes in magmatic-hydrothermal fluids exsolved from underlying crystallising cumulates that were redissolved in stratigraphically higher and fluid undersaturated interstitial melt, resulting in the precipitation of PGE-sulphides and/or PGM (Boudreau 1988, 2019). Barnes and Liu (2012) have shown that Pd and, less so, Pt may be transported in hydrothermal fluids as bisulphide or chloride complexes under certain conditions. Holwell *et al.* (2017) suggested that PGE may be mobile following extreme desulphurisation of primary magmatic sulphides. Examples for hydrothermal PGE enrichment occur at Salt Chuck, Alaska, which is a small (~ 11 km^2) body that is considered a Ural-Alaskan-type mafic-ultramafic complex (Watkinson and Melling 1992). Sulphides at this locality are typical of those precipitated from hydrothermal fluids in that they comprise extremely low Ni and IPGE concentrations, high Cu and Au concentrations, and high Pd/Pt values (Watkinson and Melling 1992; Loney and Himmelberg 1992; Thakurta and Findlay 2013).

A problem with the hydrothermal model of PGE reef formation is that the reefs are typically not only enriched in Pt and Pd, but also in IPGE, yet most of the available data indicate that the IPGE are immobile in fluids (Barnes and Ripley 2016). An alternative scenario may be the one proposed by Nicholson and Mathez (1991) and Mathez (1995) whereby upwelling magmatic vapour/fluid/melt reacted with partially molten, sulphide and PGE bearing, cumulates triggering recrystallisation and the formation of pegmatoid bracketed by chromitites and anorthosite.

Latypov and colleagues have proposed that the PGE reefs (and their often spatially associated chromitites; discussed below) of the Bushveld, Rum, and Lukkulaisvaara intrusions formed via *in situ* crystallisation along the temporary floor of the intrusions (Latypov *et al.* 2013; 2015; 2017). The required high *R* factors were achieved when sulphides that precipitated at the top of the cumulate pile (perhaps due to erosion

of the substrate) sequestered PGE from magmas streaming past the crystallisation front. The key evidence proposed is the persistence of PGE-rich chromitite seams of broadly uniform thickness in potholes (including their inclined and overhanging walls and undercuttings), which cannot be explained by traditional models of gravitational settling.

6.2. Magmatic Ni-Cu-(PGE) sulphides

While layered intrusions are best known for their PGE, chromite and magnetite reefs, many also host disseminated, net-textured, and/or massive sulphides. The deposits occur most commonly at or near the base of the intrusions and thus, are commonly referred to as contact-style mineralisation (Naldrett 2004; Barnes and Lightfoot 2005; McDonald and Holwell 2011). The reason for the basal setting of the deposits is two-fold: First, the formation of significant magmatic sulphides requires addition of external S to the magma which is most readily achieved at the contacts of intrusions (Keays and Lightfoot 2010; Ripley and Li 2013; Robertson *et al.* 2015). Second, the basal portions of intrusions usually crystallise from relatively unevolved, Ni-rich magma.

Many of the largest Ni-Cu-(PGE) deposits are hosted in relatively small layered intrusions (*e.g.*, Noril'sk-Talnakh, Pilgujärvi and other sills in the Pechenga belt, Voisey's Bay, Uitkomst, Nebo-Babel, Nova, CAOB, Finnish Ni belt intrusions) that are interpreted to represent magma feeder conduits. Geochemical and isotopic studies have revealed that in most of these deposits, addition of external S has played a key role in ore genesis. The nature of the contaminant can be diverse, including evaporates at Noril'sk-Tanakh (Grinenko 1985), graphitic shales at Duluth (Ripley and Barnes 1998), paragneiss at Voisey's Bay (Ripley *et al.* 2002), orthogneiss at Nebo-Babel (Seat *et al.* 2009), (v) dolomite at Uitkomst (Li *et al.* 2002), (vi) granite and shales at Eagle (Thakurta *et al.* 2019), and (vii) juvenile crust at Huangshannan (Mao *et al.* 2016). In the Platreef of the Bushveld Complex, a range of contaminants has been proposed including carbonates, sulphidic shale, and granitic gneiss (Barton et al. 1986; Harris and Chaumba 2001; Maier *et al.*, 2008; Ihlenfeld and Keays 2011; McDonald and Holwell 2011; Yudovskaya *et al.* 2017). As significant contamination can result in low *R* factors which are detrimental to high metal tenors, another key component in the formation of the conduit hosted Ni-Cu deposits is entrainment of the magmatic sulphides in the flowing magma (*e.g.*, Voisey's Bay; Li and Naldrett 1999).

A number of magmatic sulphide deposits associated with layered intrusions possess unusually high metal tenors (*e.g.*, Kevitsa, Yang *et al.* 2013, Luolavirta *et al.* 2018; Mirabela; Barnes *et al.* 2011). These high tenors

may reflect the assimilation of 'proto-ore' left from antecedent pulses of magma by new fluxes of chalcophile-undepleted magma (Maier and Groves 2011). Maier and Barnes (2010) showed that sulphide ores at Kabanga were characterised by crustal-like $\delta^{34}S$ values, yet mantle-like O isotopic signatures and argued that these results were consistent with the assimilation of sulphides that segregated from an antecedent pulse of magma in response to crustal contamination. Another potential example of cannibalization includes PGE reefs at Lac des Iles (Hinchey *et al.* 2005).

6.3. Chromitites

Chromitite seams in layered intrusions host most of the world's chromite resources. The deposits occur as stratiform monomineralic seams (*e.g.*, Bushveld Complex, Great Dyke and Stillwater), with Cr_2O_3 grade ranging from ~ 20 wt.% (*e.g.*, Rum) to ~ 55 wt.% (*e.g.*, Burakovsky and Campo Formoso), and thicknesses from < 1 cm to several dm. In some cases, the seams may reach and exceed thicknesses of several metres (notably at Kemi, Uitkomst, Jacurici, and Ring of Fire). The seams are usually located in either the lower, ultramafic portions of layered intrusions and/or near the transition from mafic to ultramafic rocks. Exceptions include Koitelainen and Akanvaara where the chromitites are in the central to upper portion of the intrusions. Most seams are enriched in PGE relative to the silicate host rocks and some seams are mined primarily for PGE, such as the UG2 of the Bushveld Complex (Mudd *et al.* 2018).

Most of the layered intrusions that host chromite deposits are > 2 Ga, including the chromite occurrences of Russia (Pados-Tundra, Burakovsky, and Imandra), India (Sukinda and Nuasahi), Finland (Koitelainden, Kemi, and Akanvaara), and Brazil (Jacurici, Formoso, and Bacuri) as well as those in the Canadian Ring of Fire, Bushveld Complex, and Great Dyke. The 20-30 cm thick chromitite of the Stolzberg complex, South Africa may be the oldest seam reported (3260-3540 Ma, Anhaeusser 2006). In our compilation, only chromitite occurrences of the Madagascan intrusions, Kettara of Morocco, and Nurali of the Russian Urals Belt are < 1 Ga in age.

The origin of chromitite seams has been explained by a range of diverse processes, including (i) fluctuations in intensive parameters (*e.g.*, Ulmer 1969; Cameron 1980; Lipin 1993); (ii) crustal contamination and/or magma mixing (*e.g.*, Irvine 1976; 1977; Alapieti *et al.* 1989; Spandler *et al.* 2005); (iii) metasomatism and recrystallisation of pyroxene-rich rocks (*e.g.*, Nicholson and Mathez 1991; Boudreau 2016; Mathez and Kinzler 2017), (iv) thermochemical erosion and *in situ* crystallisation (*e.g.*, O'Driscoll *et al.* 2010; Latypov *et al.*

2013; 2017; Friedrich *et al.* 2020), (v) intrusion of chromite-enriched magmas/slurry (Voordouw *et al.* 2009), and (vi) hydrodynamic sorting of chromite bearing crystal slurries (*e.g.*, Mondal and Mathez 2007; Maier *et al.* 2013a; Forien *et al.* 2015).

i. Early studies of the Bushveld chromitites invoked variations in fO_2 of the magma as a control on chromite precipitation (*e.g.*, Cameron and Desborough 1969; Ulmer 1969). Fluctuations in fO_2, perhaps in response to episodic magma influx, has also been proposed to explain chromitites of the Great Dyke of Zimbabwe (Wilson 1982) and Sukinda intrusion of India (Chakraborty and Chakraborty 1984). Others have argued that the lateral persistence of the chromitites is more consistent with fluctuations in total pressure exerted on a magma with a composition near the olivine-chromite phase boundary (Osborn 1980; Cameron 1980), *e.g.*, during episodes of replenishment and ejection (Lipin 1993). More recently, Latypov *et al.* (2018) proposed that basaltic magmas may become solely saturated in chromite during depressurisation upon magma ascent through the upper crust. The authors performed polybaric crystallisation simulations on Bushveld melts represented by fine grained rock of Barnes *et al.* (2010) and Cawthorn (2015) using the MELTS programme (Ghiorso and Sack 1995). However, it could be argued that the approach taken, *i.e.*, the incremental and iterative modification of the major element contents of a fine-grained rock presumed to represent a melt, to identify a pressure interval within which chromite is the sole liquidus phase, is overly speculative.

ii. Irvine (1976) proposed that a magma crystallising olivine (± chromite) may be shifted into the chromite-only stability field during the assimilation of siliceous country rock. This model was used to explain olivine-chromite-orthopyroxene cumulate assemblages of the Muskox intrusion and it has recently been applied to explain the formation of chromitites in the Ring of Fire intrusions of Canada (Woods *et al.* 2019). In a revised model, Irvine (1977) proposed mixing of fractionated tholeiitic magma with a more primitive tholeiitic magma. This model has been used to explain the formation of the Kemi chromitites (Alapieti *et al.* 1989) and Stillwater chromitites (Horan *et al.* 2001; Spandler *et al.* 2005). In a related model, O'Driscoll *et al.* (2010), Latypov *et al.* (2013) and Scoon and Costin (2018) argued that the mixing of relatively unevolved replenishing magma with a partial melt of feldspathic cumulates in the chamber triggered *in situ* formation of chromite stringers in the Rum and Bushveld intrusions. However, Naldrett *et al*. (2012) used MELTS modelling on Bushveld model magmas to show that neither an increase in pressure, mixing of

primitive and fractionated magma, felsic contamination of replenishing magma, nor addition of H_2O can promote crystallisation of spinel before orthopyroxene, and thus are inadequate to explain the formation of the chromite seams.

iii. Nicholson and Mathez (1991) proposed that the Merensky Reef chromitites formed via hydration melting of a semi-consolidated, sulphide-bearing proto-reef. Melting was triggered by magmatic vapour ascending through the semi-consolidated cumulate pile, reducing the stability of chromite at the expense of pyroxene and plagioclase. This model can account for the presence of a pegmatitic layer bracketed by chromitite stringers, the knife-sharp contacts observed between the chromitites and the other rocks and the presence of pyroxenite and noritic xenoclasts in the reef that are also rimmed by anorthosite-chromite layers. Mathez and Kinzler (2017) applied the model to the Rum chromitites.

iv. Boudreau (2019) and Marsh *et al.* (2021) proposed that Stillwater and Bushveld chromitite stringers formed due to dissolution of pyroxene and precipitation of chromite in response to volatiles ascending through the cumulates. The volatiles become undersaturated in pyroxene as they infiltrate the relatively hot rocks near the top of the crystal pile. Key evidence cited includes the Cl-rich nature of spatially associated apatite and the presence of volatile-rich polyphase inclusions in chromites.

v. Mondal and Mathez (2007) proposed that the UG2 chromitite of the Bushveld Complex may have formed by the settling of suspended chromite in batches of injected magma, which requires the pre-emplacement fractionation of chromitite in a staging chamber. In a related model, Voordouw *et al.* (2009) suggested that the Bushveld chromitite seams formed from injections of chromite-rich slurries into a largely solidified crystal pile. In contrast, Maier *et al.* (2013a) proposed that Bushveld chromitites formed via hydrodynamic sorting and sieving of pyroxene-chromite slurries deposited at the top of the crystal pile. The slurries locally injected into semi-consolidated footwall cumulates. The effectiveness of density currents for crystal sorting has been experimentally verified in flume tank experiments conducted by Forien *et al.* (2015). In the Kemi intrusion, chromitites can be seen to progressively thicken from the margins to the centre of the intrusion, consistent with hydrodynamic sorting during chamber subsidence (Alapieti *et al.* 1989). Thick chromitite seams in the Jacurici Complex of Brazil are also thought to have formed during

slumping and hydrodynamic sorting of chromite-rich crystal slurries, facilitated by the presence of volatile phases (Marques *et al.* 2017; Friedrich *et al.* 2020).

6.4. Fe-Ti-V-(P) deposits

Stratiform Fe-Ti oxide layers are usually located in the upper, relatively fractionated portions of layered intrusions. Like chromitite seams, these layers can be near-monomineralic (up to several 10s of metres in thickness; *e.g.*, Bushveld, Emeishan LIP intrusions, and Chineysky) or form thick (up to > 100m) intervals of (titano-)magnetite and ilmenite-bearing gabbro (*e.g.*, Koillismaa, Koitelainen, Akanvaara). In some cases, Fe-Ti-V oxide ores are spatially associated with apatite-rich gabbroic rocks or nelsonite from which P can be mined as a by-product, including Bushveld, Grader, Bjerkreim-Sokndal, and Fedorovka (see Charlier *et al.* 2015 and references therein). Only few layered intrusions are mined with P as the primary product, including Bikilal, Ethiopia (Woldemichael and Kimura 2008), Fanshan, China (Cheng and Sun 2008), and the Khibina massif, Russia (Kogarko and Khapaev 1987).

Several models have been proposed for the formation of Fe-Ti-V-(P) oxide layers in layered intrusions, including (i) fluctuations in intensive parameters, (ii) segregation of an immiscible Fe-Ti-(P)-rich melt, (iii) gravitational concentration augmented by hydrodynamic processes, (iv) magma mixing and/or recharge, and (v) *in situ* crystallisation and compositional convection.

i. It has been experimentally determined that oxygen fugacity and TiO_2 content of the residual melt control the stability and composition of Fe-Ti oxides (Buddington and Lindlsey 1964; Toplis and Carroll 1995; Botcharnikov *et a.* 2008). Klemm *et al.* (1985) argued that massive magnetitite layers of the Bushveld Complex formed in response to periodic increases in oxygen fugacity driven by wall-rock devolatilization (see also Reynolds 1985). An increase in oxygen fugacity through assimilation-fractional crystallisation has been invoked to explain the formation of massive Fe-Ti oxide layers at Baima (Zhang *et al.* 2012a), Panzhihua (Ganino *et al.* 2013), and Lac Doré (Mathieu 2019). In other intrusions, the formation of oxide layers was linked to increases in total pressure (Osborn 1980; Lipin 1993; Naslund and McBirney 1996). Cawthorn and Ashwal (2009) argued that magnetite-anorthosite layering in the Bushveld Complex may have formed in response to pressure fluctuation.

ii. During the advanced stages of fractionation, silicate magma may undergo segregation into dense, Fe-Ti-P-rich magma and buoyant Si-rich magma (Philpotts 1967; Reynolds 1985; Zhou *et al.* 2005; Namur *et al.* 2012; Charlier and Grove 2012; Fischer *et al.* 2016; Hou *et al.* 2018), *e.g.*, Skaergaard, Jakobsen *et al.* 2005; Sept Iles, Namur *et al.* 2012; Baima, Liu *et al.* 2016). Fe-Ti-V-(P) ores may therefore represent the crystalline products of immiscible Fe-Ti-V-P-rich melts (Zhou *et al.* 2013) or the ores may represent a cumulate assemblage crystallised from these immiscible melts (Namur *et al.* 2012).

iii. Residual melts associated with anorthositic rocks are relatively Fe-Ti-rich, causing ilmenite to be a liquidus phase together with plagioclase (Toplis and Carroll 1995). The density contrast between crystallising Fe-Ti oxides and plagioclase could lead to plagioclase flotation and Fe-Ti oxide accumulation (*e.g.*, Grader; Charlier *et al.* 2008; 2015), perhaps followed by granular flow of magnetite slurries (Vukmanovic *et al.* 2019). Similar models of gravitational fractionation have been proposed for the Fe-Ti-V deposits of the Emeishan LIP intrusions, such as Panzhihua, Hongge, and Baima (*e.g.*, Pang *et al.* 2008a; 2008b; Zhang *et al.*, 2012; Song *et al.* 2013) and for magnetitites in the Jameson Range intrusion (Karykowski *et al.* 2017b).

iv. The Main Magnetite Layer of the Bushveld Complex has been explained through magma mixing between resident and replenishing magma of the same lineage but at a different stage of fractionation (Molyneux 1974; Irvine and Sharpe 1986; Harney *et al.* 1990; Von Gruenewaldt 1993). However, Cawthorn *et al.* (2005) disputed that magnetite oversaturation occurs in response to magma mixing and Cawthorn and Ashwal (2009) argued that the lack of compositional reversals in cumulate plagioclase above magnetite seams is inconsistent with mixing of resident and replenishing magma.

v. Kruger and Latypov (2020) suggested that magnetite crystallises *in situ* along the floor of the magma chamber, a model initially proposed by Cawthorn and McCarthy (1981). The key evidence cited comprises the rapid decrease in Cr (and V) content of magnetite with height. The authors use a partition coefficient for Cr into magnetite of 525 (based on Lindstrom 1976), whereas the maximum *D* value reported in Dare *et al.* (2012) is 340, and the Geomean is 67.

6.5. Other notable mineral deposits

In addition to PGE-Cu-Ni-Cr-Ti-V, layered intrusions may host other types of economically important mineral deposits, including REE and Nb (in alkaline intrusions of the Gardar and Kola mineral belts), chrysotile asbestos and magnesite (notably in many of the Archean layered intrusions of the Barberton greenstone belt), andalusite as well as building stone (*e.g.*, in the Bushveld Complex, further discussed below) and Ni-laterites (*e.g.*, in the Kibaran Fold belt intrusions of Musongati, Kapalugulu, and Waga.

Because the Bushveld Complex is the largest layered intrusion, it is not surprising that it hosts the greatest range of economically exploitable mineral resources. During the emplacement of the Complex, the country rocks were extensively metamorphosed, leading to the development of biotite-chlorite, cordierite-sillimanite, and andalusite hornfels (Botha 2010), the latter hosting the world's largest reserves of andalusite, presently exploited at several localities, notably Thabazimbi (> 59 wt.% Al_2O_3), Penge (> 58.5 wt.% Al_2O_3), and Lydenburg (> 59 wt.% Al_2O_3; Oosterhuis 1998; Botha 2010). Secondly, Kraubath-type magnesite deposits (*i.e.*, stockwork magnesite veins in ultramafic rocks) are reported in hydrothermally altered ultramafic rocks in the lower zone of the Rustenburg Layered Series (Pohl 1990). Thirdly, gabbro and gabbronorite are quarried at several localities in the Main Zone (Pivko 2004). In addition, the felsic phase of the Bushveld event comprises tin-bearing granite plutons (*e.g.*, Mutele *et al.* 2017). The Zaaiplaats Tin Field in the northern limb of the Bushveld Complex is host to the stanniferous Bobbejaankop and Lease granites that were first discovered in 1908 (Coetzee and Twist 1989; Vonopartis *et al.* 2020). The Phalaborwa Carbonatite Complex is thought to represent the early phase in the formation of the Bushveld Complex, whereby carbonatite magmatism formed during partial melting of metasomatized lithospheric mantle during plume underplating (Wu *et al.* 2011). The complex hosts economic deposits of Cu, U, Zr, P, and Ti (*e.g.*, Wu *et al.* 2011).

Approximately 85% of the world's Ni laterite resources occur in accretionary terranes in the Circum-Pacific Belt and the remainder occur in serpentinised ultramafic cumulates of layered intrusions, notably Kapalagulu-Musongati (Tanzania/Burundi), Wingellina Hills (Australia), and Niquelandia and Barro Alto (Brazil; Butt and Cluzel 2013). Musongati is one of the largest Ni laterite deposits in the world formed through alteration of ultramafic cumulates (Bandyayera 1997). It is also characterised by relatively high PGE contents (~ 0.5-2 ppm; Bandyayera 1997; Maier *et al.* 2008).

Most layered alkaline intrusions that are prospective for REE-Nb mineralisation occur in the Gardar Province of southern Greenland and the Kola peninsula of NW Russia. Due to their incompatibility, the REEs concentrate in the peralkaline residual liquid during differentiation, giving rise to mineralised syneitic and/or

pegmatitic rocks at the roof of intrusions (Marks *et al.* 2011; Paulick *et al.* 2015). The Gardar Province represents a Mesoproterozoic failed rift system that is host to several layered alkaline intrusions that are prospective for REE mineralisation, including Illimaussaq (hosting the Kvanefjeld and Kringlerne deposits) and the Motzfeldt intrusions (Tukianinen 2014; Paulick *et al.* 2015). Mineralised kakortokites and lujavrites of the Kvanefjeld and Kringlerne deposits formed during the advanced stages of fractional crystallisation, where the former represents one of the world's largest REE and U-Th deposits (Thrane *et al.* 2014; Paulick *et al.* 2015). Significant REE-U-Th-Ta-Zr-Nb mineralisation (~ 80 Mt at 0.6-1.1% TREO) is documented at the margins and roof of the Motzfeldt intrusion (Tukiainen 2014). Other notable alkaline intrusions include the Khibina, Lovozero, Kurga, and Niva syenitic plutons of the Kola Alkaline Carbonatite Province, which in turn is part of the Kola-Dnieper LIP (Puchkov *et al.* 2016), of Russia and eastern Finland (see Downes 2005 and references therein). The Khibina massif comprises one of the world's largest apatite deposits, which also comprises considerable amounts of SrO (~ 4.5 wt.%) and REE_2O_3 (< 8.891 ppm; Arzamastsev *et al.* 1987*;* Kogarko 2018)

7. Implications and areas for further study

Layered intrusions have been natural laboratories to advance the understanding of igneous and ore-forming processes, from the early days of Bushveld research in the 1920s focussing on the origin of the PGE deposits (Wagner 1929), through the seminal publication of Layered Intrusions by Wager and Brown in 1968 highlighting the similarities to magmatic sediments, to the application of fluid dynamics in the 1980s (Huppert and Sparks 1981; Sparks *et al.* 1984), and the recognition of the role of magmatic metasomatism and constitutional zone refining (Irvine 1980, McBirney 1987, Boudreau 1988) and *in situ* crystallisation (Campbell 1978). The concept of out-of-sequence sills was introduced by Bedard *et al.* (1988) at Rum and subsequently applied to the Bushveld Complex by authors such as Lee and Butcher (1990), Maier and Barnes (1998), Manyeruke *et al.* (2005), Kinnaird (2005), Scoon and Mitchell (2007), Mungall *et al.* (2016), Wall *et al.* (2018), and Scoates *et al.* (2021).

In the present contribution, we highlight that layered intrusions are volumetrically important components of Earth's crust. This is particularly evident in regions that have a long history of mineral exploration and research, such as Fennoscandia, Western Australia. and South Africa. In these areas, the density of layered intrusions is on the order of 100/M km^2. If this rule holds for other regions of the globe, 100s of intrusions remain to be discovered. Amongst the most recent examples are well mineralised intrusions, such as in the McFauld's Lake

Area (or 'Ring of Fire') and at Sunday Lake in Ontario (Bleeker and Houlé 2020) as well as Nova in Western Australia (Maier *et al.* 2016).

While the scientific advances in understanding the petrogenesis of the intrusions have been considerable, many questions remain. Amongst these, the following may be highlighted:

(i) *Tectonic setting*: It is evident from our compilation that many notable layered igneous intrusions correlate with episodes of voluminous magmatism associated with inter- or intra- continental rift environments, possibly involving slab delamination or mantle plume impingement at the base of the lithosphere. Many others occur in magmatic arc environments (*e.g.*, obducted ophiolite-hosted intrusions, Ural-Alaskan type intrusions, back-arc extension). Post-collisional intrusions (*e.g.*, Variscan and CAOB intrusions) appear to commonly host Ni-Cu mineralisation, seldom Fe-Ti-V (*e.g.*, Bjerkreim-Sokndal, few CAOB intrusions), and no Cr occurrences. The tectonic setting of the CAOB intrusions remains controversial, possibly reflecting the relatively recent onset of research in this region. Intrusions located in syn-orogenic/convergent settings appear to be rare.

(ii) *Mantle sources*: Are the parent magmas generated in the asthenosphere, the SCLM, or both? In view of the high PGE budget of some intrusions, could there be mantle domains that are relatively PGE enriched, perhaps representing incompletely dissolved late veneer material, and if so, how can this be tested? Is the plume model universally applicable, or is there evidence for plate-driven magmatism in some provinces (*e.g.*, Musgrave/Giles Complex; Smithies *et al.* 2015).

(iii) *Composition of magmas*: Examination of fine-grained sills and dykes in the floor of intrusions (*e.g.*, Barnes *et al.* 2010) and chilled margins at their basal contact (Wilson 2012, Maier *et al.* 2016) as well as the trace element content of cumulate rocks and minerals (*e.g.*, Godel *et al.* 2011) indicates that there are 2 types of magma (SHMB and Al-tholeiite) in several of the most prominent intrusions (*e.g.*, Bushveld, Stillwater, Finnish 2.45 Ga intrusions). Does this reflect contamination of komatiitic parent magmas with progressively more refractory crust (Maier *et al.* 2000) or melting of different mantle sources (Richardson and Shirey 2008)

(iv) *Magma emplacement*: Do the magmas intrude as crystal mushes, crystal-poor melts, or both? What is the key evidence, and which factors control the mode of emplacement (*e.g.*, could upper crustal subsidence, induced by magma emplacement, trigger magma ascent from mid-crustal staging chambers? Could this control the size of intrusions in addition to the size of the thermal mantle

anomaly? How common is out-of-sequence sill emplacement, and what is the precision and accuracy of the geochronological methods on which this idea is largely based?

(v) *Origin of layering*: To what degree is the layering of primary magmatic origin, resulting *i.e.,* from granular flow and sill emplacement. If it is largely secondary, as argued by Bedard (2015) and Boudreau (2017), why are there relatively few hydrous phases such as magmatic mica and hornblende?

(vi) *Origin of sulphide and oxide reefs*: While most authors argue that the reefs are of magmatic origin (but see *e.g.* Boudreau 2019), the mechanism of sulphide melt saturation and the mode of sulphide concentration remain debated. The most controversial question is probably whether sulphides and oxides were concentrated within the intrusions (*e.g.,* via phase settling, or granular flow and kinetic sieving/percolation), or in a staging chamber or feeder conduit from where they were entrained by the ascending magma (*e.g.,* Yao & Mungall 2021).

(vii) *Broader implications*: Mafic-ultramafic intrusions volumetrically comprise a significant proportion of Earth's crust and as such, their emplacement may have a significant impact on Earth's atmosphere. Many layered igneous intrusions are associated with the emplacement of large igneous provinces, which in turn correlate with mass extinction events (Wignall 2005; Bond & Wignall 2014). The emplacement of LIPs may be most devastating when emplaced amongst carbonate host rocks (*e.g.,* Bushveld LIP, Siberian Traps; Ganino and Arndt 2009; Stordal *et al.* 2017; Le Vaillant *et al.* 2017).

In terms of investigative approach, future advances will likely depend on combining thermodynamic modelling *(e.g.,* Boudreau 2008; Mungall *et al.* 2015; Schoneveld *et al.* 2020) and machine learning (*e.g.,* Linday *et al.* 2021) with large geochemical databases, analogue experiments (Forien *et al.* 2015), microtextural analysis (Holness 2007; Vukmanovic *et al.* 2018), and element mapping techniques such as microXRF and FESEM (Barnes *et al.* 2020; Smith *et al.* 2021, Maier *et al.* 2021).

Conclusions

Layered igneous intrusions occur across the globe and geological time, with a clustering in Archean cratons and during supercontinent rifting and dispersal. Both asthenospheric and lithospheric mantle sources have been proposed, with the former likely being predominant. The intrusions are not only natural laboratories

for studies of igneous petrology, but are also invaluable repositories for a wide range of mineral deposits, notably PGE reefs, disseminated or massive Ni-Cu-PGE deposits, stratiform massive or disseminated Fe-Ti-V-(P) layers, and chromite seams. Additional mineral deposits include REE, Nb, P, Au, building stone, andalusite, asbestos, magnesite, and, in associated felsic intrusives, tin and fluorite. Based on the abundance of layered intrusions in relatively well explored terranes (*e.g.*, Fennoscandia, South Africa, Western Australia), we propose that many layered intrusions remain to be discovered on Earth, particularly in poorly explored and relatively inaccessible regions of Africa, Australia, Russia, Greenland, Antarctica, South America, and northern Canada.

Acknowledgements

We thank Christian Tegner and Richard Ernst for their constructive reviews that helped improve an earlier version of this contribution. Christina Yan Wang is thanked for the editorial handling of this manuscript. The authors would like to acknowledge fruitful collaboration and discussion with many colleagues over the years, amongst them Hugh Eales, Bernd Teigler, Billy de Klerk, Julian (Goonie) Marsh, Roger Scoon and Steve Prevec (Rhodes University), Sarah-Jane Barnes, Paul Bedard and Dany Savard (UQAC), Sybrand de Waal, Tawanda Manyeruke, Ian Graham, Geoff Grantham and Hassina Mouri (Univ. Pretoria), Chusi Li and Ed Ripley (Indiana University), Nick Arndt (Univ. Grenoble), Dave Reid and Chris Harris (Univ. Cape Town), Lew Ashwal, Grant Cawthorn, Carl Anhaeusser and Marina Yudovskaya (Wits University), Jim Mungall (Carleton University), Haroldo da Silva Sa (Univ. Bahia), Hugh Smithies (GSWA), Steve Barnes and Belinda Godel (CSIRO), Marco Fiorentini, Birger Rasmussen and David Groves (UWA), Petri Peltonen (Univ. Helsinki), Eero Hanski and Shenghong Yang (Oulu University), Tapio Halkoaho, Hannu Huhma, Yann Lahaye and Hugh O'Brien (GTK), Pavel Lipachkin and Nikolay Groshev (Kola Science Center), James Scoates (UBC), Alan Boudreau (Duke University), Thomas Oberthür (BGR), Mario Fischer-Gödde (Uni. Köln), Jens Anderson (Univ. Exeter), Brian O'Driscoll (Univ. Manchester), Luke Hepworth (Keele University), Tom Blenkinsop, Hazel Prichard and Duncan Muir (Cardiff University), and Dean Bullen and James Darling (Univ. Portsmouth). We benefitted enormously from the support of our industry partners, namely Danie Grobler (Ivanplats), Ian Bliss and Christine Vaillancourt (Northern Shield), Les Patton (Impala), Chris Lee and Bruce Walters (Anglo Platinum), Genario de Oliveira (Caraiba mine), Mark Bristow (Rand Mines), Mike Bowen (Gold Fields), Volker Gartz (Harmony Gold), Eckhard Freyer and Solly Theron (Anglo American SA), Tim Livesey (Barrick), James Abson (Southern Era), John Blaine and Dave Dodd (Falconbridge SA and Caledonia Mining), Jock Harmer (Pan Palladium), Hennie Theart (Anglovaal), Leslie Terreblanche and Koos Beukes (Okiep Cu Company), Marco Andreoli (NECSA), and Paul Polito (Anglo American base metals Australia).

Declaration of interests

The authors declare that they have no known competing financial interests or personal relationships that could have appeared to influence the work reported in this paper.

Supplementary data

Suppmentary material

References

Abdel Halim AH, Helmy HM, Abd El-Rahman YM, et al (2016) Petrology of the Motaghairat mafic-ultramafic complex, Eastern Desert, Egypt: A high-Mg post-collisional extension-related layered intrusion. J Asian Earth Sci 116:164–180.

Abernethy KE. (2020) Assimilation of Dolomite by Bushveld Magmas in the Flatreef; Implications for the Origin of Ni-Cu-PGE Mineralization and the Precambrian Atmosphere. Cardiff University PhD Thesis.

Ahmat AL (1986) Petrology, structure, regional geology and age of the gabbroic Windimurra complex, Western Australia: University of Western Australia, PhD Thesis unpub.

Alapieti TT, Kujanpaa J, Lahtinen JJ, Papunen H (1989) The Kemi stratiform chromitite deposit, northern Finland. Econ Geol 84:1057–1077.

Andersen JCO, Rasmussen H, Nielsen TFD, Ronsbo JG (1998) The Triple Group and the Platinova gold and palladium reefs in the Skaergaard Intrusion; stratigraphic and petrographic relations. Econ Geol 93:488–509

Anhaeusser CR (2006) A reevaluation of Archean intracratonic terrane boundaries on the Kaapvaal Craton, South Africa: Collisional suture zones? Spec Pap - Geol Soc Am 405:193

Anhaeusser, CR (1983). Archaean Layered Ultramafic Complexes in the Barberton Mountain Land South Africa (No. 161-162). Economic Geology Research Unit, University of the Witwatersrand.

Ariskin A, Danyushevsky L, Nikolaev G, et al (2018) The Dovyren Intrusive Complex (Southern Siberia, Russia): Insights into dynamics of an open magma chamber with implications for parental magma origin, composition, and Cu-Ni-PGE fertility. Lithos 302:242–262

Ariskin AA, Danyushevsky L V, Fiorentini M, et al (2020) Petrology, geochemistry, and the origin of sulfide-bearing and PGE-mineralized troctolites from the Konnikov zone in the Yoko-Dovyren layered intrusion. Russ Geol Geophys 61:611–633

Ariskin AA, Kislov E V., Danyushevsky L V., et al (2016) Cu–Ni–PGE fertility of the Yoko-Dovyren layered massif (northern Transbaikalia, Russia): thermodynamic modeling of sulfide compositions in low mineralized dunite based on quantitative sulfide mineralogy. Miner Deposita 51:993–1011.

Arndt N, Lesher CM, Czamanske GK (2005) Mantle-derived magmas and magmatic Ni-Cu-(PGE) deposits. Econ Geol 5–24

Arndt NT (2011) Insights into the geologic setting and origin of Ni-Cu-PGE sulfide deposits of the Norilsk-Talnakh region, Siberia. Rev Econ Geol 17:199–215

Arzamastsev AA, Ivanova TN, Korobeinikova AN (1987) Petrology of ijolite-urtite series of the Khibina alkaline massif and apatite-nepheline mineralization. Nauka, Leningrad. 112 pp. (in Russian).

Ashley P, Craw D, Mackenzie D, et al (2012) Mafic and ultramafic rocks, and platinum mineralisation potential, in the Longwood Range, Southland, New Zealand. New Zeal J Geol Geophys 55:3–19.

Ashwal LD (2013) Anorthosites. Volume 21. Springer Science & Business Media

Augé T, Cocherie A, Genna A, et al (2003) Age of the Baula PGE mineralization (Orissa, India) and its implications concerning the Singhbhum Archaean nucleus. Precambrian Res 121:85–101.

Bailly L, Augé T, Trofimov N, et al (2011) The mineralization potential of the Burakovsky layered intrusion, Karelia, Russia. Can Mineral 49:1455–1478

Ballhaus C, Glikson AY (1989) Magma mixing and intraplutonic quenching in the Wingellina Hills Intrusion, Giles Complex, central Australia. J Petrol 30:1443–1469

Ballhaus CG, Stumpfl EF (1986) Sulfide and platinum mineralization in the Merensky Reef: evidence from hydrous silicates and fluid inclusions. Contrib to Mineral Petrol 94:193–204

Bandyayera D (1997) Formation des latérites nickélifères et mode de distribution des éléments du groupe du platine dans les profils latéritiques du complexe de Musongati, Burundi. Université du Québec à Chicoutimi. PhD Thesis.

Barkov AY, Fedortchouk Y, Campbell RA, Halkoaho TAA (2015) Coupled substitutions in PGE-enriched cobaltite: new evidence from the Rio Jacaré layered complex, Bahia state, Brazil. Mineral Mag 79:1185–1193

Barnes SJ (1993) Partitioning of the platinum group elements and gold between silicate and sulphide magmas in the Munni Munni Complex, Western Australia. Geochim Cosmochim Acta 57:1277–1290

Barnes SJ, Anderson JAC, Smith TR, Bagas L (2008) The Mordor Alkaline Igneous Complex, Central Australia: PGE-enriched disseminated sulfide layers in cumulates from a lamprophyric magma. Miner Depos 43:641–662.

Barnes SJ, Fisher LA, Godel B, et al (2016) Primary cumulus platinum minerals in the Monts de Cristal Complex, Gabon: magmatic microenvironments inferred from high-definition X-ray fluorescence microscopy. Contrib to Mineral Petrol 171:1–18.

Barnes S-J, Francis D (1995) The distribution of platinum-group elements, nickel, copper, and gold in the Muskox layered intrusion, Northwest Territories, Canada. Econ Geol 90:135–154.

Barnes S-J, Gowne TS (2011) The Pd Deposits of the Lac des Iles Complex , Northwestern Ontario. Rev Econ Geol 17:351–370

Barnes SJ, Hoatson DM (1994) The Munni Munni Complex, western Australia: stratigraphy, structure and petrogenesis. J Petrol 35:715–751

Barnes SJ, Latypov R, Chistyakova S, et al (2021) Idiomorphic oikocrysts of clinopyroxene produced by a peritectic reaction within a solidification front of the Bushveld Complex. Contrib to Mineral Petrol 176:1–19

Barnes S-J, Lightfoot PC (2005) Formation of Magmatic Nickel Sulfide Ore Deposits and Processes Affecting Their Copper and Platinum Group Element Contents. Econ Geol 179–213

Barnes SJ, Liu W (2012) Pt and Pd mobility in hydrothermal fluids: evidence from komatiites and from thermodynamic modelling. Ore Geol Rev 44:49–58

Barnes S-J, Maier WD (2002) Platinum-Group Element Distributions in the Rustenburg Layered Suite of the Bushveld Complex , South Africa. Geol geochemistry Mineral Miner Benef Platinum-gr Elem Canad Inst Min Met Petro CIM Sp 54:431–458

Barnes S-J, Maier WD, Curl EA (2010) Composition of the marginal rocks and sills of the Rustenburg Layered Suite, Bushveld Complex, South Africa: implications for the formation of the platinum-group element deposits. Econ Geol 105:1491–1511

Barnes SJ, Malitch KN, Yudovskaya MA (2020) Introduction to a Special Issue on the Norilsk-Talnakh Ni-Cu-Platinum Group Element Deposits. Econ Geol 115:1157–1172

Barnes SJ, Melezhik VA, Sokolov S V. (2001) The composition and mode of formation of the Pechenga nickel deposits, Kola Peninsula, Northwestern Russia. Can Mineral 39:447–471.

Barnes SJ, Mole DR, Le Vaillant M, et al (2016) Poikilitic Textures, Heteradcumulates and Zoned Orthopyroxenes in the Ntaka Ultramafic Complex , Tanzania : Implications for Crystallization Mechanisms of Oikocrysts. J Petrol 57:1171–1198. https://doi.org/10.1093/petrology/egw036

Barnes SJ, Mungall JE (2018) Blade-shaped dikes and nickel sulfide deposits: a model for the emplacement of ore-bearing small intrusions. Econ Geol 113:789–798

Barnes SJ, Mungall JE, Le Vaillant M, et al (2017) Sulfide-silicate textures in magmatic Ni-Cu-PGE sulfide ore deposits: Disseminated and net-textured ores. Am Mineral 102:473–506

Barnes SJ, Osborne GA, Cook D, et al (2011) The Santa Rita nickel sulfide deposit in the Fazenda Mirabela intrusion, Bahia, Brazil: Geology, sulfide geochemistry, and genesis. Econ Geol 106:1083–1110

Barnes S-J, Pagé P, Zientek M (2020) The Lower Banded series of the Stillwater Complex, Montana: whole-rock lithophile, chalcophile, and platinum-group element distributions. Miner Depos 55:163–186

Barnes S-J, Ripley EM (2016) Highly siderophile and strongly chalcophile elements in magmatic ore deposits. Rev Mineral Geochemistry 81:725–774

Barton JM, Cawthorn RG, White J (1986) The role of contamination in the evolution of the Platreef of the Bushveld Complex. Econ Geol 81:1096–1104

Bédard JH (2015) Ophiolitic magma chamber processes, a perspective from the Canadian Appalachians. In: Layered intrusions. Springer, pp 693–732

Bédard JH, Sparks RSJ, Renner R, et al (1988) Peridotite sills and metasomatic gabbros in the Eastern Layered Series of the Rhum complex. J Geol Soc London 145:207–224

Bekker A, Grokhovskaya TL, Hiebert R, et al (2016) Multiple sulfur isotope and mineralogical constraints on the genesis of Ni-Cu-PGE magmatic sulfide mineralization of the Monchegorsk Igneous Complex, Kola Peninsula, Russia. Miner Depos 51:1035–1053

Bennett M, Gollan M, Staubmann M, Bartlett J (2014) Motive, means, and opportunity: key factors in the discovery of the Nova-Bollinger magmatic nickel-copper sulfide deposits in Western Australia. Soc Econ Geol Spec Publ 18:301–320

Berlo K, Blundy J, Turner S, Hawkesworth C (2007) Textural and chemical variation in plagioclase phenocrysts from the 1980 eruptions of Mount St. Helens, USA. Contrib to Mineral Petrol 154:291–308

Bierlein FP, Groves DI, Goldfarb RJ, Dubé B (2006) Lithospheric controls on the formation of provinces hosting giant orogenic gold deposits. Miner Depos 40:874

Bleeker W (2003) The late Archean record: a puzzle in ca. 35 pieces. Lithos 71:99–134

Bleeker W, Houlé MG (2020) Targeted Geoscience Initiative 5: Advances in the understanding of Canadian Ni-Cu-PGE and Cr ore systems – Examples from the Midcontinent Rift, the Circum-Superior Belt, the

Archean Superior Province, and Cordilleran Alaskan-type intrusions. Geological Survey of Canada Open File 8722

Bolle O, Diot H, Duchesne J-C (2000) Magnetic fabric and deformation in charnockitic igneous rocks of the Bjerkreim–Sokndal layered intrusion (Rogaland, Southwest Norway). J Struct Geol 22:647–667

Bond DPG, Wignall PB (2014) Large igneous provinces and mass extinctions: an update. Volcanism, impacts, mass extinctions causes Eff 505:29–55

Boorman SL, McGuire JB, Boudreau AE, Kruger FJ (2003) Fluid overpressure in layered intrusions: Formation of a breccia pipe in the Eastern Bushveld Complex, Republic of South Africa. Miner Depos 38:356–369.

Botcharnikov RE, Almeev RR, Koepke J, Holtz F (2008) Phase relations and liquid lines of descent in hydrous ferrobasalt—implications for the Skaergaard intrusion and Columbia River flood basalts. J Petrol 49:1687–1727

Botha BW (2010) An Overview of Andalusite from Southern Africa: Geology and Mineralogy. In: The Southern African Institute of Mining and Metallurgy, Refractories 2010 Conference, 8p

Boudreau AE (1987) The role of fluids in the petrogenesis of platinum-group element deposits in the Stillwater Complex, Montana. PhD Thesis.

Boudreau AE (1988) Investigations of the Stillwater Complex; 4, The role of volatiles in the petrogenesis of the JM Reef, Minneapolis adit section. Can Mineral 26:193–208

Boudreau AE (2008) Modeling the Merensky Reef, Bushveld Complex, Republic of South Africa. Contrib to Mineral Petrol 156:431–437

Boudreau AE (2017) A personal perspective on layered intrusions. Elem An Int Mag Mineral Geochemistry, Petrol 13:380–381

Boudreau AE (2019) Hydromagmatic processes and platinum-group element deposits in layered intrusions. Cambridge University Press

Boudreau AE, Mathez EA, McCallum IS (1986) Halogen geochemistry of the Stillwater and Bushveld Complexes: evidence for transport of the platinum-group elements by Cl-rich fluids. J Petrol 27:967–986

Boudreau AE, McBirney AR (1997) The Skaergaard layered series. Part III. Non-dynamic layering. J Petrol 38:1003–1020

Boudreau AE, McCallum IS (1992) Infiltration metasomatism in layered intrusions - An example from the Stillwater Complex, Montana. J Volcanol Geotherm 52(1-3): 171-183.

Bowen NL (1915) Crystallization-differentiation in silicate liquids. Am J Sci 175–191

Bowles JFW, Suárez S, Prichard HM, Fisher PC (2017) Weathering of PGE sulfides and Pt–Fe alloys in the Freetown Layered Complex, Sierra Leone. Miner Depos 52:1127–1144

Bruegmann GE, Naldrett AJ, Macdonald AJ (1989) Magma mixing and constitution zone refining in the Lac des Iles Complex, Ontario; genesis of platinum-group element mineralization. Econ Geol 84:1557–1573

Buddington AF, Lindsley DH (1964) Iron-titanium oxide minerals and synthetic equivalents. J Petrol 5:310–357

Butcher AR, Pirrie D, Prichard HM, Fisher P (1999) Platinum-group mineralization in the Rum layered intrusion, Scottish Hebrides, UK. J Geol Soc London 156:213–216

Butcher AR, Young IM, Faithfull JW (1985) Finger structures in the Rhum Complex. Geol Mag 122:491–502

Butt CRM, Cluzel D (2013) Nickel laterite ore deposits: weathered serpentinites. Elements 9:123–128

Callegaro S, Marzoli A, Bertrand H, et al (2017) Geochemical constraints provided by the Freetown Layered Complex (Sierra Leone) on the origin of high-Ti tholeiitic CAMP magmas. J Petrol 58:1811–1840

Cameron EN (1980) Evolution of the Lower Critical Zone, central sector, eastern Bushveld Complex, and its chromite deposits. Econ Geol 75:845–871

Cameron EN, Desborough GA (1969) Occurrence and characteristics of chromite deposits—eastern Bushveld Complex. Econ Geol Monogr 4:23–40

Cameron EN, Emerson ME (1959) The origin of certain chromite deposits of the eastern part of the Bushveld Complex. Econ Geol 54:1151–1213

Campbell IH (1977) A study of macro-rhythmic layering and cumulate processes in the Jimberlana intrusion, Western Australia. part I: The upper layered series. J Petrol 18:183–215.

Campbell IH (1978) Some problems with the cumulus theory. Lithos 11:311–323

Campbell IH, Naldrett AJ (1979) The influence of silicate:sulfide ratios on the geochemistry of magmatic sulfides. Econ Geol 74:1503–1506

Campbell IH, Naldrett AJ, Barnes SJ (1983) A model for the origin of the platinum-rich sulfide horizons in the Bushveld and Stillwater Complexes. J Petrol 24:133–165

Carr HW, Kruger FJ, Groves DI, Cawthorn RG (1999) The petrogenesis of Merensky Reef potholes at the Western Platinum Mine, Bushveld Complex: Sr-isotopic evidence for synmagmatic deformation. Miner Depos 34:335–347

Cashman K V, Sparks RSJ, Blundy JD (2017) Vertically extensive and unstable magmatic systems: a unified view of igneous processes. Science, 355(1280):1-9

Cashman K, Blundy J (2013) Petrological cannibalism: the chemical and textural consequences of incremental magma body growth. Contrib to Mineral Petrol 166:703–729

Cawthorn RG (2015) The Bushveld Complex, South Africa. In: Layered Intrusions. Springer, pp 517–587

Cawthorn RG, Ashwal LD (2009) Origin of anorthosite and magnetitite layers in the Bushveld Complex, constrained by major element compositions of plagioclase. J Petrol 50:1607–1637

Cawthorn RG, Barnes SJ, Ballhaus C, Malitch KN (2005) Platinum-group element, chromium, and vanadium deposits in mafic and ultramafic rocks. Econ Geol 100:215–249

Cawthorn RG, Meyer FM (1993) Petrochemistry of the Okiep copper district basic intrusive bodies, northwestern Cape Province, South Africa. Econ Geol 88:590–605

Chakraborty KL, Chakraborty TL (1984) Geological features and origin of the chromite deposits of Sukinda valley, Orissa, India. Miner Depos 19:256–265

Chalokwu CI (2001) Petrology of the Freetown Layered Complex, Sierra Leone: part II. Magma evolution and crystallisation conditions. J African Earth Sci 32:519–540

Charlier B, Grove TL (2012) Experiments on liquid immiscibility along tholeiitic liquid lines of descent. Contrib to Mineral Petrol 164:27–44

Charlier B, Namur O, Bolle O, et al (2015) Fe–Ti–V–P ore deposits associated with Proterozoic massif-type anorthosites and related rocks. Earth-Science Rev 141:56–81

Charlier B, Sakoma E, Sauvé M, et al (2008) The Grader layered intrusion (Havre-Saint-Pierre Anorthosite, Quebec) and genesis of nelsonite and other Fe–Ti–P ores. Lithos 101:359–378

Chashchin V V, Galkin AS, Ozeryanskii V V, Dedyukin AN (1999) Sopcha lake chromite deposit and its platinum potential, Monchegorsk pluton, Kola Peninsula (Russia). Geol Ore Depos 41:460–468

Cheng C, Sun S (2003) The Fanshan apatite-magnetite deposit in the potassic ultramafic layered intrusion, North China. Resour Geol 53:163–174

Choban EA, Semenov VS, Glebovitsky VA (2006) Rhythmic layering in the magma chamber of basic-ultrabasic intrusions due to diffusion and intermittent convection. Izv Phys Solid Earth 42:362–376

Choudhary BR, Ernst RE, Xu Y-G, et al (2019) Geochemical characterization of a reconstructed 1110 Ma large igneous province. Precambrian Res 332:105382

Christopher Jenkins M, Mungall JE, Zientek ML, et al (2020) The Nature and Composition of the JM Reef, Stillwater Complex, Montana, USA. Econ Geol 115:1799–1826

Christopher TE, Blundy J, Cashman K, et al (2015) Crustal-scale degassing due to magma system destabilization and magma-gas decoupling at Soufrière Hills Volcano, Montserrat. Geochemistry, Geophys Geosystems 16:2797–2811

Cimon J (1998) L'unité à apatite de Rivière-des-Rapides, Complexe de Sept-Îles: localisation stratigraphique et facteurs à l'origine de sa formation. Le Complexe Sept-Îles Québec, Canada, Ministère l'Ènergie des Ressources du Québec 5–97

Clifford TN, Barton ES (2012) The O'okiep Copper District, Namaqualand, South Africa: A review of the geology with emphasis on the petrogenesis of the cupriferous Koperberg Suite. Miner Depos 47(8): 837-857.

Coetzee J, Twist D (1989) Disseminated tin mineralization in the roof of the Bushveld granite pluton at the Zaaiplaats Mine, with implications for the genesis of magmatic hydrothermal tin systems. Econ Geol 84:1817–1834

Condie KC (2001) Continental growth during formation of Rodinia at 1.35-0.9 Ga. Gondwana Res 4:5–16

Conrad ME, Naslund HR (1989) Modally-graded rhythmic layering in the Skaergaard intrusion. J Petrol 30:251–269

Cooper KM (2015) Timescales of crustal magma reservoir processes: insights from U-series crystal ages. Geol Soc London, Spec Publ 422:141–174

Costa F, Coogan LA, Chakraborty S (2010) The time scales of magma mixing and mingling involving primitive melts and melt–mush interaction at mid-ocean ridges. Contrib to Mineral Petrol 159:371–387

Cruden AR, McCaffrey KJW, Bunger AP (2018) Geometric scaling of tabular igneous intrusions: implications for emplacement and growth. In: Breitkreuz C, Rocchu S (eds) Physical Geology of Shallow Magmatic Systems: Dykes, Sills, and Laccoliths. Springer

Dare SAS, Barnes S-J, Beaudoin G (2012) Variation in trace element content of magnetite crystallized from a fractionating sulfide liquid , Sudbury , Canada: Implications for provenance discrimination. Geochim Cosmochim Acta 88:27–50.

Darwin C (1845) Geological Observations on the Volcanic Islands visited during the voyage of HMS Beagle, together with some brief notices on the geology of Australia and the Cape of Good Hope; being the

second part of the Geology of the Voyage of the Beagle, under the command of Capt. Fitzroy, RN, during the years 1832 to 1836: London, pp. 176, with a map of the Island of Ascension.

Davies G, Cawthorn RG, Barton JM, Morton M (1980) Parental magma to the Bushveld Complex. Nature 287:33–35

Day JMD, Pearson DG, Hulbert LJ (2008) Rhenium - Osmium isotope and platinum-group element constraints on the origin and evolution of the 1.27 Ga Muskox layered intrusion. J Petrol 49:1255–1295.

De Waal SA, Maier WD, Armstrong RA, Gauert CDK (2001) Parental magma and emplacement of the stratiform Uitkomst Complex, South Africa. Can Mineral 39:557–571

Deblond A (1994) Géologie et pétrologie des massifs basiques et ultrabasiques de la ceinture Kabanga-Musongati au Burundi. Ann Roy Mus for C Af. Geol Sci 279:

Dharma Rao C V., Windley BF, Choudhary AK (2011) The Chimalpahad anorthosite Complex and associated basaltic amphibolites, Nellore Schist Belt, India: Magma chamber and roof of a Proterozoic island arc. J Asian Earth Sci 40:1027–1043.

Ding X, Ripley EM, Li C (2012) PGE geochemistry of the Eagle Ni-Cu-(PGE) deposit, Upper Michigan: Constraints on ore genesis in a dynamic magma conduit. Miner Depos 47:89–104.

Dobmeier C (2006) Emplacement of Proterozoic massif-type anorthosite during regional shortening: evidence from the Bolangir anorthosite complex (Eastern Ghats Province, India). Int J Earth Sci 95:543–555

Dostal J (2016) Rare metal deposits associated with alkaline/peralkaline igneous rocks. Rev Econ Geol 18:33–54

Downes H, Balaganskaya E, Beard A, et al (2005) Petrogenetic processes in the ultramafic, alkaline and carbonatitic magmatism in the Kola Alkaline Province: a review. Lithos 85:48–75

Duchesne J-C, Charlier B (2005) Geochemistry of cumulates from the Bjerkreim–Sokndal layered intrusion (S. Norway). Part I: Constraints from major elements on the mechanism of cumulate formation and on the jotunite liquid line of descent. Lithos 83:229–254

Eales H V, Field M, De Klerk WJ, Scoon RN (1988) Regional trends of chemical variation and thermal erosion in the Upper Critical Zone, western Bushveld Complex. Mineral Mag 52:63–79

Eales H V, Marsh JS, Mitchell AA, et al (1986) Some geochemical constraints upon models for the crystallization of the upper critical zone-main zone interval, northwestern Bushveld complex. Mineral Mag 50:567–582

Eales H V., de Klerk WJ, Teigler B (1990) Evidence for magma mixing processes within the Critical and Lower Zones of the northwestern Bushveld Complex, South Africa. Chem Geol 88(3-4): 261-278.

Edmonds M, Cashman K V, Holness M, Jackson M (2019) Architecture and dynamics of magma reservoirs. Phil. Trans R Soc A 377: 20180298.

Elardo SM, McCubbin FM, Shearer CK (2012) Chromite symplectites in Mg-suite troctolite 76535 as evidence for infiltration metasomatism of a lunar layered intrusion. Geochim Cosmochim Acta 87:154–177.

Emslie RF (1965) The Michikamau anorthositic intrusion, Labrador. Can J Earth Sci 2:385–399

Ernst RE (2014) Large igneous provinces. Cambridge University Press

Ernst RE (2014) Large igneous provinces. Cambridge University Press

Ernst RE, Bell K (2010) Large igneous provinces (LIPs) and carbonatites. Mineral Petrol 98:55–76

Ernst RE, Bleeker W, Söderlund U, Kerr AC (2013) Large Igneous Provinces and supercontinents: Toward completing the plate tectonic revolution. Lithos 174:1–14

Ernst RE, Buchan KL (1997) Layered mafic intrusions: a model for their feeder systems and relationship with giant dyke swarms and mantle plume centres: Plumes, Plates and Mineralisation'97 Symposium. South African J Geol 100:319–334

Ernst RE, Jowitt SM (2013) Large igneous provinces (LIPs) and metallogeny. Soc Econ Geol Spec Publ 17:17–51

Ernst RE, Liikane DA, Jowitt S, et al (2019) A new plumbing system framework for mantle plume-related continental Large Igneous Provinces and their mafic-ultramafic intrusions. J Volcanol Geotherm Res 384:75–84

Evans DM (2017) Chromite compositions in nickel sulphide mineralized intrusions of the Kabanga-Musongati-Kapalagulu Alignment, East Africa: petrologic and exploration significance. Ore Geol Rev 90:307–321

Faure F, Arndt N, Libourel G (2006) Formation of spinifex texture in komatiites: an experimental study. J Petrol 47:1591–1610

Ferguson J (1964) Geology of the Ilímaussaq alkaline intrusion, South Greenland. Reitzel

Ferguson J, Pulvertaft TCR (1963) Contrasted styles of igneous layering in the Gardar province of South Greenland. Spec Pap Miner Soc Am 1:10–21

Ferreira Filho C, Naldrett AJ, Asif M (1995) Distribution of platinum-group elements in the Niquelandia layered mafic-ultramafic intrusion, Brazil; implications with respect to exploration. Can Mineral 33:165–184

Ferreira Filho CF, Cunha JC, Cunha EM, Canela JHC (2013) Depósito de níquel-cobre sulfetado de Santa Rita, Itagibá, Bahia, Brasil. Série Arq Abertos 39.

Ferreira-Filho CF, Kamo SL, Fuck RA, et al (1994) Zircon and rutile U-Pb geochronology of the Niquelândia layered mafic and ultramafic intrusion, Brazil: constraints for the timing of magmatism and high grade metamorphism. Precambrian Res 68:241–255

Ferris JK, Storey BC, Vaughan APM, et al (2003) The Dufek and Forrestal intrusions, Antarctica: A centre for Ferrar large igneous province dike emplacement? Geophys Res Lett 30(6):1-4.

Fiorentini ML, Beresford SW, Rosengren N, et al (2010) Contrasting komatiite belts, associated Ni–Cu–(PGE) deposit styles and assimilation histories. Aust J Earth Sci 57:543–566

Fiorentini ML, O'Neill C, Giuliani A, et al (2020) Bushveld superplume drove Proterozoic magmatism and metallogenesis in Australia. Sci Rep 10:1–10.

Fischer LA, Yuan Q (2016) Fe-Ti-V-(P) resources in the upper zone of the Bushveld complex, South Africa. In: Papers and Proceedings of the Royal Society of Tasmania. pp 15–22

Ford AB (1983) The Dufek intrusion of Antarctica and a survey of its minor metals and possible resources. Pet Miner Resour Antarct US Geol Surv Circ 909:51–75

Forien M, Tremblay J, Barnes S-J, et al (2015) The role of viscous particle segregation in forming chromite layers from slumped crystal slurries: insights from analogue experiments. J Petrol 56:2425–2444

Francis D (2011) Columbia Hills - An exhumed layered igneous intrusion on Mars? Earth Planet Sci Lett 310:59–64.

Friedrich BM, Marques JC, Olivo GR, et al (2020) Petrogenesis of the massive chromitite layer from the Jacurici Complex, Brazil: evidence from inclusions in chromite. Miner Depos 55:1105–1126

Frimmel HE, Groves DI, Kirk J, et al (2005) The formation and preservation of the Witwatersrand goldfields, the world's largest gold province. Econ Geol 100:769–797

Ganino C, Arndt NT (2009) Climate changes caused by degassing of sediments during the emplacement of large igneous provinces. Geology 37:323–326

Ganino C, Harris C, Arndt NT, et al (2013) Assimilation of carbonate country rock by the parent magma of the Panzhihua Fe-Ti-V deposit (SW China): evidence from stable isotopes. Geosci Front 4:547–554

Garuti G, Zaccarini F, Proenza JA, et al (2012) Platinum-group minerals in chromitites of the Niquelândia layered intrusion (Central Goias, Brazil): Their magmatic origin and low-temperature reworking during serpentinization and lateritic weathering. Minerals 2:365–384

Gauert CDK, De Waal SA, Wallmach T (1995) Geology of the ultrabasic to basic Uitkomst complex, eastern Transvaal, South Africa: an overview. J African Earth Sci 21:553–570.

Ghebre WM (2010) Geology and mineralization of Bikilal phosphate deposit, western Ethiopia, implication and outline of gabbro intrusion to east Africa zone. Iran J of Earth Sci 2(2): 158-167.

Ginibre C, Wörner G, Kronz A (2002) Minor-and trace-element zoning in plagioclase: implications for magma chamber processes at Parinacota volcano, northern Chile. Contrib to Mineral Petrol 143:300–315

Godel B (2015) Platinum-group element deposits in layered intrusions: recent advances in the understanding of the ore forming processes. In: Layered Intrusions. Springer, pp 379–432

Godel B, Barnes S-J, Maier WD (2011) Parental magma composition inferred from trace element in cumulus and intercumulus silicate minerals: An example from the Lower and Lower Critical Zones of the Bushveld Complex, South-Africa. Lithos 125:537–552

Godel B, Rudashevsky NS, Nielsen TFD, et al (2014) New constraints on the origin of the Skaergaard intrusion Cu–Pd–Au mineralization: Insights from high-resolution X-ray computed tomography. Lithos 190:27–36

Goff BH, Weinberg R, Groves DI, et al (2004) The giant Volgeno Eg fluorite deposit in a magnetite-fluorite-fayalite REE pipe: A hydrothermally-altered carbonatite-related pegmatoid? Mineral Petrol 80:173–199.

Goldfarb RJ, Bradley D, Leach DL (2010) Secular variation in economic geology. Econ Geol 105:459–465

Good DJ, Cabri LJ, Ames DE (2017) PGM facies variations for Cu-PGE deposits in the Coldwell Alkaline Complex, Ontario, Canada. Ore Geol Rev 90:748–771

Goode ADT (1970) The petrology and structure of the Kalka and Ewarara layered basic intrusions, Giles Complex, central Australia. University of Adelaide. PhD Thesis.

Goode ADT (1976) Small scale primary cumulus igneous layering in the kalka layered intrusion, giles complex, central Australia. J Petrol 17(3): 379-397.

Goode ADT (1977) Vertical igneous layering in the Ewarara layered intrusion , central Australia. Geol Mag 114:365–374

Goode ADT, Moore AC (1975) High pressure crystallization of the Ewarara, Kalka and Gosse Pile intrusions, Giles Complex, central Australia. Contrib to Mineral Petrol 51:77–97.

Gorring ML, Naslund HR (1995) Geochemical reversals within the lower 100 m of the Palisades sill, New Jersey. Contrib to Mineral Petrol 119(2-3): 263-276.

Grieve RAF (1994) An impact model of the Sudbury structure. In: Proceedings of the Sudbury±Noril'sk Symposium. Ministry of Northern Development and Mines, Ontario. pp 119–132

Grinenko LN (1985) Hydrogen sulfide-containing gas deposits as a source of sulfur for sulfurization of magma in ore-bearing intrusives of the Noril'sk area. Int Geol Rev 27:290–292

Grobler DF, Brits JAN, Maier WD, Crossingham A (2019) Litho- and chemostratigraphy of the Flatreef PGE deposit, northern Bushveld Complex. Miner Depos 54(1): 3-28.

Grokhovskaya TL, Bakaev GF, Shelepina EP, et al (2000) PGE mineralization in the Vuruchuaivench gabbronorite massif, Monchegorsk pluton (Kola Peninsula, Russia). Geol Ore Depos 42:133–146

Grokhovskaya TL, Bakaev GF, Sholokhnev V V, et al (2003) The PGE ore mineralization in the Monchegorsk magmatic layered complex (Kola Peninsula, Russia). Geol Ore Depos 45:287–308

Groves DI, Bierlein FP (2007) Geodynamic settings of mineral deposit systems. J Geol Soc London 164:19–30

Halkoaho TAA, Alapieti TT, Lahtinen JJ (1990a) The Sompujärvi PGE Reef in the Penikat layered intrusion, northern Finland. Mineral Petrol 42:39–55

Halkoaho TAA, Alapieti TT, Lahtinen JJ, Lerssi JM (1990b) The Ala-Penikka PGE reefs in the Penikat layered intrusion, northern Finland. Mineral Petrol 42:23–38

Hammerbeck ECI (1986) Andalusite in the metamorphic aureole of the Bushveld Complex. In: Mineral Deposits of Southern Africa. pp 993–1004

Hannah, JL, Stein, HJ, Zimmerman, A, et al. (2008). Re-Os geochronology of shungite: A 2.05 Ga fossil oil field in Karelia. Geochim. Cosmochim. Acta, 72, p. A351.

Hanski E, Huhma H, Smolkin VF, Vaasjoki M (1990) The age of the ferropicritic volcanics and comagmatic Ni-bearing intrusions at Pechenga, Kola Peninsula, USSR. Bull Geol Soc Finl 62:123–133

Hanski E, Walker RJ, Huhma H, Suominen I (2001) The Os and Nd isotopic systematics of c. 2.44 Ga Akanvaara and Koitelainen mafic layered intrusions in northern Finland. Precambrian Res 109:73–102.

Hanski EJ (1992) Petrology of the Pechenga ferropicrites and cogenetic Ni-bearing gabbro-wehrlite intrusions, Kola Peninsula, Russia. Bull Surv Finl

Harney DMW, Merkle RKW, Von Gruenewaldt G (1990) Plagioclase Composition in the Upper Zone, Eastern Bushveld Complex: Support for Magma Mixing at the Main Magnetite Layer. Institute for Geological Research on the Bushveld Complex, University of Pretoria.

Harris C, Chaumba JB (2001) Crustal contamination and fluid–rock interaction during the formation of the Platreef, northern limb of the Bushveld Complex, South Africa. J Petrol 42:1321–1347

Haskjn LA, Salpas PA (1992) Genesis of compositional characteristics of Stillwater AN-I and AN-II thick anorthosite units. Geochim Cosmochim Acta 56:1187–1212

Hawkes DD (1967) Order of Abundant Crystal Nucleation in a Natural Magma. Geol Mag 104(5): 473-486.

Hayes B, Ashwal LD, Webb SJ, Bybee GM (2017) Large-scale magmatic layering in the Main Zone of the Bushveld Complex and episodic downward magma infiltration. Contrib to Mineral Petrol 172(2-3): 13.

Hepworth LN, Kaufmann FED, Hecht L, et al (2020) Braided peridotite sills and metasomatism in the Rum Layered Suite, Scotland. Contrib to Mineral Petrol 175:17

Hess HH (1939) Extreme fractional crystallization of a basaltic magma: the Stillwater igneous complex. Eos, Trans Am Geophys Union 20:420–432

Hess HH, Smith JR (1960) Stillwater igneous complex, Montana a quantitative mineralogical study. Geological Society of America Volume 80.

Higgins MD (1991) The origin of laminated and massive anorthosite, Sept Iles layered intrusion, Quebec, Canada. Contrib to Mineral Petrol 106:340–354

Higgins MD (2002) A crystal size-distribution study of the Kiglapait layered mafic intrusion, Labrador, Canada: evidence for textural coarsening. Contrib to Mineral Petrol 144:314–330

Higgins MD (2005) A new interpretation of the structure of the Sept Iles Intrusive suite, Canada. Lithos 83:199–213

Higgins MD, Van Breemen O (1998) The age of the Sept Iles layered mafic intrusion, Canada: implications for the late Neoproterozoic/Cambrian history of southeastern Canada. J Geol 106:421–432

Hill GJ, Caldwell TG, Heise W, et al (2009) Distribution of melt beneath Mount St Helens and Mount Adams inferred from magnetotelluric data. Nat Geosci 2:785–789

Himmelberg GR, Loney RA (1995) Characteristics and petrogenesis of Alaskan-type ultramafic-mafic intrusions, southeastern Alaska. US Government Printing Office

Hinchey JG, Hattori KH, Lavigne MJ (2005) Geology, petrology, and controls on PGE mineralization of the southern Roby and Twilight zones, Lac des Iles mine, Canada. Econ Geol 100:43–61

Hoatson DM, Keays RR (1989) Formation of platiniferous sulfide horizons by crystal fractionation and magma mixing in the Munni Munni layered intrusion, West Pilbara Block, Western Australia. Econ Geol 84:1775–1804

Hoatson DMDM, Blake DH (2000) Geology and economic potential of the Palaeoproterozoic layered mafic-ultramafic intrusions in the East Kimberley, Western Australia. Australian Geological Survey Organisation

Holness MB (2007) Textural immaturity of cumulates as an indicator of magma chamber processes: infiltration and crystal accumulation in the Rum Eastern Layered Intrusion. J Geol Soc London 164:529–539

Holness MB, Farr R, Neufeld JA (2017) Crystal settling and convection in the Shiant Isles Main Sill. Contrib to Mineral Petrol 172:1–25.

Holness MB, Hallworth MA, Woods A, Sides RE (2007) Infiltration metasomatism of cumulates by intrusive magma replenishment: The wavy horizon, Isle of Rum, Scotland. J Petrol 48(3): 563-587.

Holness MB, Sides R, Prior DJ, et al (2012) The peridotite plugs of Rum: Crystal settling and fabric development in magma conduits. Lithos 134: 23-40

Holness MB, Stock MJ, Geist D (2019) Magma chambers versus mush zones: constraining the architecture of sub-volcanic plumbing systems from microstructural analysis of crystalline enclaves. Philos Trans R Soc A 377:20180006

Holwell DA, Adeyemi Z, Ward LA, et al (2017) Low temperature alteration of magmatic Ni-Cu-PGE sulfides as a source for hydrothermal Ni and PGE ores: A quantitative approach using automated mineralogy. Ore Geol Rev 91:718–740.

Holwell DA, Blanks DE (2020) Emplacement of magmatic Cu-Au-Te (-Ni-PGE) sulfide blebs in alkaline mafic rocks of the Mordor Complex, Northern Territory, Australia. Miner Depos 1–15

Holwell DA, Keays RR (2014) The formation of low-volume, high-tenor magmatic PGE-Au sulfide mineralization in closed systems: evidence from precious and base metal geochemistry of the Platinova Reef, Skaergaard Intrusion, East Greenland. Econ Geol 109:387–406

Hou T, Charlier B, Holtz F, et al (2018) Immiscible hydrous Fe–Ca–P melt and the origin of iron oxide-apatite ore deposits. Nat Commun 9:1–8

Houlé MG, Lesher CM, Metsaranta R, et al (2020) Magmatic architecture of the Esker intrusive complex in the Ring of Fire intrusive suite, McFaulds Lake greenstone belt, Superior Province, Ontario: Implications for the genesis of Cr and Ni-Cu-(PGE) mineralization in an inflationary dyke-chonolith- sill complex. In Targeted Geoscience Initiative 5: Advances in the understanding of Canadian Ni-Cu-PGE and Cr ore systems – Examples from the Midcontinent Rift, the Circum-Superior Belt, the Archean Superior Province, and Cordilleran Alaskan-type intrusions, (ed.) W. Bleeker and M.G. Houlé; Geological Survey of Canada, Open File 8722, p. 141–163. https://doi.org/10.4095/326892

Huhtelin TA, Alapieti TT, Lahtinen JJ (1990) The Paasivaara PGE reef in the Penikat layered intrusion, northern Finland. Mineral Petrol 42:57–70

Huppert HE, Sparks RSJ (1981) The fluid dynamics of a basaltic magma chamber replenished by influx of hot, dense ultrabasic magma. Contrib to Mineral Petrol 75:279–289

Huthmann FM, Yudovskaya MA, Kinnaird JA, et al (2018) Geochemistry and PGE of the lower mineralized Zone of the Waterberg Project, South Africa. Ore Geol Rev 92:161–185

Ihlenfeld C, Keays RR (2011) Crustal contamination and PGE mineralization in the Platreef, Bushveld Complex, South Africa: evidence for multiple contamination events and transport of magmatic sulfides. Miner Depos 46:813–832

Iljina M, Hanski E (2005) Layered mafic intrusions of the Tornio—Näränkävaara belt. In: Developments in Precambrian geology. Elsevier, pp 101–137

Iljina M, Maier WD, Karinen T (2015) PGE-(Cu-Ni) deposits of the Tornio-Näränkävaara belt of intrusions (Portimo, Penikat, and Koillismaa). In: Mineral deposits of Finland. Elsevier, pp 133–164

Irvine NT (1980) Magmatic infiltration metasomatism, double diffusive fractional crystallization, and adcumulus growth in the Muskox intrusion and other layered intrusions. Phys Magmat Process, pp. 325-384. Princeton University Press.

Irvine TN (1976) Crystallization sequences in the Muskox intrusion and other layered intrusions—II. Origin of chromitite layers and similar deposits of other magmatic ores. In: Chromium: its Physicochemical Behavior and Petrologic Significance. Elsevier, pp 991–1020

Irvine TN (1977) Origin of chromitite layers in the Muskox intrusion and other stratiform intrusions: A new interpretation. Geology 5:273–277

Irvine TN (1987) Layering and related structures in the Duke Island and Skaergaard intrusions: similarities, differences, and origins (Alaska, USA, Greenland). In Origins of igneous layering, pp. 185-245. Springer, Dordrecht.

Irvine TN, Andersen JCØ, Brooks CK (1998) Included blocks (and blocks within blocks) in the Skaergaard intrusion: Geologic relations and the origins of rhythmic modally graded layers. Geol Soc Am Bull 110:1398–1447.

Ivanic TJ, Wingate MTD, Kirkland CL, et al (2010) Age and significance of voluminous mafic-ultramafic magmatic events in the Murchison Domain, Yilgarn Craton. Aust J Earth Sci 57:597–614.

Jackson ED (1960) Preliminary textures and mineral associations in the ultramafic zone of the Stillwater complex, Montana. US Geological Survey. (No. 60-79).

Jakobsen JK, Veksler I V, Tegner C, Brooks CK (2005) Immiscible iron-and silica-rich melts in basalt petrogenesis documented in the Skaergaard intrusion. Geology 33:885–888

James RS, Easton RM, Peck DC, Hrominchuk JL (2002) The East Bull Lake intrusive suite: Remnants of a ~ 2.48 Ga large igneous and Metallogenic Province in the Sudbury Area of the Canadian Shield. Econ Geol 97:1577–1606.

Järvinen V, Halkoaho T, Konnunaho J, et al (2020) Parental magma, magmatic stratigraphy, and reef-type PGE enrichment of the 2.44-Ga mafic-ultramafic Näränkävaara layered intrusion, Northern Finland. Miner Depos 55:1535–1560

Jesus AP, Mateus A, Munhá J, Pinto Á (2005) Intercumulus massive Ni-Cu-Co and PGE-bearing sulphides in pyroxenite: a new mineralization type in the layered gabbroic sequence of the Beja Igneous Complex (Portugal). Miner Depos Res Meet Glob Chall 405–407.

Jesus AP, Mateus A, Munhá JM, et al (2016) Evidence for underplating in the genesis of the Variscan synorogenic Beja Layered Gabbroic Sequence (Portugal) and related mesocratic rocks. Tectonophysics 683:148–171.

Jesus AP, Mateus A, Waerenborgh JC, et al (2003) Hypogene titanian, vanadian maghemite in reworked oxide cumulates in the Beja layered gabbro complex, Odivelas, southeastern Portugal. Can Mineral 41:1105–1124.

Jones JP (1976) Pegmatoidal nodules in the layered rocks of the Bafokeng leasehold area. South African J Geol 79:312–320

Jugo PJ (2009) Sulfur content at sulfide saturation in oxidized magmas. Geology 37:415–418.

Junge M, Oberthür T, Melcher F (2014) Cryptic variation of chromite chemistry, platinum group element and platinum group mineral distribution in the UG-2 chromitite: an example from the Karee Mine, western Bushveld Complex, South Africa. Econ Geol 109:795–810

Kaavera J, Imai A, Yonezu K, et al (2020) Controls on the disseminated Ni-Cu-PGE sulfide mineralization at the Tubane section, northern Molopo Farms Complex, Botswana: Implications for the formation of conduit style magmatic sulfide ores. Ore Geol Rev 126:103731

Kaavera J, Rajesh HM, Tsunogae T, Belyanin GA (2018) Marginal facies and compositional equivalents of Bushveld parental sills from the Molopo Farms Complex layered intrusion, Botswana: Petrogenetic and mineralization implications. Ore Geol Rev 92:506–528.

Karinen T (2010) The Koillismaa intrusion, northeastern Finland: evidence for PGE reef forming processes in the layered series. Geological Survey of Finland. Vol. 404.

Karykowski BT, Maier WD, Groshev NY, et al (2018a) Critical Controls on the Formation of Contact-Style PGE-Ni-Cu Mineralization: Evidence from the Paleoproterozoic Monchegorsk Complex , Kola Region , Russia. Econ Geol 2:911–935.

Karykowski BT, Maier WD, Groshev NY, et al (2018b) Origin of reef-style PGE mineralization in the paleoproterozoic Monchegorsk Complex, Kola Region, Russia. Econ Geol 113:1333–1358

Karykowski BT, Polito PA, Maier WD, et al (2017b) New insights into the petrogenesis of the Jameson Range layered intrusion and associated Fe Ti-PV-PGE-Au mineralisation, West Musgrave Province, Western Australia. Miner Depos 52:233–255

Karykowski BT, Yang SH, Maier WD, et al (2017a) In situ Sr isotope compositions of plagioclase from a complete stratigraphic profile of the Bushveld complex, South Africa: Evidence for extensive magma mixing and percolation. J Petrol 58(11): 2285-2308.

Keays RR, Campbell IA (1981) Precious metals in the Jimberlana intrusion, Western Australia: implications for the genesis of platiniferous ores in layered intrusions. Econ Geol 76:1118–1141.

Keays RR, Lightfoot PC (2010) Crustal sulfur is required to form magmatic Ni-Cu sulfide deposits: Evidence from chalcophile element signatures of Siberian and Deccan Trap basalts. Miner Depos 45:241–257.

Khatun S, Mondal SK, Zhou MF, et al (2014) Platinum-group element (PGE) geochemistry of Mesoarchean ultramafic-mafic cumulate rocks and chromitites from the Nuasahi Massif, Singhbhum Craton (India). Lithos 205:322–340.

Khedr MZ, El-Awady A, Arai S, et al (2020) Petrogenesis of the ~740 Ma Korab Kansi mafic-ultramafic intrusion, South Eastern Desert of Egypt: Evidence of Ti-rich ferropicritic magmatism. Gondwana Res 82:48–72.

Kilgour GN, Saunders KE, Blundy JD, et al (2014) Timescales of magmatic processes at Ruapehu volcano from diffusion chronometry and their comparison to monitoring data. J Volcanol Geotherm Res 288:62–75

Killick AM, Scheepers R (2005) Controls to hydrothermal gold mineralization in the Witwatersberg Goldfield; situated in the floor to the south of the Bushveld Complex, South Africa. J African Earth Sci 41:235–247

Kinnaird JA, Yudovskaya M, McCreesh M, et al (2017) The Waterberg platinum group element deposit: Atypical mineralization in mafic-ultramafic rocks of the Bushveld Complex, South Africa. Econ Geol 112(6): 1367-1394.

Kiser E, Palomeras I, Levander A, et al (2016) Magma reservoirs from the upper crust to the Moho inferred from high-resolution Vp and Vs models beneath Mount St. Helens, Washington State, USA. Geology 44:411–414

Kislov EV, Khudyakova LI (2020) Yoko–Dovyren Layered Massif: Composition, Mineralization, Overburden and Dump Rock Utilization. Minerals 10:682

Kistler RW, White LD, Ford AB (2000) Strontium and oxygen isotopic data and age for the layered gabbroic Dufek intrusion, Antarctica. US Department of the Interior, US Geological Survey

Klemm DD, Ketterer S, Reichhardt F, et al (1985) Implication of vertical and lateral compositional variations across the pyroxene marker and its associated rocks in the upper part of the main zone in the eastern Bushveld Complex. Econ Geol 80:1007–1015

Knight RD, Prichard HM, McDonald I, Ferreira Filho CF (2011) Platinum-group mineralogy of the Fazenda Mirabela intrusion, Brazil: the role of high temperature liquids and sulphur loss. Appl Earth Sci 120:211–224

Kogarko L (2018) Chemical composition and petrogenetic implications of apatite in the Khibiny apatite-nepheline deposits (Kola Peninsula). Minerals 8:532

Kogarko LN, Khapaev V V. (1986) The modelling of formation of apatite deposits of the Knibina massif (Kola Peninsula, USSR). In Origins of igneous layering, pp. 589-611. Springer, Dordrecht, 1987.

Kruger FJ (1994) The Sr-isotopic stratigraphy of the western Bushveld Complex. South African J Geol 97:393–398

Kruger W, Latypov R (2020) Fossilized solidifications from in the Bushveld Complex argues for liquid-dominated magmatic systems. Nat Commun 11:1–11

Langford RL, Ivanic TJ, Arculus RJ, Wills KJA (2020) Ti–V magnetite stratigraphy of the Upper Zone of the Windimurra Igneous Complex, Western Australia. Ore Geol Rev 103922

Langworthy AP, Black LP (1978) The Mordor Complex: A highly differentiated potassic intrusion with kimberlitic affinities in central Australia. Contrib to Mineral Petrol 67:51–62.

Latypov R, Chistyakova S, Barnes SJ, Hunt EJ (2017) Origin of Platinum Deposits in Layered Intrusions by In Situ Crystallization: Evidence from Undercutting Merensky Reef of the Bushveld Complex. J Petrol 58:715–762.

Latypov R, Chistyakova S, Page A, Hornsey R (2015) Field evidence for the in situ crystallization of the Merensky Reef. J Petrol 56:2341–2372

Latypov R, Costin G, Chistyakova S, et al (2018) Platinum-bearing chromite layers are caused by pressure reduction during magma ascent. Nat Commun 9:1–7

Latypov R, O'Driscoll B, Lavrenchuk A (2013) Towards a model for the in situ origin of PGE reefs in layered intrusions: insights from chromitite seams of the Rum Eastern Layered Intrusion, Scotland. Contrib to Mineral Petrol 166:309–327

Latypov RM (2003) The origin of basic–ultrabasic sills with S-, D-, and I-shaped compositional profiles by in situ crystallization of a single input of phenocryst-poor parental magma. J Petrol 44:1619–1656

Le Vaillant M, Barnes SJ, Mole DR, et al (2020) Multidisciplinary study of a complex magmatic system: The Savannah Ni-Cu-Co Camp, Western Australia. Ore Geol Rev 117:103292

Le Vaillant M, Barnes SJ, Mungall JE, Mungall EL (2017) Role of degassing of the Noril'sk nickel deposits in the Permian–Triassic mass extinction event. Proc Natl Acad Sci 114:2485–2490

Lee CA, Butcher AR (1990) Cyclicity in the Sr isotope stratigraphy through the Merensky and Bastard Reef units, Atok section, eastern Bushveld Complex. Econ Geol 85:877–883

Leelanandam C (1997) The Kondapalli layered complex, Andhra Pradesh, India: A synoptic overview. Gondwana Res 1:95–114.

Lesher CM, Thurston PC (2002) A special issue devoted to the mineral deposits of the Sudbury basin. Econ Geol 97:1373–1375

Li C, Lightfoot PC, Amelin Y, Naldrett AJ (2000) Contrasting petrological and geochemical relationships in the Voisey's Bay and Mushuau intrusions, Labrador, Canada: Implications for ore genesis. Econ Geol 95:771–799.

Li C, Naldrett AJ (1999) Geology and petrology of the Voisey's Bay intrusion: reaction of olivine with sulfide and silicate liquids. Lithos 47:1–31

Li C, Ripley EM (2005) Empirical equations to predict the sulfur content of mafic magmas at sulfide saturation and applications to magmatic sulfide deposits. Miner Depos 40:218–230.

Li C, Ripley EM, Maier WD, Gomwe TES (2002) Olivine and sulfur isotopic compositions of the Uitkomst Ni–Cu sulfide ore-bearing complex, South Africa: evidence for sulfur contamination and multiple magma emplacements. Chem Geol 188:149–159

Li C, Zhang M, Fu P, et al (2012) The Kalatongke magmatic Ni–Cu deposits in the Central Asian Orogenic Belt, NW China: product of slab window magmatism? Miner Depos 47:51–67

Lightfoot PC (2016) Nickel sulfide ores and impact melts: Origin of the Sudbury Igneous Complex. Elsevier

Lindsay JJ, Hughes HSR, Yeomans CM, et al (2021) A machine learning approach for regional geochemical data: Platinum-group element geochemistry vs geodynamic settings of the North Atlantic Igneous Province. Geosci Front 12:101098

Lindstrom DJ (1976) Experimental study of the partitioning of the transition metals between clinopyroxene and coexisting silicate liquids. University of Oregon. PhD Thesis.

Lipin BR (1993) Pressure increases, the formation of chromite seams, and the development of the ultramafic series in the Stillwater Complex, Montana. J Petrol 34:955–976

Lissenberg CJ, MacLeod CJ, Bennett EN (2019) Consequences of a crystal mush-dominated magma plumbing system: a mid-ocean ridge perspective. Philos Trans R Soc A 377:20180014

Litherland M, Annells RN, Llanos A, et al (1986) The geology and mineral resources of the Bolivian Precambrian shield. Overseas Mem-Br. Geol. Surv., 99. pp. 153.

Liu P-P, Zhou M-F, Ren Z, et al (2016) Immiscible Fe-and Si-rich silicate melts in plagioclase from the Baima mafic intrusion (SW China): Implications for the origin of bi-modal igneous suites in large igneous provinces. J Asian Earth Sci 127:211–230

Loney RA, Himmelberg GR (1992) Petrogenesis of the Pd-rich intrusion at Salt Chuck, Prince of Wales Island; an early Paleozoic alaskan-type ultramafic body. Can Mineral 30:1005–1022

Loomis TP (1983) Compositional zoning of crystals: a record of growth and reaction history. In: Kinetics and Equilibrium in Mineral Reactions. Springer, pp 1–60

Luan Y, Song XY, Chen LM, et al (2014) Key factors controlling the accumulation of the Fe-Ti oxides in the Hongge layered intrusion in the Emeishan large igneous province, SW China. Ore Geol Rev 57:518–538.

Lubnina NV, Stepanova AV, Ernst RE, et al (2016) New U–Pb baddeleyite age, and AMS aLubnina NV, Stepanova AV, Ernst RE, et al (2016) New U–Pb baddeleyite age, and AMS and paleomagnetic data for dolerites in the Lake Onega region belonging to the 1.98–1.95 Ga regional Pechenga–Onega Large Igneous Provinc. GFF 138:54–78

Luolavirta K, Hanski E, Maier W, Santaguida F (2018) Whole-rock and mineral compositional constraints on the magmatic evolution of the Ni-Cu-(PGE) sulfide ore-bearing Kevitsa intrusion, northern Finland. Lithos 296–299:37–53.

Maes SM, Tikoff B, Ferré EC, et al (2007) The Sonju Lake layered intrusion, northeast Minnesota: Internal structure and emplacement history inferred from magnetic fabrics. Precambrian Res 157:269–288

Magee C, Stevenson CTE, Ebmeier SK, et al (2018) Magma plumbing systems: a geophysical perspective. J Petrol 59:1217–1251

Maier RP (2021) Characterisation of Fe-Ti-V mineralisation at Lac Fabien, Quebec and comparison to anorthosite-hosted Fe-Ti-V deposits

Maier WD (2005) Platinum-group element (PGE) deposits and occurrences: Mineralization styles, genetic concepts, and exploration criteria. J African Earth Sci 41:165–191.

Maier WD, Andreoli MAG, Groves DI, Barnes S-J (2012) Petrogenesis of Cu-Ni sulphide ores from O'okiep and Kliprand, Namaqualand, South Africa: constraints from chalcophile metal contents. South African J Geol 115:499–514

Maier WD, Arndt NT, Curl EA (2000) Progressive crustal contamination of the Bushveld Complex: evidence from Nd isotopic analyses of the cumulate rocks. Contrib to Mineral Petrol 140:316–327

Maier WD, Barnes S-J (1998) Concentrations of rare earth elements in silicate rocks of the Lower, Critical and Main Zones of the Bushveld Complex. Chem Geol 150:85–103

Maier WD, Barnes S-J (2004) Pt/Pd and Pd/Ir ratios in mantle-derived magmas: a possible role for mantle metasomatism. South African J Geol 107:333–340

Maier WD, Barnes S-J (2010) The Kabanga Ni sulfide deposits, Tanzania: II. Chalcophile and siderophile element geochemistry. Miner Depos 45:443–460

Maier WD, Barnes S-J, Bandyayera D, et al (2008) Early Kibaran rift-related mafic–ultramafic magmatism in western Tanzania and Burundi: Petrogenesis and ore potential of the Kapalagulu and Musongati layered intrusions. Lithos 101:24–53

Maier WD, Barnes SJ, Gartz V, Andrews G (2003a) Pt-Pd reefs in magnetitites of the Stella layered intrusion, South Africa: A world of new exploration opportunities for platinum group elements. Geology 31:885–888.

Maier WD, Barnes S-J, Groves DI (2013a) The Bushveld Complex, South Africa: formation of platinum–palladium, chrome-and vanadium-rich layers via hydrodynamic sorting of a mobilized cumulate slurry in a large, relatively slowly cooling, subsiding magma chamber. Miner Depos 48:1–56

Maier WD, Barnes S-J, Karykowski BT (2016a) A chilled margin of komatiite and Mg-rich basaltic andesite in the western Bushveld Complex, South Africa. Contrib to Mineral Petrol 171:57

Maier WD, Barnes S-J, Muir D, et al (2021) Formation of Bushveld anorthosite by reactive porous flow. Contrib to Mineral Petrol 176:1–12

Maier WD, Barnes S-J, Peltet T (1996) The economic significance of the Bell River complex, Abitibi subprovince, Quebec. Can J Earth Sci 33:967–980

Maier WD, Barnes S-J, Sarkar A, et al (2010) The Kabanga Ni sulfide deposit, Tanzania: I. Geology, petrography, silicate rock geochemistry, and sulfur and oxygen isotopes. Miner Depos 45:419–441

Maier WD, Groves DI (2011) Temporal and spatial controls on the formation of magmatic PGE and Ni-Cu deposits. Miner Depos 46:841–857.

Maier WD, Halkoaho T, Huhma H, et al (2018b) The Penikat intrusion, Finland: geochemistry, geochronology, and origin of platinum–palladium reefs. J Petrol 59:967–1006

Maier WD, Hanski EJ (2017) Layered mafic-ultramafic intrusions of Fennoscandia: Europe's treasure chest of magmatic metal deposits. Elements 13:415–420.

Maier WD, Howard HM, Smithies RH, et al (2015c) Magmatic ore deposits in mafic-ultramafic intrusions of the Giles Event, Western Australia. Ore Geol Rev 71:405–436.

Maier WD, Määttää S, Yang S, et al (2015a) Composition of the ultramafic–mafic contact interval of the Great Dyke of Zimbabwe at Ngezi mine: Comparisons to the Bushveld Complex and implications for the origin of the PGE reefs. Lithos 238:207–222

Maier WD, Peltonen P, Grantham G, Mänttäri I (2003b) A new 1.9 Ga age for the Trompsburg intrusion, South Africa. Earth Planet Sci Lett 212:351–360.

Maier WD, Prevec SA, Scoates JS, et al (2018a) The Uitkomst intrusion and Nkomati Ni-Cu-Cr-PGE deposit, South Africa: trace element geochemistry, Nd isotopes and high-precision geochronology. Miner Depos 53:67–88

Maier WD, Rasmussen B, Fletcher IR, et al (2013b) The Kunene anorthosite complex, Namibia, and its satellite intrusions: Geochemistry, geochronology, and economic potential. Econ Geol 108:953–986.

Maier WD, Rasmussen B, Fletcher IR, et al (2015b) Petrogenesis of the ~2.77 Ga Monts de Cristal complex, Gabon: Evidence for direct precipitation of Pt-arsenides from basaltic magma. J Petrol 56:285–1308.

Maier WD, Smithies RH, Spaggiari C V., et al (2016b) Petrogenesis and Ni-Cu sulphide potential of mafic-ultramafic rocks in the Mesoproterozoic Fraser Zone within the Albany-Fraser Orogen, Western Australia. Precambrian Res 281:27–46.

Mäkisalo A (2019) Geological characterization of anorthositic rocks in the Otanmäki intrusion, central Finland: constraints on magma evolution and Fe-Ti-V oxide ore genesis MSc thesis, University of Oulu, Finland

Makkonen H V. (2015) Nickel Deposits of the 1.88 Ga Kotalahti and Vammala Belts. Elsevier Inc.

Malitch KN, Belousova EA, Griffin WL, et al (2010) Magmatic evolution of the ultramafic-mafic Kharaelakh intrusion (Siberian Craton, Russia): Insights from trace-element, U-Pb and Hf-isotope data on zircon. Contrib to Mineral Petrol 159:753–768.

Mansur ET, Ferreira Filho CF (2016) Magmatic structure and geochemistry of the Luanga Mafic–Ultramafic Complex: Further constraints for the PGE-mineralized magmatism in Carajás, Brazil. Lithos 266:28–43

Mansur ET, Ferreira Filho CF, Oliveira DPL (2020) The Luanga deposit, Carajás Mineral Province, Brazil: Different styles of PGE mineralization hosted in a medium-size layered intrusion. Ore Geol Rev 118:103340

Manyeruke TD, Maier WD, Barnes S-J (2005) Major and trace element geochemistry of the Platreef on the farm Townlands, northern Bushveld Complex. South African J Geol 108:381–396

Mao Y-J, Dash B, Qin K-Z, et al (2018) Comparisons among the Oortsog, Dulaan, and Nomgon mafic-ultramafic intrusions in central Mongolia and Ni-Cu deposits in NW China: implications for economic Ni-Cu-PGE ore exploration in central Mongolia. Russ Geol Geophys 59:1–18

Mao Y-J, Qin K-Z, Li C, et al (2014) Petrogenesis and ore genesis of the Permian Huangshanxi sulfide ore-bearing mafic-ultramafic intrusion in the Central Asian Orogenic Belt, western China. Lithos 200:111–125

Mao Y-J, Qin K-Z, Tang D-M, et al (2016) Crustal contamination and sulfide immiscibility history of the Permian Huangshannan magmatic Ni-Cu sulfide deposit, East Tianshan, NW China. J Asian Earth Sci 129:22–37

Maré LP, Cole J (2006) The Trompsburg complex, South Africa: A preliminary three dimensional model. J African Earth Sci 44:314–330

Marks M, Markl G (2001) Fractionation and assimilation processes in the alkaline augite syenite unit of the Ilimaussaq Intrusion, South Greenland, as deduced from phase equilibria. J Petrol 42:1947–1969

Marks MAW, Hettmann K, Schilling J, et al (2011) The mineralogical diversity of alkaline igneous rocks: critical factors for the transition from miaskitic to agpaitic phase assemblages. J Petrol 52:439–455

Marks MAW, Markl G (2015) The ilímaussaq alkaline complex, South Greenland. In: Layered Intrusions. Springer, pp 649–691

Marques JC, Dias JRP, Friedrich BM, et al (2017) Thick chromitite of the Jacurici Complex (NE Craton São Francisco, Brazil): Cumulate chromite slurry in a conduit. Ore Geol Rev 90:131–147

Marsh BD (1996) Solidification fronts and magmatic evolution. Mineral Mag 60:5–40

Marsh BD (2006) Dynamics of magmatic systems. Elements 2:287–292

Marsh BD (2013) On some fundamentals of igneous petrology. Contrib to Mineral Petrol 166:665–690

Marsh JS, Pasecznyk MJ, Boudreau AE (2021) Formation of chromitite seams and associated anorthosites in layered intrusion by reactive volatile-rich fluid infiltration. J Petrol 1-23

Mathez EA (1995) Magmatic metasomatism and formation of the Merensky reef, Bushveld Complex. Contrib to Mineral Petrol 119:277–286

Mathez EA, Kinzler RJ (2017) Metasomatic chromitite seams in the bushveld and rum layered intrusions. In: Elements. pp 397–402

Mathieu L (2019) Origin of the Variegated Serpentine–Magnetite Rocks of the Mt. Sorcerer Area, Lac Doré Layered Intrusion, Chibougamau, Québec. Geosciences 9:110

Mavrogenes JA, O'Neill HSC (1999) The relative effects of pressure, temperature and oxygen fugacity on the solubility of sulfide in mafic magmas. Geochim Cosmochim Acta 63:1173–1180.

McBirney AR (1987) Constitutional zone refining of layered intrusions. In: Origins of igneous layering. Springer, pp 437–452

McBirney AR (1996) The Skaergaard intrusion. In: Developments in Petrology. Elsevier, pp 147–180

McBirney AR, Nakamura Y (1974) Immiscibility in late-stage magmas of the Skaergaard intrusion. Carnegie Inst Washingt Yearb 73:348–352

McBirney AR, Noyes RM (1979) Crystallization and layering of the Skaergaard intrusion. J Petrol 20:487–554

McBirney AR, White CM, Boudreau AE (1990) Spontaneous development of concentric layering in a solidified siliceous dike, East Greenland. Earth-Science Rev 29:321–330

McCallum IS (1996) The stillwater complex. In Developments in petrology Vol. 15, pp. 441-483. Elsevier.

McDonald I, Holwell DA (2011) Geology of the northern Bushveld Complex and the setting and genesis of the Platreef Ni-Cu-PGE deposit. Rev Econ Geol 297–327

McEnroe SA, Skilbrei JR, Robinson P, et al (2004) Magnetic anomalies, layered intrusions and Mars. Geophys Res Lett 31:31–34.

McNaughton NJ, Pollard PJ, Groves DI, Taylor RG (1993) A long-lived hydrothermal system in Bushveld granites at the Zaaiplaats tin mine; lead isotope evidence. Econ Geol 88:27–43

Melezhik VA, Huhma H, Condon DJ, et al (2007) Temporal constraints on the Paleoproterozoic Lomagundi-Jatuli carbon isotopic event. Geology 35:655–658

Mikoshiba MU, Takahashi Y, Takahashi Y, et al (1999) Rb-Sr isotopic study of the Chilas Igneous Complex ,

Miller Jr J, Loucks RR, Ashraf M (1991) Platinum-group element mineralization in the Jijal layered ultramafic-mafic complex, Pakistani Himalayas. Econ Geol 86:1093–1102

Miller Jr JD, Ripley EM (1996) Layered intrusions of the Duluth complex, Minnesota, USA. In Developments in petrology. Vol. 15, pp. 257–301. Elsevier.

Mitchell AA, Scoon RN (2007) The Merensky Reef at Winnaarshoek, Eastern Bushveld Complex: a primary magmatic hypothesis based on a wide reef facies. Econ Geol 102:971–1009

Mohanty JK, Paul AK (2008) Fe-Ti-oxide ore of the Mesoarchean Nuasahi ultramafic-mafic complex, Orissa and its utilization potential. Jour Geol Soc India 72:623–633

Molyneux TG (1974) A geological investigation of the Bushveld Complex in Sekhukhuneland and part of the Steelpoort valley. South African J Geol 77:329–338

Mondal SK, Mathez EA (2007) Origin of the UG2 chromitite layer, Bushveld Complex. J Petrol 48:495–510

Mondal SK, Zhou MF (2010) Enrichment of PGE through interaction of evolved boninitic magmas with early formed cumulates in a gabbro-breccia zone of the Mesoarchean Nuasahi massif (eastern India). Miner Depos 45:69–91.

Monjoie P, Bussy F, Lapierre H, Pfeifer H-R (2005) Modeling of in-situ crystallization processes in the Permian mafic layered intrusion of Mont Collon (Dent Blanche nappe, western Alps). Lithos 83:317–346

Moore AC (1973) Studies of igneous and tectonic textures and layering in the rocks of the Gosse Pile intrusion, Central Australia. J Petrol 14:49–79

Morgan DJ, Blake S, Rogers NW, et al (2004) Time scales of crystal residence and magma chamber volume from modelling of diffusion profiles in phenocrysts: Vesuvius 1944. Earth Planet Sci Lett 222:933–946

Morse SA (1969) The Kiglapait layered intrusion, Labrador. Vol. 112. Geological Society of America

Morse SA (2015) Kiglapait Intrusion, Labrador. In: Layered Intrusions. Springer, pp 589–648

Mouri H, Maier WD, Brandl G (2013) On the possible occurrence of komatiites in the archaean high-grade polymetamorphic central zone of the Limpopo Belt, South Africa. South African J Geol 116:55–66

Mudd GM, Jowitt SM, Werner TT (2018) Global platinum group element resources, reserves and mining–a critical assessment. Sci Total Environ 622:614–625

Mungall J, Brenan J (2014) Partitioning of platinum-group elements and Au between sulfide liquid and basalt and the origins of mantle-crust fractionation of the chalcophile elements. Geochim Cosmochim Acta 125:265–289.

Mungall JE, Brenan JM, Godel B, et al (2015) Transport of metals and sulphur in magmas by flotation of sulphide melt on vapour bubbles. Nat Geosci 8:216–219

Mungall JE, Christopher Jenkins M, Robb SJ, et al (2020) Upgrading of Magmatic Sulfides, Revisited. Econ Geol 115:1827–1833.

Mungall JE, Harvey JD, Balch SJ, et al (2010) Eagle's nest: A magmatic Ni-sulfide deposit in the James Bay Lowlands, Ontario, Canada. Soc Econ Geol 15:539–557

Mungall JE, Kamo SL, McQuade S (2016) U–Pb geochronology documents out-of-sequence emplacement of ultramafic layers in the Bushveld Igneous Complex of South Africa. Nat Commun 7:1–13

Mungall JE, Naldrett AJ (2008) Ore deposits of the platinum-group elements. Elements 4:253–258

Munoz Taborda CM (2010) Distribution of platinum-group elements in the Ebay claim, central part of the Bell River Complex, Matagami, Quebec. Université du Québec à Chicoutimi

Mutanen T, Huhma H (2001) U-Pb geochronology of the Koitelainen, Akanvaara and Keivitsa layered intrusions and related rocks. Spec Pap Geol Surv Finl 229–246

Mutele L, Billay A, Hunt JP (2017) Knowledge-driven prospectivity mapping for granite-related polymetallic Sn–F–(REE) mineralization, Bushveld Igneous Complex, South Africa. Nat Resour Res 26:535–552

Naldrett AJ (2004) Magmatic sulfide deposits: Geology, geochemistry and exploration. Springer Science & Business Media

Naldrett AJ, Asif M, Krstic S, Li C (2000) The Composition of Mineralization at the Voisey's Bay Ni-Cu Sulfide Deposit, with Special Reference to Platinum-Group Elements. Econ Geol 95:845–865

Naldrett AJ, Lightfoot PC, Fedorenko V, et al (1992) Geology and geochemistry of intrusions and flood basalts of the Noril'sk region, USSR, with implications for the origin of the Ni-Cu ores. Econ Geol 87:975–1004

Naldrett AJ, Wilson A, Kinnaird J, Chunnett G (2009) PGE tenor and metal ratios within and below the Merensky Reef, Bushveld Complex: implications for its genesis. J Petrol 50:625–659

Naldrett AJ, Wilson A, Kinnaird J, et al (2012) The origin of chromitites and related PGE mineralization in the Bushveld Complex: new mineralogical and petrological constraints. Miner Depos 47:209–232

Namur O, Abily B, Boudreau AE, et al (2015) Igneous layering in basaltic magma chambers. In: Layered intrusions. Springer, pp 75–152

Namur O, Charlier B (2012) Efficiency of compaction and compositional convection during mafic crystal mush solidification: the Sept Iles layered intrusion, Canada. Contrib to Mineral Petrol 163:1049–1068

Namur O, Charlier B, Holness MB (2012) Dual origin of Fe-Ti-P gabbros by immiscibility and fractional crystallization of evolved tholeiitic basalts in the Sept Iles layered intrusion. Lithos 154: 100-114.

Namur O, Charlier B, Toplis MJ, et al (2011) Differentiation of tholeiitic basalt to A - type granite in the Sept Iles layered intrusion, Canada. J Petrol 52(3): 487-539.

Naslund HR (1986) Disequilibrium partial melting and rheomorphic layer formation in the contact aureole of the Basistoppen sill, East Greenland. Contrib to Mineral Petrol 93(3): 350-367.

Naslund HR, McBirney AR (1996) Mechanisms of formation of igneous layering. In: Developments in petrology. Elsevier, pp 1–43

Naslund HR, Turner PA, Keith DW (1991) Crystallization and layer formation in the middle zone of the Skaergaard Intrusion. Bull Geol Soc Denmark 38

Nicholson DM, Mathez EA (1991) Petrogenesis of the Merensky Reef in the Rustenburg section of the Bushveld Complex. Contrib to Mineral Petrol 107(3): 293-309.

Nielsen TFD, Andersen JCØ, Holness MB, et al (2015) The Skaergaard PGE and gold deposit: the result of in situ fractionation, sulphide saturation, and magma chamber-scale precious metal redistribution by immiscible Fe-rich melt. J Petrol 56:1643–1676

O'Driscoll B, Donaldson CH, Daly JS, Emeleus CH (2009) The roles of melt infiltration and cumulate assimilation in the formation of anorthosite and a Cr-spinel seam in the Rum Eastern Layered Intrusion, NW Scotland. Lithos 111:6–20.

O'Driscoll B, Emeleus CH, Donaldson CH, et al (2010) Cr-spinel seam petrogenesis in the Rum Layered Suite, NW Scotland: cumulate assimilation and in situ crystallization in a deforming crystal mush. J Petrol 51:1171–1201.

O'Driscoll B, González-Jiménez JM (2016) Petrogenesis of the platinum-group minerals. Rev Mineral Geochemistry 81:489–578

O'Hara MJ (1998) Volcanic plumbing and the space problem—thermal and geochemical consequences of large-scale assimilation in ocean island development. J Petrol 39:1077–1089

Oberthür T, Junge M, Rudashevsky N, et al (2016) Platinum-group minerals in the LG and MG chromitites of the eastern Bushveld Complex, South Africa. Miner Depos 51:71–87

Oosterhuis WR (1998) Andalusite, sillimanite and kyanite. The mineral resources of South Africa 16:53-58

Orsoev DA (2019) Anorthosites of the Low-sulfide Platiniferous Horizon (Reef I) in the Upper Riphean Yoko–Dovyren Massif (Northern Cisbaikalia): New Data on the Composition, PGE–Cu–Ni Mineralization, Fluid Regime, and Formation Conditions. Geol Ore Depos 61:306–332

Osborn EF (1980) On the cause of the reversal of the normal fractionation trend; an addendum to the paper by EN Cameron," Evolution of the Lower Critical Zone, central sector, eastern Bushveld Complex, and its chromite deposits". Econ Geol 75:872–875

Owen-Smith TM, Ashwal LD (2015) Evidence for multiple pulses of crystal-bearing magma during emplacement of the Doros layered intrusion, Namibia. Lithos 238:120–139

Pang K-N, Li C, Zhou M-F, Ripley EM (2008) Abundant Fe–Ti oxide inclusions in olivine from the Panzhihua and Hongge layered intrusions, SW China: evidence for early saturation of Fe–Ti oxides in ferrobasaltic magma. Contrib to Mineral Petrol 156:307–321

Pang K-N, Li C, Zhou M-F, Ripley EM (2009) Mineral compositional constraints on petrogenesis and oxide ore genesis of the late Permian Panzhihua layered gabbroic intrusion, SW China. Lithos 110:199–214

Pang K-N, Zhou M-F, Lindsley D, et al (2008) Origin of Fe–Ti oxide ores in mafic intrusions: evidence from the Panzhihua intrusion, SW China. J Petrol 49:295–313

Parsons I, Becker SM (1987) Layering, compaction and post-magmatic processes in the Klokken intrusion. In: Origins of igneous layering. Springer, pp 29–92

Parsons I, Becker SM (1987) Layering, compaction and post-magmatic processes in the Klokken intrusion. In: Origins of igneous layering. Springer, pp 29–92

Paulick H, Rosa D, Kalvig P (2015) Rare Earth Element projects and exploration potential in Greenland. eds JK Keiding P Kalvig, MiMa Rapp 2:

Pearson DG, Irvine GJ, Ionov DA, et al (2004) Re–Os isotope systematics and platinum group element fractionation during mantle melt extraction: a study of massif and xenolith peridotite suites. Chem Geol 208:29–59

Peltonen P (1995) Petrogenesis of ultramafic rocks in the Vammala Nickel Belt: implications for crustal evolution of the early Proterozoic Svecofennian arc terrane. Lithos 34:253–274

Pfaff K, Krumrei T, Marks M, et al (2008) Chemical and physical evolution of the 'lower layered sequence' from the nepheline syenitic Ilímaussaq intrusion, South Greenland: Implications for the origin of magmatic layering in peralkaline felsic liquids. Lithos 106:280–296

Philpotts AR (1967) Origin of certain iron-titanium oxide and apatite rocks. Econ Geol 62:303–315

Pimentel MM, Ferreira Filho CF, Armstrong RA (2004) SHRIMP U–Pb and Sm–Nd ages of the Niquelândia layered complex: Meso-(1.25 Ga) and Neoproterozoic (0.79 Ga) extensional events in central Brazil. Precambrian Res 132:133–153

Piña R, Lunar R, Ortega L, et al (2006) Petrology and geochemistry of mafic-ultramafic fragments from the Aguablanca Ni-Cu ore breccia, southwest Spain. Econ Geol 101:865–881

Piña R, Romeo I, Ortega L, et al (2010) Origin and emplacement of the Aguablanca magmatic Ni-Cu-(PGE) sulfide deposit, SW Iberia: A multidisciplinary approach. Bull Geol Soc Am 122:915–925.

Pinto VM, Koester E, Debruyne D, et al (2020) Petrogenesis of the mafic-ultramafic Canindé layered intrusion, Sergipano Belt, Brazil: constraints on the metallogenesis of the associated Fe–Ti oxide ores. Ore Geol Rev 103535

Pirajno F, Hoatson DM (2012) A review of Australia's Large Igneous Provinces and associated mineral systems: Implications for mantle dynamics through geological time. Ore Geol Rev 48:2–54

Pivko D (2004) World's quarries of commercial granites-localization and geology. In: Proceedings of the international conference in dimension stone, Prague. pp 147–152

Podmore F, Wilson AH (1987) A reappraisal of the structure, geology and emplacement of the Great Dyke, Zimbabwe. In: Mafic dyke swarms. Geological Association of Canada Special Paper 34, pp 317–330

Prendergast MD (1991) The Wedza–Mimosa platinum deposit, Great Dyke, Zimbabwe: layering and stratiform PGE mineralization in a narrow mafic magma chamber. Geol Mag 128:235–249

Prendergast MD (2000) Layering and precious metals mineralization in the; Rincón del Tigre Complex, Eastern Bolivia. Econ Geol 95:113–130

Prendergast MD (2012) The molopo farms complex, southern botswana - A reconsideration of structure, evolution, and the bushveld connection. South African J Geol 115:77–90.

Prendergast MD (2021) Variant Offset-Type Platinum Group Element Reef Mineralization in Basal Olivine Cumulates of the Kapalagulu Intrusion, Western Tanzania. Econ Geol

Prendergast MD, Keays RR (1989) Controls of platinum-group element mineralization and the origin of the PGE-rich Main Sulphide Zone in the Wedza Subchamber of the Great Dyke, Zimbabwe: implications for the genesis of, and exploration for, stratiform PGE mineralization in layered intrusi. In: Magmatic sulphides field conference, Zimbabwe. 5. pp 43–69

Pringle IC (1986) The Zwartkloof fluorite deposits, Warmbaths district. In: Mineral Deposits of southern Africa. pp 1343–1349

Pripachkin P, Rundkvist T, Groshev N, et al (2020) Archean Rocks of the Diorite Window Block in the Southern Framing of the Monchegorsk (2.5 Ga) Layered Mafic-Ultramafic Complex (Kola Peninsula, Russia). Minerals 10:848

Puchkov V, Ernst RE, Hamilton MA, et al (2016) A Devonian> 2000-km-long dolerite dyke swarm-belt and associated basalts along the Urals-Novozemelian fold-belt: part of an East-European (Baltica) LIP tracing the Tuzo Superswell. GFF 138:6–16:459–481

Rajesh HM, Chisonga BC, Shindo K, et al (2013) Petrographic, geochemical and SHRIMP U–Pb titanite age characterization of the Thabazimbi mafic sills: Extended time frame and a unifying petrogenetic model for the Bushveld Large Igneous Province. Precambrian Res 230:79–102

Reid DL, Basson IJ (2002) Iron-rich ultramafic pegmatite replacement bodies within the upper critical zone, Rustenburg layered suite, Northam platinum mine, South Africa. Mineral Mag 66:895–914

Reynolds IM (1985) The nature and origin of titaniferous magnetite-rich layers in the upper zone of the Bushveld Complex; a review and synthesis. Econ Geol 80:1089–1108

Rhodes RC (1975) New evidence for impact origin of the Bushveld Complex, South Africa. Geology 3:549–554

Richardson SH, Shirey SB (2008) Continental mantle signature of Bushveld magmas and coeval diamonds. Nature 453:910–913

Ripley EM, Li C (2003) Sulfur isotope exchange and metal enrichment in the formation of magmatic Cu-Ni-(PGE) deposits. Econ Geol. 98(3). 635-641.

Ripley EM, Li C (2013) Sulphide Saturation in Mafic Magmas: Is External Sulfur Required for Magmatic Ni-Cu-(PGE) Ore Genesis? Econ Geol 108:45–58

Ripley EM, Li C, Shin D (2002) Paragneiss Assimilation in the Genesis of Magmatic Ni-Cu-Co Sulfide Mineralization at Voisey's Bay, Labrador: δ34S, δ13C, and Se/S Evidence. Econ Geol 97:1307–1318

Ripley EM, Wernette BW, Ayre A, et al (2017) Multiple S isotope studies of the Stillwater Complex and country rocks: An assessment of the role of crustal S in the origin of PGE enrichment found in the JM Reef and related rocks. Geochim Cosmochim Acta 214:226–245

Robertson JC, Barnes SJ, Le Vaillant M (2015) Dynamics of magmatic sulphide droplets during transport in silicate melts and implications for magmatic sulphide ore formation. J Petrol 56:2445–2472

Rousell DH, Fedorowich JS, Dressler BO (2003) Sudbury Breccia (Canada): a product of the 1850 Ma Sudbury Event and host to footwall Cu–Ni–PGE deposits. Earth-Science Rev 60:147–174

Ryder G (1984) Oxidation and layering in the Stillwater intrusion. In: Geologist Society of America Conference Abstract. p 642

Sá JHS, Barnes S-J, Prichard HM, Fisher PC (2005) The distribution of base metals and platinum-group elements in magnetitite and its host rocks in the Rio Jacaré Intrusion, Northeastern Brazil. Econ Geol 100:333–348

Sappin AA, Constantin M, Clark T (2011) Origin of magmatic sulfides in a Proterozoic island arc-an example from the Portneuf-Mauricie Domain, Grenville Province, Canada. Miner Depos 46:211–237.

Sappin A-A, Constantin M, Clark T, van Breemen O (2009) Geochemistry, geochronology, and geodynamic setting of Ni–Cu±PGE mineral prospects hosted by mafic and ultramafic intrusions in the Portneuf–Mauricie Domain, Grenville Province, Quebec. Can J Earth Sci 46:331–353.

Savelieva GN, Sharaskin AY, Saveliev AA, et al (1997) Ophiolites of the southern Uralides adjacent to the East European continental margin. Tectonophysics 276:117–137

Schiffries CM (1982) The petrogenesis of a platiniferous dunite pipe in the Bushveld Complex; infiltration metasomatism by a chloride solution. Econ Geol 77:1439–1453

Schönenberger J, Köhler J, Markl G (2008) REE systematics of fluorides, calcite and siderite in peralkaline plutonic rocks from the Gardar Province, South Greenland. Chem Geol 247:16–35

Schoneveld L, Barnes SJ, Godel B, et al (2020) Oxide-sulfide-melt-bubble interactions in spinel-rich taxitic rocks of the Norilsk-Talnakh intrusions, polar Siberia. Econ Geol 115:1305–1320

Scoates JS, Lindsley DH, Frost BR (2010) Magmatic and structural evolution of an anorthositic magma chamber: the Poe Mountain intrusion, Laramie anorthosite complex, Wyoming. Can Mineral 48:851–885

Scoates JS, Wall CJ, Friedman RM, et al (2021) Dating the Bushveld Complex: Timing of Crystallization, Duration of Magmatism, and Cooling of the World's Largest Layered Intrusion and Related Rocks. J Petrol

Scoon RN, Costin G (2018) Chemistry, morphology and origin of magmatic-reaction chromite stringers associated with anorthosite in the Upper Critical Zone at Winnaarshoek, Eastern Limb of the Bushveld Complex. J Petrol 59:1551–1578

Scoon RN, Mitchell AA (1994) Discordant iron-rich ultramafic pegmatites in the Bushveld Complex and their relationship to iron-rich intercumulus and residual liquids. J Petrol 35:881–917

Scoon RN, Mitchell AA (2004) The platiniferous dunite pipes in the eastern limb of the Bushveld Complex: review and comparison with unmineralized discordant ultramafic bodies. South African J Geol 107:505–520

Seat Z, Beresford SW, Grcuric BA, et al (2009) Re-valuation of the role of external sulfur addition in the genesis of Ni-Cu-PGE deposits: Evidence from the nebo-babel Ni-Cu-PGE deposit, west musgrave, Western Australia. Econ Geol 104:521–538.

Seat Z, Beresford SW, Grguric BA, et al (2007) Architecture and emplacement of the Nebo-Babel gabbronorite-hosted magmatic Ni-Cu-PGE sulphide deposit, West Musgrave, Western Australia. Miner Depos 42:551–581.

Semenov VS, Mikhailov VM, Koptev-Dvornikov E V., et al (2014) Layered Jurassic intrusions in Antarctica. Petrology 22:547–573.

Sharkov E V., Bogatikov OA, Grokhovskaya TL, et al (1995) Petrology and Ni-Cu-Cr-PGE mineralization of the largest mafic pluton in Europe: The early Proterozoic Burakovsky layered intrusion, Karelia, Russia. Int Geol Rev 37:509–525.

Sharman ER, Penniston-Dorland SC, Kinnaird JA, et al (2013) Primary origin of marginal Ni-Cu-(PGE) mineralization in layered intrusions: δ33S evidence from the Platreef, Bushveld, South Africa. Econ Geol 108:365–377

Sharpe MR (1981) The chronology of magma influxes to the eastern compartment of the Bushveld Complex as exemplified by its marginal border groups. J Geol Soc London 138:307–326

She YW, Song XY, Yu SY, He HL (2015) Variations of trace element concentration of magnetite and ilmenite from the Taihe layered intrusion, Emeishan large igneous province, SW China: Implications for magmatic fractionation and origin of Fe-Ti-V oxide ore deposits. J Asian Earth Sci 113:1117–1131.

Skryzalin PA, Ramirez C, Durrheim RJ, et al (2016) No Evidence for Connectivity between the Bushveld Igneous Complex and the Molopo Farms Complex from Forward Modeling of Receiver Functions. AGUFM 2016:T11B-2603

Smith WD, Maier WD, Barnes SJ, et al (2021) Element mapping the Merensky Reef of the Bushveld Complex. Geosci Front 12:101101

Smithies RH, Kirkland CL, Korhonen FJ, et al (2015) The Mesoproterozoic thermal evolution of the Musgrave Province in central Australia—Plume vs. the geological record. Gondwana Res 27:1419–1429

Song X, Qi H, Hu R, et al (2013) Formation of thick stratiform Fe-Ti oxide layers in layered intrusion and frequent replenishment of fractionated mafic magma: evidence from the Panzhihua intrusion, SW China. Geochemistry, Geophys Geosystems 14:712–732

Song X-Y, Xie W, Deng Y-F, et al (2011) Slab break-off and the formation of Permian mafic–ultramafic intrusions in southern margin of Central Asian Orogenic Belt, Xinjiang, NW China. Lithos 127:128–143

Sonnenthal EL (1990) Part I. Metasomatic replacement and the behavior of fluorine and chlorine during differentiation of the Skaergaard intrusion, East Greenland. Part II. Geochemical and physical aspects of melt segregation in the Picture Gorge basalt, Oregon

Sørensen H (2006) Ilimaussaq Alkaline Complex, South Greenland: An Overview of 200 Years of Research and an Outlook

Spandler C, Worden K, Arculus R, Eggins S (2005) Igneous rocks of the brook street terrane, New Zealand: Implications for permian tectonics of eastern gondwana and magma genesis in modern intra-oceanic volcanic arcs. New Zeal J Geol Geophys 48:167–183.

Spandler CJ, Eggins SM, Arculus RJ, Mavrogenes JA (2000) Using melt inclusions to determine parent-magma compositions of layered intrusions: Application to the Greenhills Complex (New Zealand), a platinum group minerals-bearing, island-arc intrusion. Geology 28:991–994.

Sparks RSJ, Cashman K V (2017) Dynamic magma systems: implications for forecasting volcanic activity. Elements 13:35–40

Sparks RSJ, Huppert HE, Turner JS (1984) The fluid dynamics of evolving magma chambers. Philos Trans R Soc London Ser A, Math Phys Sci 310:511–534

Stordal F, Svensen HH, Aarnes I, Roscher M (2017) Global temperature response to century-scale degassing from the Siberian Traps large igneous province. Palaeogeogr Palaeoclimatol Palaeoecol 471:96–107

Su BX, Qin KZ, Zhou MF, et al (2014) Petrological, geochemical and geochronological constraints on the origin of the Xiadong Ural-Alaskan type complex in NW China and tectonic implication for the evolution of southern Central Asian Orogenic Belt. Lithos 200–201:226–240.

Sun T, Qian ZZ, Deng YF, et al (2013a) PGE and Isotope (Hf-Sr-Nd-Pb) Constraints on the Origin of the Huangshandong Magmatic Ni-Cu Sulfide Deposit in the Central Asian Orogenic Belt, Northwestern China. Econ Geol 108:1849–1864.

Sun T, Qian Z-Z, Li C, et al (2013b) Petrogenesis and economic potential of the Erhongwa mafic–ultramafic intrusion in the Central Asian Orogenic Belt, NW China: constraints from olivine chemistry, U–Pb age and Hf isotopes of zircons, and whole-rock Sr–Nd–Pb isotopes. Lithos 182:185–199

Tack L, Liégeois J-P, Deblond A, Duchesne J-C (1994) Kibaran A-type granitoids and mafic rocks generated by two mantle sources in a late orogenic setting (Burundi). Precambrian Res 68:323–356

Takahashi Y, Mikoshiba MU, Takahashi Y, et al (2007) Geochemical modelling of the Chilas Complex in the Kohistan Terrane, northern Pakistan. J Asian Earth Sci 29:336–349.

Tanner D, Mavrogenes JA, Arculus RA, Jenner FE (2014) Trace element stratigraphy of the Bellevue Core, Northern Bushveld: multiple magma injections obscured by diffusive processes. J Petrol 55:859–882

Teixeira W, Hamilton MA, Lima GA, et al (2015) Precise ID-TIMS U–Pb baddeleyite ages (1110–1112 Ma) for the Rincón del Tigre–Huanchaca large igneous province (LIP) of the Amazonian Craton: Implications for the Rodinia supercontinent. Precambrian Res 265:273–285

Tessalina SG, Bourdon B, Gannoun A, et al (2007) Complex Proterozoic to Paleozoic history of the upper mantle recorded in the Urals lherzolite massifs by Re–Os and Sm–Nd systematics. Chem Geol 240:61–84

Thakurta J, Findlay J (2013) Geochemical constraints on the origin of palladium, copper and gold mineralization in the Salt Chuck mafic-ultramafic intrusion in southeastern Alaska. AGUFM 2013:V33B-2750

Thakurta J, Hinks B, Rose K (2019) Spatial distribution of sulfur isotope ratios associated with the Eagle Ni-Cu sulfide deposit in Upper Peninsula, Michigan: Implications on country-rock contamination in a dynamic magma conduit. Ore Geol Rev 106:176–191

Thakurta J, Ripley EM, Li C (2014) Platinum group element geochemistry of sulfide-rich horizons in the Ural-Alaskan–type ultramafic complex of Duke Island, southeastern Alaska. Econ Geol 109:643–659

Theriault RD, Barnes S-J (1998) Compositional variations in Cu-Ni-PGE sulfides of the Dunka Road deposit, Duluth Complex, Minnesota: The importance of combined assimilation and magmatic processes. Can Mineral 36:869–886

Thrane K, Kalvig P, Keulen N (2014) REE deposits and occurrences in Greenland. In: ERES2014: 1st European Rare Earth Resources Conference, Milos, Greece

Tolstykh N, Kozlov A, Telegin Y (2015) Platinum mineralization of the Svetly Bor and nizhny tagil intrusions, Ural Platinum Belt. Ore Geol Rev 67:234–243

Tolstykh ND, Sidorov EG, Kozlov AP (2004) Platinum-group minerals in lode and placer deposits associated with the Ural-Alaskan-type Gal'moenan complex, Koryak–Kamchatka platinum belt, Russia. Can Mineral 42:619–630

Tolstykh ND, Sidorov EG, Krivenko AP, Mungall JE (2005) Platinum-group element placers associated with Ural-Alaska type complexes. Mineral Assoc Canada Short Course 35:113–143

Toplis MJ, Carroll MR (1995) An experimental study of the influence of oxygen fugacity on Fe-Ti oxide stability, phase relations, and mineral—melt equilibria in ferro-basaltic systems. J Petrol 36:1137–1170

Tukiainen T (2014) The Motzfeld of the Igaliko nepheline syenite complex, South Greenland—a major resource of REE elements. In: ERES2014, proceedings of the 1st European rare earth resources conference, Milos Greece. pp 4–7

Turnbull RE, Size WB, Tulloch AJ, Christie AB (2017) The ultramafic–intermediate Riwaka Complex, New Zealand: summary of the petrology, geochemistry and related Ni–Cu–PGE mineralisation. New Zeal J Geol Geophys 60:270–295.

Ulmer G (1969) Experimental investigations of chromite spinels. Magmat Ore Depos 114–131

Upton BGJ, Parsons I, Emeleus CH, Hodson ME (1996) Layered alkaline igneous rocks of the Gardar Province, South Greenland. In: Developments in Petrology. Elsevier, pp 331–363

Upton BGJ, Skovgaard AC, McClurg J, et al (2002) Picritic magmas and the Rum ultramafic complex, Scotland. Geol Mag 139:437–452.

Von Gruenewaldt G (1993) Ilmenite-apatite enrichments in the Upper Zone of the Bushveld Complex: a major titanium-rock phosphate resource. Int Geol Rev 35:987–1000

Vonopartis L, Nex P, Kinnaird J, Robb L (2020) Evaluating the Changes from Endogranitic Magmatic to Magmatic-Hydrothermal Mineralization: The Zaaiplaats Tin Granites, Bushveld Igneous Complex, South Africa. Minerals 10:373

Voordouw R, Gutzmer J, Beukes NJ (2009) Intrusive origin for upper group (UG1, UG2) stratiform chromitite seams in the Dwars River area, Bushveld Complex, South Africa. Mineral Petrol 97:75

Vukmanovic Z, Holness MB, Monks K, Andersen JCØ (2018) The Skaergaard trough layering: sedimentation in a convecting magma chamber. Contrib to Mineral Petrol 173:43

Vukmanovic Z, Holness MB, Stock MJ, Roberts RJ (2019) The creation and evolution of crystal mush in the Upper Zone of the Rustenburg Layered Suite, Bushveld Complex, South Africa. J Petrol 60:1523–1542

Wadsworth WJ (1961) The layered ultrabasic rocks of south-west Rhum, Inner Hebrides. Philos Trans R Soc Lond B Biol Sci 244:21–64

Wager LR, Brown GM (1968) Layered igneous intrusions. Edinburgh London Oliver Boyd 1–588

Wager LR, Brown GM, Wadsworth WJ (1960) Types of igneous cumulates. J Petrol 1:73–85

Wagner PA (1929) Platinum deposits and mines of South Africa: Cape Town, C. Struik Ltd 338:

Wall CJ, Scoates JS, Weis D, et al (2018) The Stillwater Complex: integrating zircon geochronological and geochemical constraints on the age, emplacement history and crystallization of a large, open-system layered intrusion. J Petrol 59:153–190

Wallmach T, Hatton CJ, Droop GT. (1989) Extreme facies of contact metamorphism developed in calc-silicate xenoliths in the eastern Bushveld Complex. Can Mineral 27:509–523

Wang CY, Wei B, Zhou M-F, et al (2018) A synthesis of magmatic Ni-Cu-(PGE) sulfide deposits in the~ 260 Ma Emeishan large igneous province, SW China and northern Vietnam. J Asian Earth Sci 154:162–186

Wang M, Wang CY (2020) Crystal Size Distributions and Trace Element Compositions of the Fluorapatite from the Bijigou Fe–Ti Oxide-Bearing Layered Intrusion, Central China: Insights for the Expulsion Processes of Interstitial Liquid from Crystal Mush. J Petrol 61(7): 69

Watkinson DH, Melling DR (1992) Hydrothermal origin of platinum-group mineralization in low-temperature copper sulfide-rich assemblages, Salt Chuck intrusion, Alaska. Econ Geol 87:175–184

Weiblen PW, Morey GB (1980) A summary of the stratigraphy, petrology, and structure of the Duluth Complex. Yale University, Kline Geology Laboratory pp 88-133.

Wiebe RA (1993) The Pleasant Bay layered gabbro—diorite, coastal Maine: ponding and crystallization of basaltic injections into a silicic magma chamber. J Petrol 34:461–489

Wiebe RA, Wild T (1983) Fractional crystallization and magma mixing in the Tigalak layered intrusion, the Nain anorthosite complex, Labrador. Contrib to Mineral Petrol 84:327–344

Wignall P (2005) The link between large igneous province eruptions and mass extinctions. Elements 1:293–297

Wilhelmij HR, Cabri LJ (2016) Platinum mineralization in the Kapalagulu Intrusion, western Tanzania. Miner Depos 51:343–367

Wilson AH (1982) The geology of the Great 'Dyke', Zimbabwe: the ultramafic rocks. J Petrol 23:240–292

Wilson AH (1992) The geology of the great dyke, Zimbabwe: Crystallization, layering, and cumulate formation in the P1 pyroxenite of cyclic unit 1 of the Darwendale subchamber. J Petrol 33:611–663.

Wilson AH (2012) A chill sequence to the Bushveld Complex: insight into the first stage of emplacement and implications for the parental magmas. J Petrol 53:1123–1168

Wilson AH, Tredoux M (1990) Lateral and vertical distribution of platinum-group elements and petrogenetic controls on the sulfide mineralization in the P1 pyroxenite layer of the Darwendale subchamber of the Great Dyke, Zimbabwe. Econ Geol 85:556–584

Wilson JR, Menuge JF, Pedersen S, Engell-Sørensen O (1987) The southern part of the Fongen-Hyllingen layered mafic complex, Norway: emplacement and crystallization of compositionally stratified magma. In: Origins of igneous layering. Springer, pp 145–184

Woldemichael BW, Kimura JI (2006) Petrogenesis of the Neoproterozoic Bikilal-Ghimbi gabbro, Western Ethiopia. J Mineral Petrol Sci 103:23–46.

Woldemichael BW, Kimura J I, Dunkley DJ, et al (2010) SHRIMP U–Pb zircon geochronology and Sr–Nd isotopic systematic of the Neoproterozoic Ghimbi-Nedjo mafic to intermediate intrusions of Western Ethiopia: a record of passive margin magmatism at 855 Ma? Int J Earth Sci 99:1773–1790

Woodruff LG, Schulz KJ, Nicholson SW, Dicken CL (2020) Mineral deposits of the Mesoproterozoic Midcontinent Rift System in the Lake Superior region-A space and time classification. Ore Geol Rev 103716

Woods K, Keltie E, Brenan J, et al (2019) The role of country rock assimilation on chromite crystallization in the Ring of Fire, James Bay lowlands, Ontario, Canada. Atlantic Geology, 2019, Volume 55 Atlantic Geoscience Society Abstracts – 45th Colloquium & Annual General Meeting 2019

Wu F-Y, Yang Y-H, Li Q-L, et al (2011) In situ determination of U–Pb ages and Sr–Nd–Hf isotopic constraints on the petrogenesis of the Phalaborwa carbonatite Complex, South Africa. Lithos 127:309–322

Xie W, Song X-Y, Chen L-M, et al (2014) Geochemistry insights on the genesis of the subduction-related Heishan magmatic Ni-Cu-(PGE) deposit, Gansu, northwestern China, at the southern margin of the Central Asian Orogenic Belt. Econ Geol 109:1563–1583

Yakubchuk A, Nikishin A (2004) Noril'sk–Talnakh Cu–Ni–PGE deposits: a revised tectonic model. Miner Depos 39:125–142

Yang S-H, Maier WD, Godel B, et al (2019) Parental magma composition of the Main Zone of the Bushveld Complex: evidence from in situ LA-ICP-MS trace element analysis of silicate minerals in the cumulate rocks. J Petrol 60:359–392

Yang S-H, Maier WD, Hanski EJ, et al (2015) Origin of ultra-nickeliferous olivine in the Kevitsa Ni–Cu–PGE-mineralized intrusion, northern Finland. Contrib to Mineral Petrol 166:81–95

Yao Z-S, Mungall JE (2021) Linking the Siberian Flood Basalts and Giant Ni-Cu-PGE Sulfide Deposits at Norilsk. J Geophys Res Solid Earth 126(3).

Yudovskaya M, Belousova E, Kinnaird J, et al (2017) Re-Os and S isotope evidence for the origin of Platreef mineralization (Bushveld Complex). Geochim Cosmochim Acta 214:282–307

Yudovskaya MA, Naldrett AJ, Woolfe JAS, et al (2015) Reverse compositional zoning in the Uitkomst chromitites as an indication of crystallization in a magmatic conduit. J Petrol 56:2373–2394

Zaccarini F, Pushkarev VE, Fershtater BG, et al (2002) Platinum-Group Element Mineralogy and Geochemistry in Chromitites of the Nurali Mafic-Ultramafic Complex (Southern Urals, Russia). In: 9th International Platinum Symposium Extended Abstracts, Billings, Montana, USA. pp 487–490

Zhang M, Yang J-H, Sun J-F, et al (2012b) Juvenile subcontinental lithospheric mantle beneath the eastern part of the Central Asian Orogenic Belt. Chem Geol 328:109–122

Zhang X-Q, Song X-Y, Chen L-M, et al (2012a) Fractional crystallization and the formation of thick Fe–Ti–V oxide layers in the Baima layered intrusion, SW China. Ore Geol Rev 49:96–108

Zhang Y-L, Liu C-Z, Ge W-C, et al (2011) Ancient sub-continental lithospheric mantle (SCLM) beneath the eastern part of the Central Asian Orogenic Belt (CAOB): Implications for crust–mantle decoupling. Lithos 126:233–247

Zhou M-F, Chen WT, Wang CY, et al (2013) Two stages of immiscible liquid separation in the formation of Panzhihua-type Fe-Ti-V oxide deposits, SW China. Geosci Front 4:481–502

Zhou M-F, Robinson PT, Lesher CM, et al (2005) Geochemistry, petrogenesis and metallogenesis of the Panzhihua gabbroic layered intrusion and associated Fe–Ti–V oxide deposits, Sichuan Province, SW China. J Petrol 46:2253–2280

Zientek ML, Cooper RW, Corson SR, Geraghty EP (2002) Platinum-group element mineralization in the Stillwater Complex, Montana. Geol Geochemistry, Mineral Miner Benef Platin Gr Elem Can Inst Mining, Metall Pet Spec 54

Figure 1. Global distribution of layered igneous intrusions coloured by their age and sized by their arial extent (km^2). The spatial distribution of cratons is that of Bleeker (2003), which have been buffered to 500 km. The map was produced in ArcMap 10.7.1. Giant > 10,000 km^2, large > 1,000 km^2, medium > 100 km^2, and small < 100 km^2.

Figure 2. Temporal distribution of layered igneous intrusions *versus* their arial extent (km^2). (A) Linear scale highlighting the ten largest known layered intrusions coloured by continent. Note the exceptional size of the Bushveld Complex (> 100,000 km^2) compared with the rest of the compiled intrusions. (B) Logarithmic scale highlighting the secular distribution of layered igneous intrusions coloured by continent and (C) the same plot coloured by type of mineralisation. (D) Secular occurrence of supercontinents and their associated juvenile

crustal production (Condie 2001; Goldfarb *et al.* 2010; modified from Maier and Groves 2011). Note the correlation between clusters of layered igneous intrusions and juvenile crust production.

Figure 3. Enhanced area of Figure 1 showing the distribution of layered intrusions in Africa coloured by their age and sized by their arial extent (km^2). The spatial distribution of cratons is that of Bleeker (2003), which have been buffered to 500 km. Giant > 10,000 km^2, large > 1,000 km^2, medium > 100 km^2, and small < 100 km^2.

Figure 4. Enhanced area of Figure 1 showing the distribution of layered intrusions in Asia coloured by their age and sized by their arial extent (km^2). The spatial distribution of cratons is that of Bleeker (2003), which have been buffered to 500 km. Giant > 10,000 km^2, large > 1,000 km^2, medium > 100 km^2, and small < 100 km^2.

Figure 5. Enhanced area of Figure 1 showing the distribution of layered intrusions in Europe coloured by their age and sized by their arial extent (km^2). The spatial distribution of cratons is that of Bleeker (2003), which have been buffered to 500 km. Giant > 10,000 km^2, large > 1,000 km^2, medium > 100 km^2, and small < 100 km^2.

Figure 6. Enhanced area of Figure 1 showing the distribution of layered intrusions in North America coloured by their age and sized by their arial extent (km^2). The spatial distribution of cratons is that of Bleeker (2003), which have been buffered to 500 km. Giant > 10,000 km^2, large > 1,000 km^2, medium > 100 km^2, and small < 100 km^2.

Figure 7. Enhanced area of Figure 1 showing the distribution of layered intrusions in Oceania coloured by their age and sized by their arial extent (km^2). The spatial distribution of cratons is that of Bleeker (2003), which have been buffered to 500 km. Giant > 10,000 km^2, large > 1,000 km^2, medium > 100 km^2, and small < 100 km^2.

Figure 8. Enhanced area of Figure 1 showing the distribution of layered intrusions in South America coloured by their age and sized by their arial extent (km^2). The spatial distribution of cratons is that of Bleeker (2003), which have been buffered to 500 km. Giant > 10,000 km^2, large > 1,000 km^2, medium > 100 km^2, and small < 100 km^2.

Figure 9. Size distribution of layered igneous intrusions (n = 480) with an enhanced plot showing the 10 largest layered igneous intrusions.

Figure 10. Global distribution of layered igneous intrusions coloured by their mineral occurrences and sized by their arial extent (km^2). The spatial distribution of cratons is that of Bleeker (2003), which have been buffered to 500 km.

Figure 11. Temporal distribution of layered igneous intrusions divided by their host continent *versus* their arial extent (km^2). Notable large igneous provinces (Ernst 2014) have been annotated on associated intrusions and clusters of intrusions.

Figure 12. Enhanced area of Figure 10 showing the distribution of layered intrusions in Africa coloured by their mineral occurrences and sized by their arial extent (km^2). The spatial distribution of cratons is that of Bleeker (2003), which have been buffered to 500 km. Giant > 10,000 km^2, large > 1,000 km^2, medium > 100 km^2, and small < 100 km^2.

Figure 13. Enhanced area of Figure 10 showing the distribution of layered intrusions in Asia coloured by their mineral occurrences and sized by their arial extent (km^2). The spatial distribution of cratons is that of Bleeker (2003), which have been buffered to 500 km. Giant > 10,000 km^2, large > 1,000 km^2, medium > 100 km^2, and small < 100 km^2.

Figure 14. Enhanced area of Figure 10 showing the distribution of layered intrusions in Europe coloured by their mineral occurrences and sized by their arial extent (km^2). The spatial distribution of cratons is that of Bleeker (2003), which have been buffered to 500 km. Giant > 10,000 km^2, large > 1,000 km^2, medium > 100 km^2, and small < 100 km^2.

Figure 15. Enhanced area of Figure 10 showing the distribution of layered intrusions in North America coloured by their mineral occurrences and sized by their arial extent (km^2). The spatial distribution of cratons is that of Bleeker (2003), which have been buffered to 500 km. Giant > 10,000 km^2, large > 1,000 km^2, medium > 100 km^2, and small < 100 km^2.

Figure 16. Enhanced area of Figure 10 showing the distribution of layered intrusions in Oceania coloured by their mineral occurrences and sized by their arial extent (km^2). The spatial distribution of cratons is that of Bleeker (2003), which have been buffered to 500 km. Giant > 10,000 km^2, large > 1,000 km^2, medium > 100 km^2, and small < 100 km^2.

Figure 17. Enhanced area of Figure 10 showing the distribution of layered intrusions in South America coloured by their mineral occurrences and sized by their arial extent (km^2). The spatial distribution of cratons is that of Bleeker (2003), which have been buffered to 500 km. Giant > 10,000 km^2, large > 1,000 km^2, medium > 100 km^2, and small < 100 km^2.

Table 1. Summary of dynamic and non-dynamic layer-forming processes operating during the formation of layered igneous intrusions.

Process	Description	Layer and layering characteristics	Notable examples	References
Dynamic				
Syn-emplacement processes				
Flow segregation	Crystals suspended within a propagating magma conduit will migrate to the area of minimum shear (*i.e.*, Bagnold Effect). The efficiency of this is also monitored partly by the Magnus and Wall Effects.	Most commonly seen in sills and dykes, whereby the margins are phenocryst-poor (often smaller in grain size) and the centres are phenocryst-rich (often coarsest in the centre).	Skaergaard (Greenland), Palisades (USA)	Irvine (1987), Gorring and Naslund (1995)
Magma replenishment	Within open-system chambers, the volume of magma will grow progressively or episodically with magma replenishment. This may cause out-of-sequence sill injection, incorporation of magma batches with different crystal loads, compositional or density stratification of a magma chamber, and different degrees of differentiation between layers.	Each episode of replenishment and differentiation will result in the constructure of cyclic layers, where its thickness is proportional to the volume of magma influx. Cryptic layering in mineral and whole rock chemistry (*i.e.*, increase in mafic cations) may indicate new fluxes of magma.	Duros (Namibia), Panzhihua (China), Bjerkreim-Sokndal (Norway), Muskox (Canada)	Irvine and Smith (1967), Jensen et al. (2003), Song et al. (2013), Owen-Smith and Ashwal (2015)
Magma mixing	Mixing can refer to: (i) mixing of two magmas (*e.g.*, hybridisation); (ii) mixing of magma and country rock (*e.g.*, crustal contamination); or (iii) mixing of magma and crystalline rock (*e.g.*, cannibalisation).	Magma hybridisation may cause monomineralic layers (*e.g.*, chromitite). Contamination may lead to cryptic compositional layering or units dominated by one phase.	Munni Munni (Australia), Tigalak (Canada), Bushveld (South Africa)	Weibe and Wild (1983), Hoatson and Keays (1989), Harney et al. (1990), Eales and Cawthorn (1996), Karykowski et al. (2017)
In situ crystallisation	The concept suggests that magmas are primarily liquid and crystals nucleate directly on the interior walls of the magma chamber.	Laterally-persisent layers of fairly uniform thickness. The may be monomineralic (or close too).	Bushveld (South Africa), Mont Collon (Switzerland), Jacurici (Brazil)	Monjoie *et al.* (2005), Latypov *et al.* (2017), Friedrich *et al.* (2020)
Convection-relatied processes				
Continuous convection	Refers to the continuous thermal and physical churning of magma, which keeps crystals suspended if the convective velocities exceed settling velocities. Once a critical concentration of suspended phases is reached, they will settle according to their physical properties	Keeping minerals in continuous suspension will create laterally-persistent, thick, modally-graded layers (potentially monomineralic layers), which may display a coarsening-up texture. Continuous convection may also homogenise a system if particles are unable to settle out.	Shiant (Scotland), Bijigou (China), Khibina (Russia)	Kogarko and Khapaev (1987), Holness et al. (2017), Wang and Wang (2020)
Intermittent convection	Refers to convective and stagnant periods, where crystals are suspended and 'dropped' episodically	Thick, laterally-persistent and modally-graded layers. Phases of convection-stagnation will lead to cyclic layering.	Skaergaard (Greenland), Kivakka (Finland),	Naslund *et al.* (1991); Choban *et al.* (2006)

			Akanvaara (Finland)	
Double-diffusive convection	Refers to a stratified magma chamber with two dependent contemporaneous parameters with different diffusion rates. For example, heat diffuses in the direction Mg and Fe will diffusive.	Laterally-persistent layers resulting in extreme whole-rock and mineral compositional gradients and modal layering.	Fongen-Hyllingen (Norway), Pleasant Bay (USA)	Wilson *et al.* (1987); Weibe (1993)
Mechanical processes				
Gravitational settling	The phenomena in which solid particles suspended in a melt will settle according to Stoke's Law. That is where denser minerals will settle faster relative to light minerals.	Laterally-persistent layers which are modally-graded and fine upward. Coupled with replenishment, this will produce cyclic layering.	Rum (Scotland), Sonju Lake (USA), Ilímaussaq (Greenland)	Maes *et al.* (2007), Pfaff *et al.* (2008), Holness et al. (2012)
Crystal flotation	The phenomena in which solid particles suspended in a melt with float according to Stoke's Law. That is where the solid phase is essentially lighter than the host melt.	It is possible that plagioclase will float in basaltic magma, leading to the formation of anorthosites in the upper portions of magma chambers.	Kalka (Australia), Sept Iles (Canada)	Goode (1976; 1977), Namur et al. (2011)
Density currents and Kinetic sieving	In a manner similar to turbidite deposits, crystal slurries may flow or collapse (*e.g.*, in response to subsidence or siesmicity) and become mechanically-sorted according to the properties of the suspended load	Density currents will produce coarsening-up and near-monomineralic trough layers. These layers may truncate other layers or bifurcate. Such processes are potentially augmented by seismicity.	Skaergaard (Greenland), Bushveld (South Africa), Canindé (Brazil), Dais (Antarctica)	Irvine *et al.* (1998), Maier *et al.* (2013a), Pinto *et al.* (2020)
Compation	May also be referred to as filter-pressing, whereby a porous cumulus pile contracts or is compacted leading to the expulsion of intercumulus liquid and the formation of solid rock.	Deformed or laminated layers with variable crystal:liquid ratios. This process may form monomineralic or polymineralic adcumulates.	Sept Iles (Canada), Klokken (Greenland)	Parsons and Becker (1987), Namur and Charlier (2012)
Deformation	Deformation can come in two forms: (i) magmatic deformation, whereby shearing and viscous flow cause strongly laminated rocks and aid processes such as kinetic sieving and melt expulsion and (ii) tectonic deformation may trigger subsidence and changes in intensive parameters.	Shearing may form laminated and size-graded layers with variable crystal:liquid ratios. Tectonic deformation may cause density currents (see above) and the accompanying mechanical processes.	Fongen-Hyllingen (Norway), Bjerkreim–Sokndal (Norway), Sept Iles (Canada), Gosse Pile (Australia)	Moore (1973), Higgins (1991), Bolle et al. (2000)
Late-stage mush-related processes				
Metasomatism	Infiltration metasomatism represents the re-equilibration of cumulus phases with allochthonous intercumulus fluids ascending in response to tectonism, buoyancy, or	May produce abrupt and potentially monomineralic zones. May also produce sharp changes in grain-size.	Muskox (Canada), Rum (Scotland), Stillwater (USA), 76535 (Lunar)	Irvine (1980), Boudreau and McCallum (1992), Holness *et al.* (2007), Elardo *et al.* (2012)

	compaction.			
Contact metamorphism	Contact metamorphism occurs at the boundary between magma and contry rock. Through diffusion or devolatilisation, the bounding magma may be subject to rheomorphism, become compositional distinct or crystallise at different rates.	May produce cryptic layering or rhythmic layering in response to rheomorphism.	Skaergaard (Greenland)	Naslund (1986)
Reactive porous flow or constitutional zone refining	Represents the migration of fluxing agents through a cumulate pile, which may alter the melting point and nucleation rate of grains it interacts with.	This may produce laterally-persistent changes in grain-size and cause cryptic zoning. In addition, it may produce oscillatory zoning on cumulus minerals	Stillwater (USA), Bushveld (South Africa), Sept Iles (Canada)	Boudreau (1988), Nicholson and Mathez (1991), Karykowski et al. (2017a)
Ostwald Ripening	The process in which larger cumulus grains grow at the expense of smaller grains in order to minimise the suirface free energy of the system.	May produce adcumulates (sometimes monomineralic) with a mosaic-like texture of fairly homogeneous grain size. Mode and grain-size should positively correlate.	Stillwater (USA), Kiglapait (Canada)	Boudreau (1987), Higgins (2002)
Liquid immiscibility	In addition to silicate-fluid and silicate-sulphide immiscibility, two contrasting silicate magma compositions may unmix causing distinct layers. An extremely Fe-rich (plus other mafic cations) melt may segregate from an Si-rich (plus other felsic cations) melt.	Sulphide-bearing layers are generally laterally-persistent and thin. Immiscibility between a silicate melt and a fluid may produce a layer of pegmatitic granophyre. Immiscibility between two sillicate melts would produce abrupt compositional and mineralogical changes.	Stillwater (USA), Bushveld (South Africa), Sept Iles (Canada)	McBirney and Nakamura (1974), Reynolds (1985), Namur et al. (2012)
Non-dynamic				
Fluctiations in intensive parameters				
Pressure variation	Crystallisation occurs down a liquid line of descent primarily according to temperature, pressure, and composition. Pressure changes in response to deformation, chamber replenishment, or eruption will alter crystal assemblages and nucelation rates.	Laterally-persistent cyclic or rhythmic layers, which genrally fine upward. This may also produce flotation cumulates due to instigating plagioclase supersaturation.	Ilimaussaq (Greenland), Stillwater (USA), Panzhihua (China)	Ferguson and Pulvertaft (1963), Lipin (1993), Pang et al. (2009)
Oxygen fugacity changes	Changes in oxygen fugacity can alter the stability of the liquidus assemblage and in particular, modify phases that comprise multi-valent cations (*i.e.*, feldspar and Fe-Ti oxides).	May produce an alternating sequence of silicate and oxide assemblages. Can also produce modal and cryptic layering (*i.e.*, plagioclase Eu/Eu* composition).	Stillwater (USA), Bushveld (South Africa)	Ryder (1984), Reynolds (1985)
Self-organising crystal nucleation				

Nucleation and crystal growth rate fluctuation	A liquid must be supersaturated and undercooled in order for crystal nucleation to occur, which is in essence, a response to return the system to compositional equilibrium. Nucleation rate is controlled by volume and surface free energy, whereas growth rate is controlled by volume free energy.	Modal layering in that mode and average grain-size share a negative correlation. In turn, nucleation density and grain-size share a negative corerlation. The formation of crescumulates occurs in response to changes in crystal growth rate	Skaergarrd (Greenland), Freetown (Sierra Leone), Klokken (Greenland), Bjerkreim-Sokndal (Norway), Rum (Scotland)	Hawkes (1967), Wager and Brown (1968), Goode (1976), Duchesne and Charlier (2005), Faure et al. (2006)
Oscillatory or diffusion-controlled nucleation	Oscillatory nucleation operates close to a eutectic point whereby constituents of a crystallising phase will diffuse toward the growing crystal, leaving a depleted boundary layer that cannot nucleate further crystals.	Alternating sequence of crystalline phases with fairly aburpt contacts. As with nucleation rate, a negative correlation between modal proportion and average grain-size should be apparent.	Skaergaard (Greenland)	McBirney and Noyes (1979); Boudreau and McBirney (1997)

Highlights

- Compilation of 565 layered and differentiated igneous intrusions
- Distribution of igneous intrusions in space and time
- Overview of notable layered igneous intrusions
- Summary of mineralisation in layered igneous intrusions

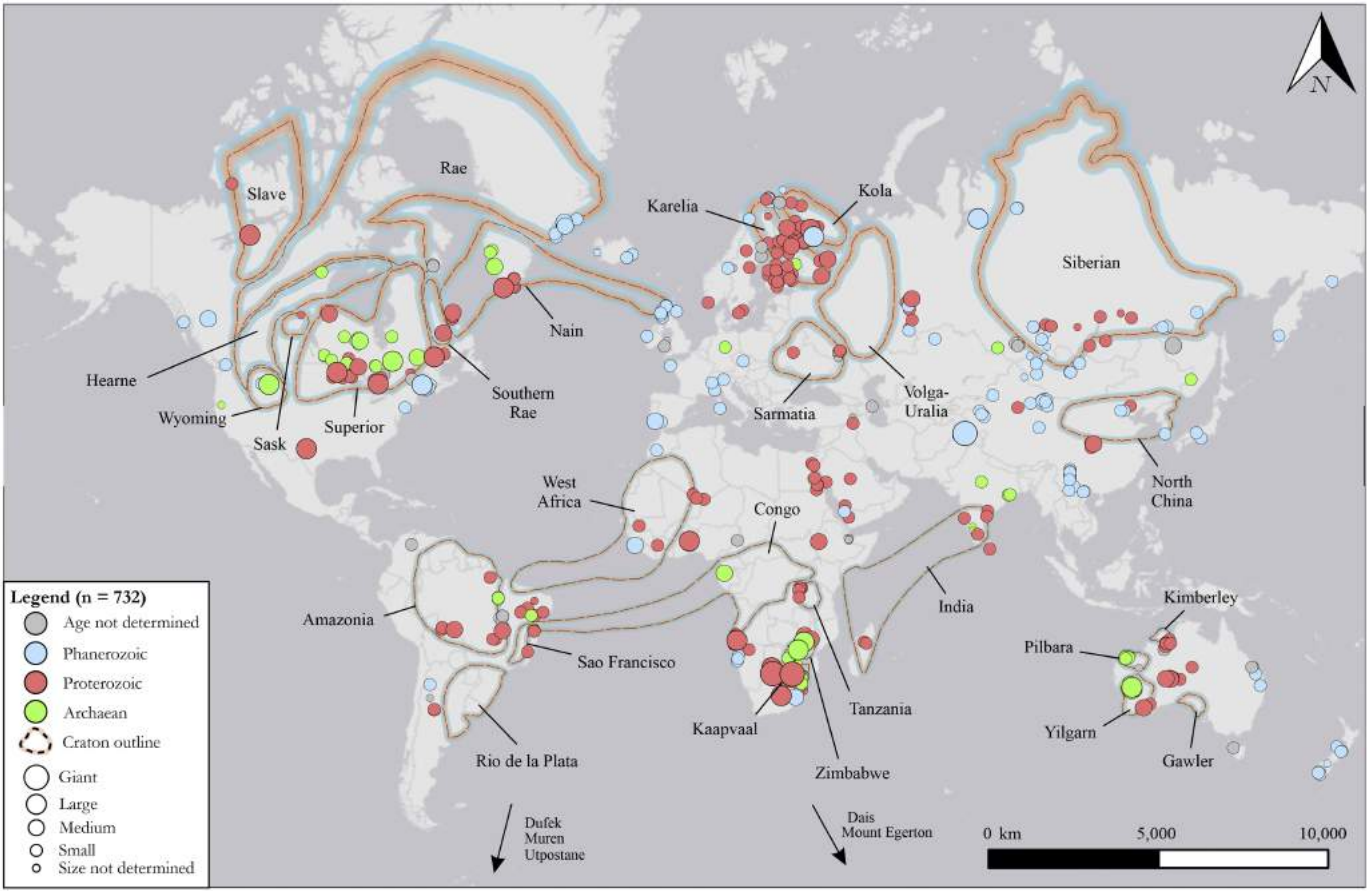
N
Slave
Rae
Karelia
Kola
Siberian
Nain
Hearne
Wyoming
Sask
Superior
Southern
Rae
Sarmatia
Volga-
Uralia
North
China
West
Africa
Congo
India
Amazonia
Sao Francisco
Kimberley
Pilbara
Yilgarn
Gawler
Kaapvaal
Tanzania
Zimbabwe
Rio de la Plata
Dufek
Muren
Utpostane
Dais
Mount Egerton
0 km
5,000
10,000
Legend (n = 732)
Age not determined
Phanerozoic
Proterozoic
Archaean
Craton outline
Giant
Large
Medium
Small
Size not determined

Figure 1

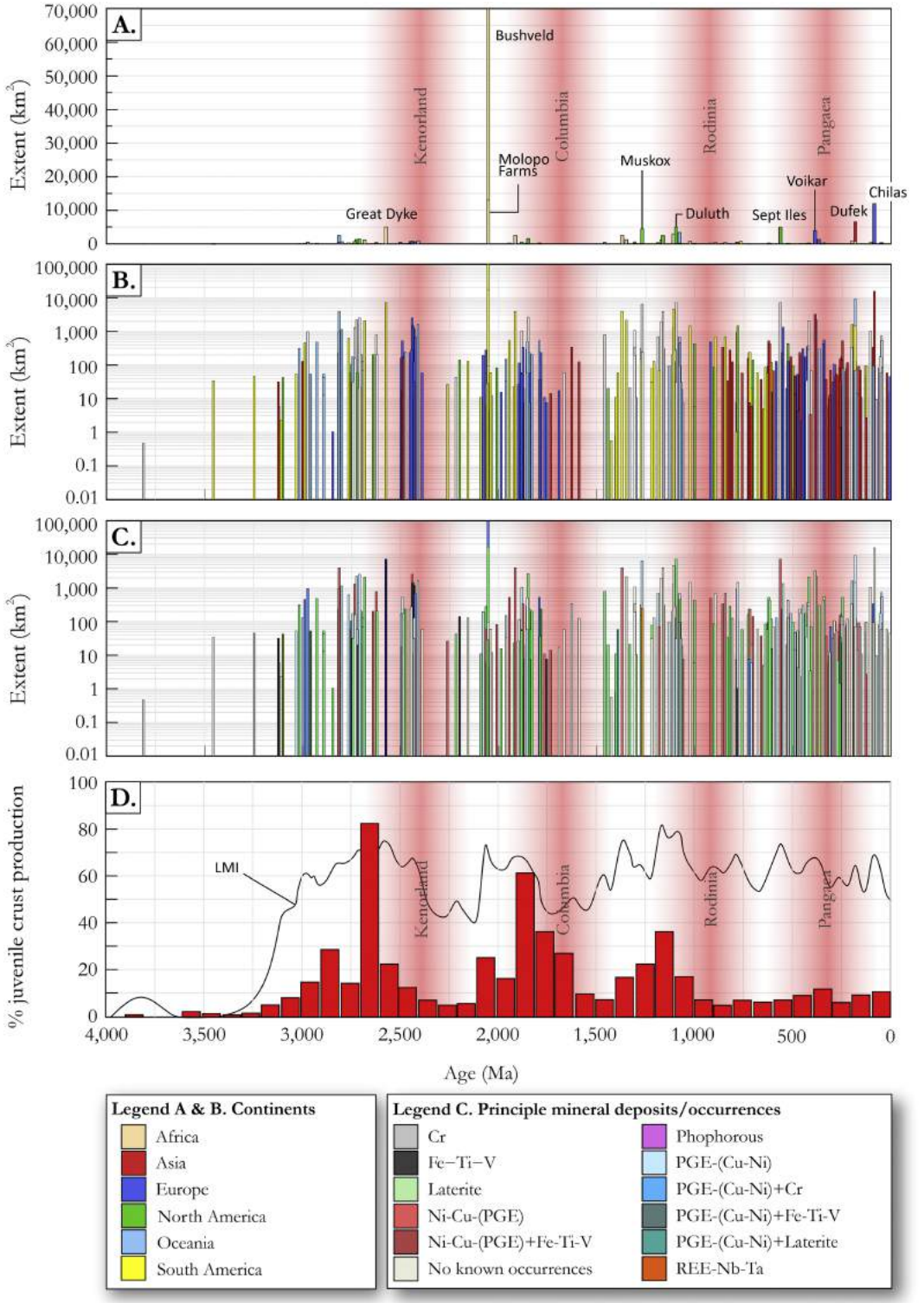
A.
B.
C.
D.
Extent (km²)
% juvenile crust production
Age (Ma)
Great Dyke
Bushveld
Molopo Farms
Muskox
Duluth
Sept Iles
Voikar
Dufek
Chilas
Kenorland
Columbia
Rodinia
Pangaea
LMI
Legend A & B. Continents
Africa
Asia
Europe
North America
Oceania
South America
Legend C. Principle mineral deposits/occurrences
Cr
Fe–Ti–V
Laterite
Ni-Cu-(PGE)
Ni-Cu-(PGE)+Fe-Ti-V
No known occurrences
Phophorous
PGE-(Cu-Ni)
PGE-(Cu-Ni)+Cr
PGE-(Cu-Ni)+Fe-Ti-V
PGE-(Cu-Ni)+Laterite
REE-Nb-Ta

Figure 2

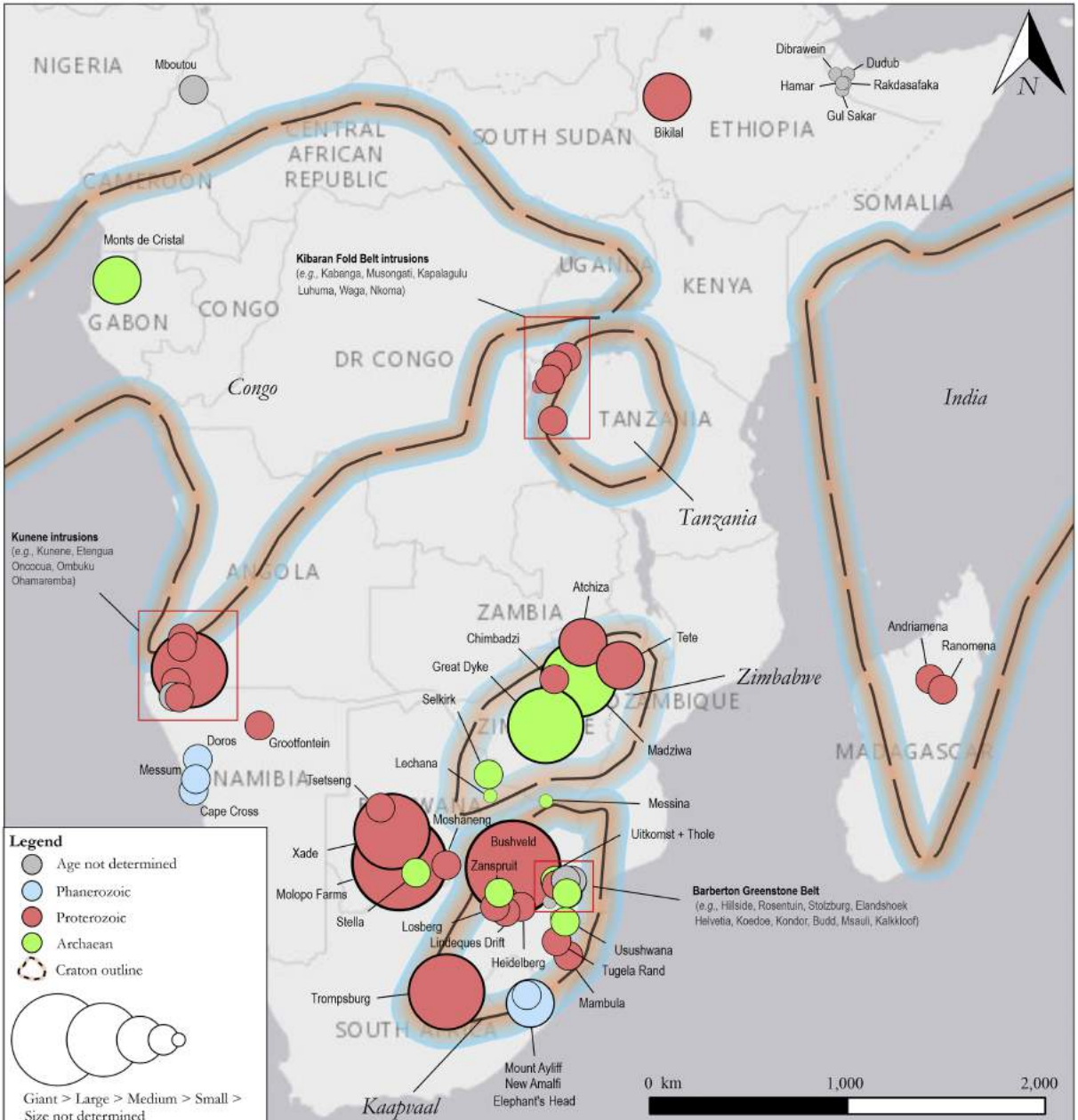
NIGERIA
Mboutou
CENTRAL AFRICAN REPUBLIC
CAMEROON
SOUTH SUDAN
Bikilal
ETHIOPIA
Dibrawein
Dudub
Hamar
Rakdasafaka
Gul Sakar
N
SOMALIA
Monts de Cristal
GABON
CONGO
Kibaran Fold Belt intrusions
(e.g., Kabanga, Musongati, Kapalagulu
Luhuma, Waga, Nkoma)
UGANDA
KENYA
DR CONGO
Congo
India
TANZANIA
Tanzania
Kunene intrusions
(e.g., Kunene, Etengua
Oncocua, Ombuku
Ohamaremba)
ANGOLA
ZAMBIA
Atchiza
Chimbadzi
Tete
Great Dyke
Zimbabwe
Selkirk
MOZAMBIQUE
Madziwa
Andriamena
Ranomena
MADAGASCAR
Doros
Grootfontein
Messum
NAMIBIA
Tsetseng
Lechana
Cape Cross
Messina
Moshaneng
Uitkomst + Thole
Bushveld
Xade
Zanspruit
Barberton Greenstone Belt
(e.g., Hillside, Rosentuin, Stolzburg, Elandshoek
Helvetia, Koedoe, Kondor, Budd, Msauli, Kalkkloof)
Molopo Farms
Stella
Losberg
Lindeques Drift
Heidelberg
Usushwana
Tugela Rand
Mambula
Trompsburg
SOUTH AFRICA
Mount Ayliff
New Amalfi
Elephant's Head
Kaapvaal
0 km
1,000
2,000
Legend
Age not determined
Phanerozoic
Proterozoic
Archaean
Craton outline
Giant > Large > Medium > Small >
Size not determined

Figure 3

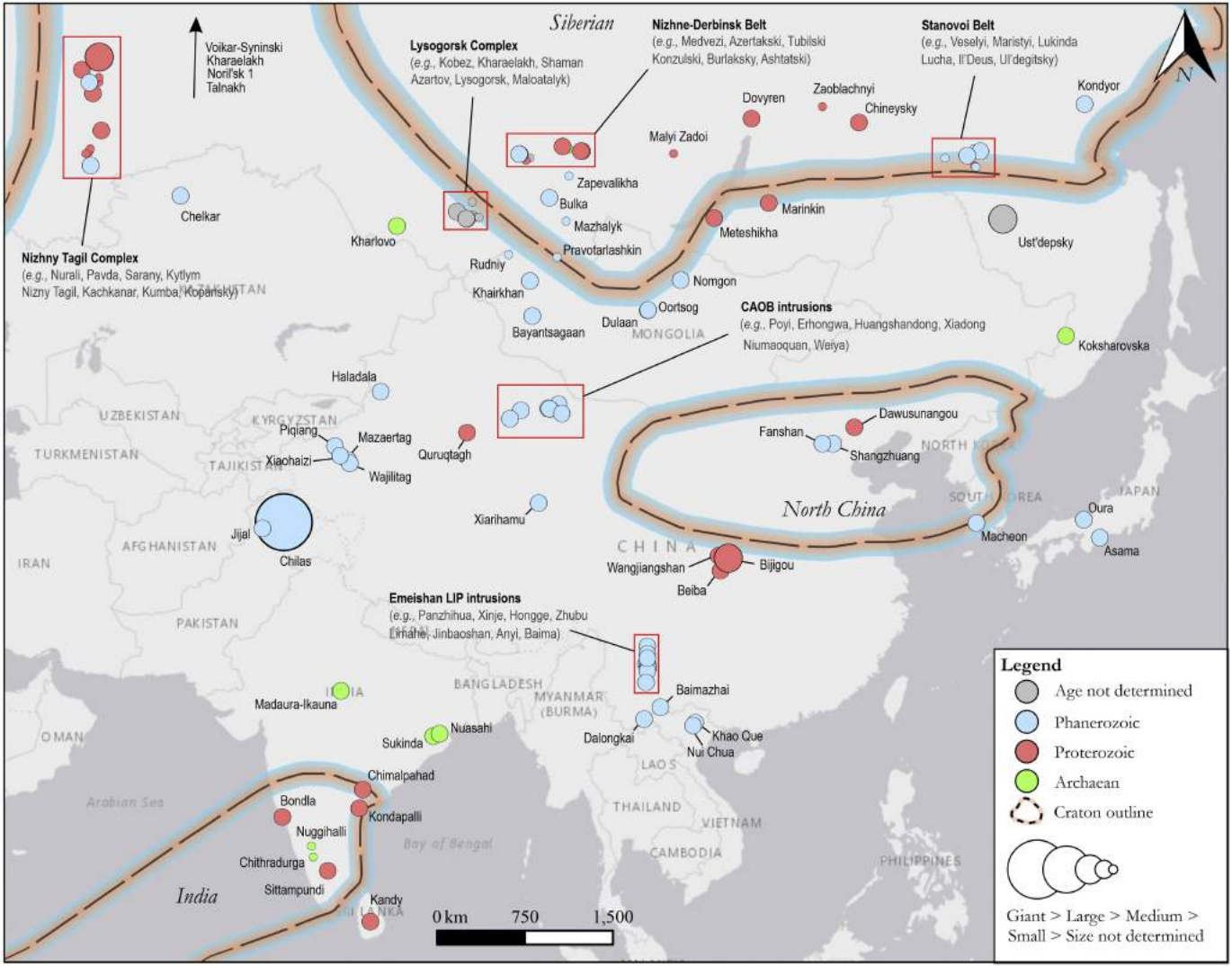
Siberian
Voikar-Syninski
Kharaelakh
Noril'sk 1
Talnakh
Lysogorsk Complex
(e.g., Kobez, Kharaelakh, Shaman
Azartov, Lysogorsk, Maloatalyk)
Nizhne-Derbinsk Belt
(e.g., Medvezi, Azertakski, Tubilski
Konzulski, Burlaksky, Ashtatski)
Stanovoi Belt
(e.g., Veselyi, Maristyi, Lukinda
Lucha, Il'Deus, Ul'degitsky)
Dovyren
Zaoblachnyi
Chineysky
Kondyor
Malyi Zadoi
Zapevalikha
Bulka
Mazhalyk
Pravotarlashkin
Marinkin
Meteshikha
Ust'depsky
Chelkar
Kharlovo
Nizhny Tagil Complex
(e.g., Nurali, Pavda, Sarany, Kytlym
Nizny Tagil, Kachkanar, Kumba, Kopansky)
Rudniy
Khairkhan
Bayantsagaan
Dulaan
Oortsog
Nomgon
CAOB intrusions
(e.g., Poyi, Erhongwa, Huangshandong, Xiadong
Niumaoquan, Weiya)
Koksharovska
Haladala
UZBEKISTAN
KYRGYZSTAN
TURKMENISTAN
TAJIKISTAN
Piqiang
Mazaertag
Xiaohaizi
Wajilitag
Quruqtagh
Dawusunangou
Fanshan
Shangzhuang
North China
Xiarihamu
Jijal
Chilas
AFGHANISTAN
IRAN
CHINA
Wangjiangshan
Bijigou
Beiba
Macheon
Oura
Asama
JAPAN
Emeishan LIP intrusions
(e.g., Panzhihua, Xinje, Hongge, Zhubu
Limahe, Jinbaoshan, Anyi, Baima)
PAKISTAN
Baimazhai
Madaura-Ikauna
BANGLADESH
MYANMAR
(BURMA)
Nuasahi
Sukinda
Dalongkai
Khao Que
Nui Chua
LAOS
OMAN
Chimalpahad
Arabian Sea
Bondla
Kondapalli
Nuggihalli
THAILAND
VIETNAM
CAMBODIA
Bay of Bengal
Chithradurga
Sittampundi
India
Kandy
PHILIPPINES
0 km
750
1,500
N
Legend
Age not determined
Phanerozoic
Proterozoic
Archaean
Craton outline
Giant > Large > Medium >
Small > Size not determined

Figure 4

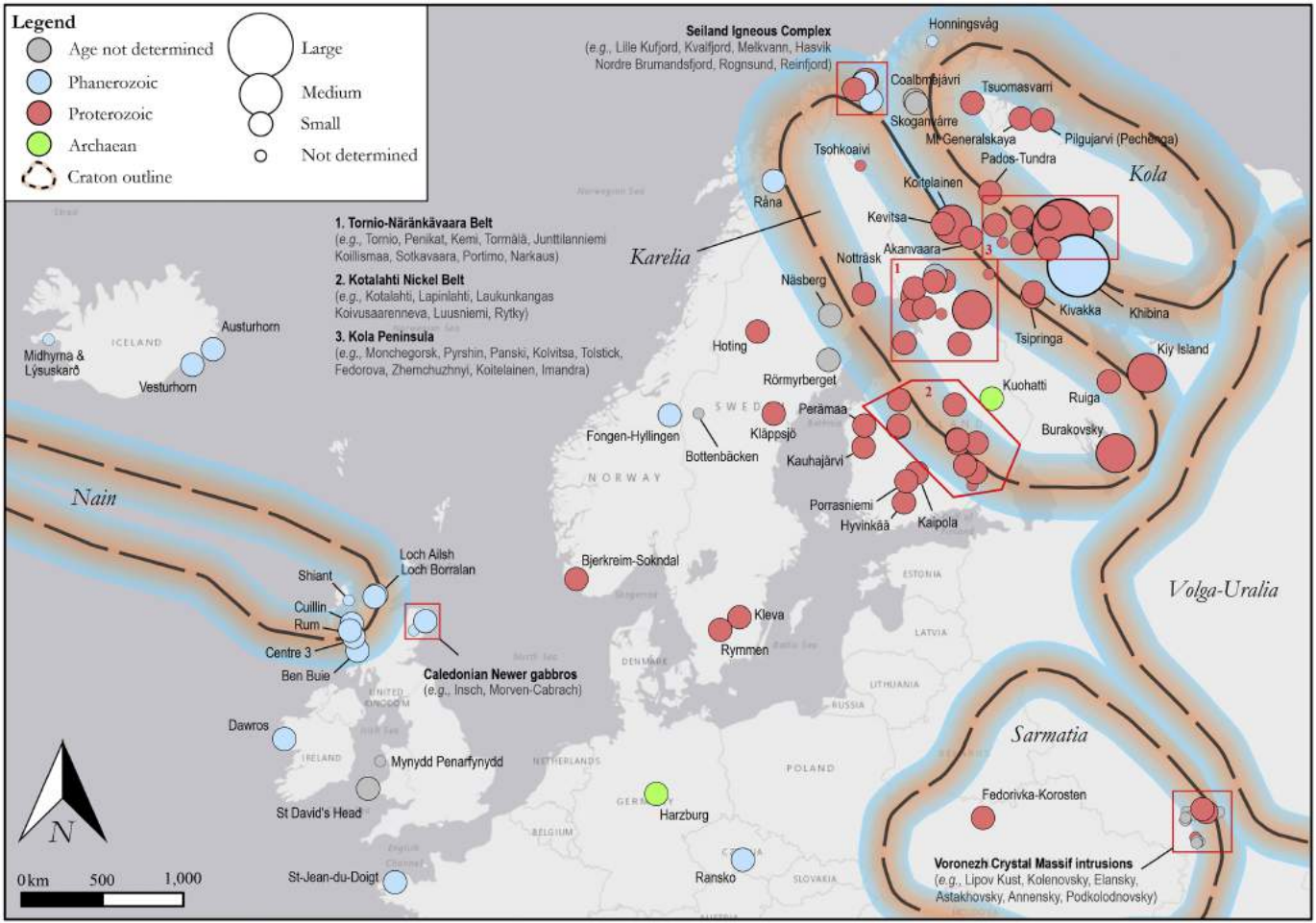
Legend
Age not determined
Phanerozoic
Proterozoic
Archaean
Craton outline
Large
Medium
Small
Not determined
Seiland Igneous Complex
(e.g., Lille Kufjord, Kvalfjord, Melkvann, Hasvik
Nordre Brumandsfjord, Rognsund, Reinfjord)
1. Tornio-Näränkävaara Belt
(e.g., Tornio, Penikat, Kemi, Tormälä, Junttilanniemi
Koillismaa, Sotkavaara, Portimo, Narkaus)
2. Kotalahti Nickel Belt
(e.g., Kotalahti, Lapinlahti, Laukunkangas
Koivusaarenneva, Luusniemi, Rytky)
3. Kola Peninsula
(e.g., Monchegorsk, Pyrshin, Panski, Kolvitsa, Tolstick,
Fedorova, Zhemchuzhnyi, Koitelainen, Imandra)
Honningsvåg
Coalbmejávri
Tsuomasvarri
Skoganvárre
Mt Generalskaya
Pilgujarvi (Pechenga)
Tsohkoaivi
Pados-Tundra
Kola
Koitelainen
Ráná
Kevitsa
Karelia
Akanvaara
Notträsk
Näsberg
Kivakka
Khibina
Tsipringa
Hoting
Kiy Island
Rörmyrberget
Kuohatti
Ruiga
Perämaa
Burakovsky
Fongen-Hyllingen
Kläppsjö
Bottenbäcken
Kauhajärvi
Porrasniemi
Hyvinkää
Kaipola
Nain
Loch Ailsh
Loch Borralan
Shiant
Cuillin
Rum
Centre 3
Ben Buie
Caledonian Newer gabbros
(e.g., Insch, Morven-Cabrach)
Bjerkreim-Sokndal
Kleva
Rymmen
Volga-Uralia
Sarmatia
Dawros
Mynydd Penarfynydd
St David's Head
Harzburg
Fedorivka-Korosten
Voronezh Crystal Massif intrusions
(e.g., Lipov Kust, Kolenovsky, Elansky,
Astakhovsky, Annensky, Podkolodnovsky)
St-Jean-du-Doigt
Ransko
Austurhorn
Midhyrna &
Lýsuskarð
Vesturhorn
ICELAND
NORWAY
SWEDEN
ESTONIA
LATVIA
LITHUANIA
RUSSIA
POLAND
DENMARK
IRELAND
NETHERLANDS
BELGIUM
SLOVAKIA
N
0 km
500
1,000

Figure 5

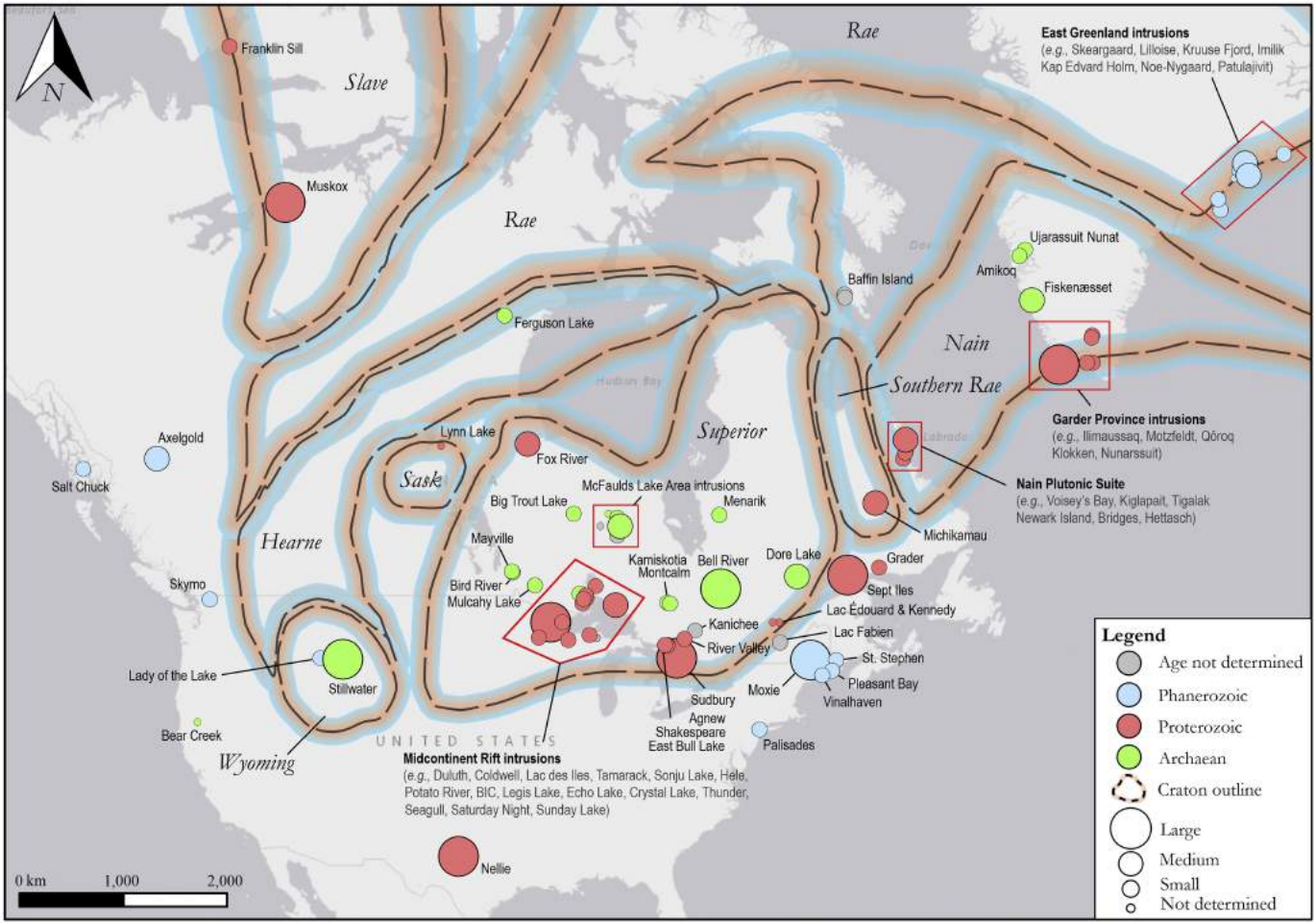
N
Franklin Sill
Slave
Muskox
Rae
Rae
East Greenland intrusions
(e.g., Skeargaard, Lilloise, Kruuse Fjord, Imilik Kap Edvard Holm, Noe-Nygaard, Patulajivit)
Ujarassuit Nunat
Amikoq
Fiskenæsset
Baffin Island
Ferguson Lake
Nain
Southern Rae
Garder Province intrusions
(e.g., Ilimaussaq, Motzfeldt, Qôroq Klokken, Nunarssuit)
Nain Plutonic Suite
(e.g., Voisey's Bay, Kiglapait, Tigalak Newark Island, Bridges, Hettasch)
Axelgold
Salt Chuck
Lynn Lake
Fox River
Superior
Sask
McFaulds Lake Area intrusions
Big Trout Lake
Menarik
Michikamau
Hearne
Mayville
Kamiskotia
Montcalm
Bell River
Dore Lake
Grader
Sept Iles
Skymo
Bird River
Mulcahy Lake
Lac Édouard & Kennedy
Kanichee
Lac Fabien
River Valley
St. Stephen
Lady of the Lake
Stillwater
Pleasant Bay
Vinalhaven
Moxie
Sudbury
Agnew
Shakespeare
East Bull Lake
Palisades
Bear Creek
UNITED STATES
Wyoming
Midcontinent Rift intrusions
(e.g., Duluth, Coldwell, Lac des Iles, Tamarack, Sonju Lake, Hele, Potato River, BIC, Legis Lake, Echo Lake, Crystal Lake, Thunder, Seagull, Saturday Night, Sunday Lake)
Nellie
0 km
1,000
2,000
Legend
Age not determined
Phanerozoic
Proterozoic
Archaean
Craton outline
Large
Medium
Small
Not determined

Figure 6

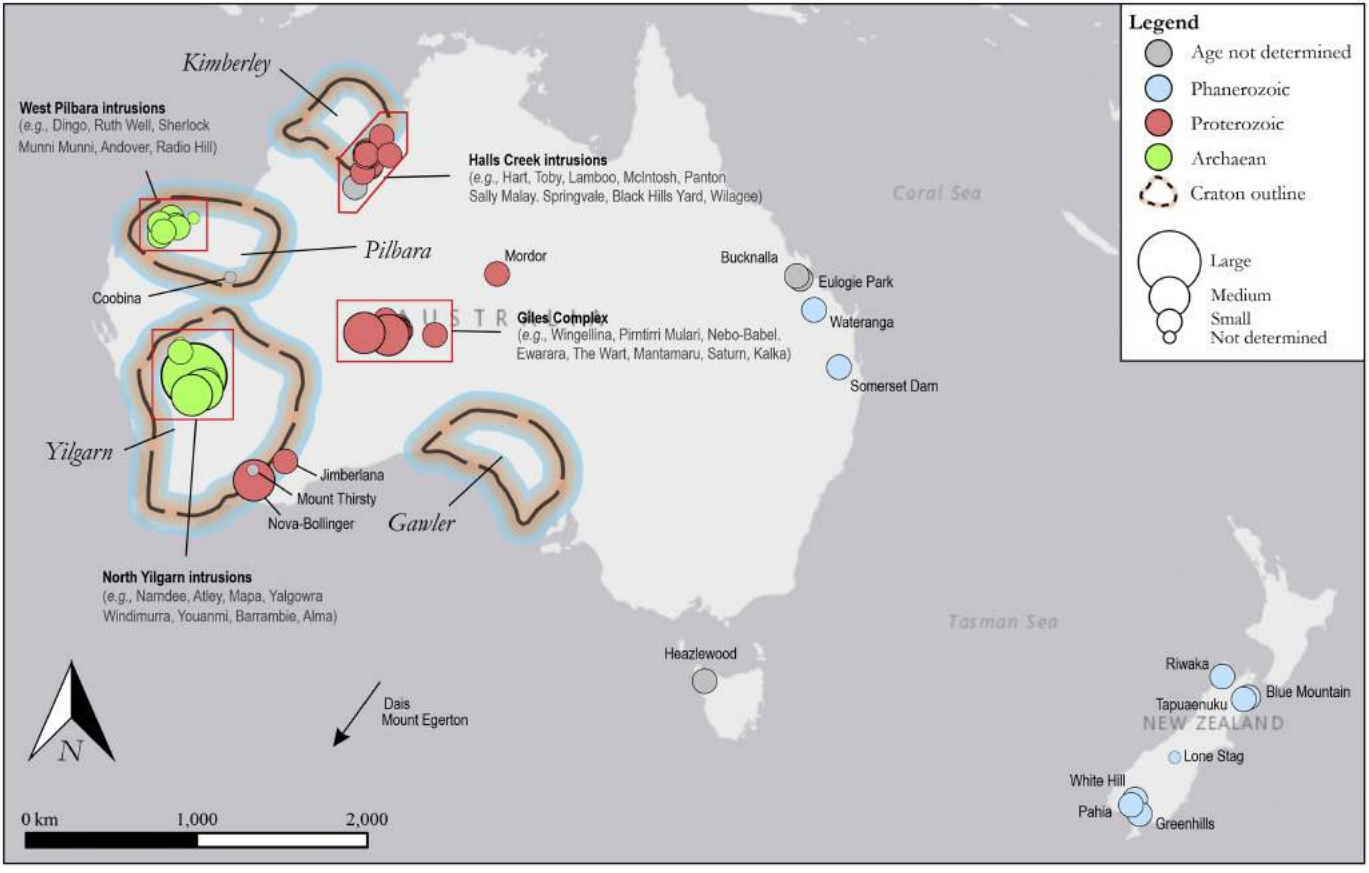
Legend
Age not determined
Phanerozoic
Proterozoic
Archaean
Craton outline
Large
Medium
Small
Not determined
Kimberley
West Pilbara intrusions
(e.g., Dingo, Ruth Well, Sherlock
Munni Munni, Andover, Radio Hill)
Halls Creek intrusions
(e.g., Hart, Toby, Lamboo, McIntosh, Panton,
Sally Malay. Springvale, Black Hills Yard, Wilagee)
Pilbara
Coobina
Mordor
Giles Complex
(e.g., Wingellina, Pirntirri Mulari, Nebo-Babel.
Ewarara, The Wart, Mantamaru, Saturn, Kalka)
Bucknalla
Eulogie Park
Wateranga
Somerset Dam
Yilgarn
Jimberlana
Mount Thirsty
Nova-Bollinger
Gawler
North Yilgarn intrusions
(e.g., Narndee, Atley, Mapa, Yalgowra
Windimurra, Youanmi, Barrambie, Alma)
Coral Sea
Tasman Sea
Heazlewood
Riwaka
Blue Mountain
Tapuaenuku
NEW ZEALAND
Lone Stag
White Hill
Pahia
Greenhills
Dais
Mount Egerton
N
0 km
1,000
2,000

Figure 7

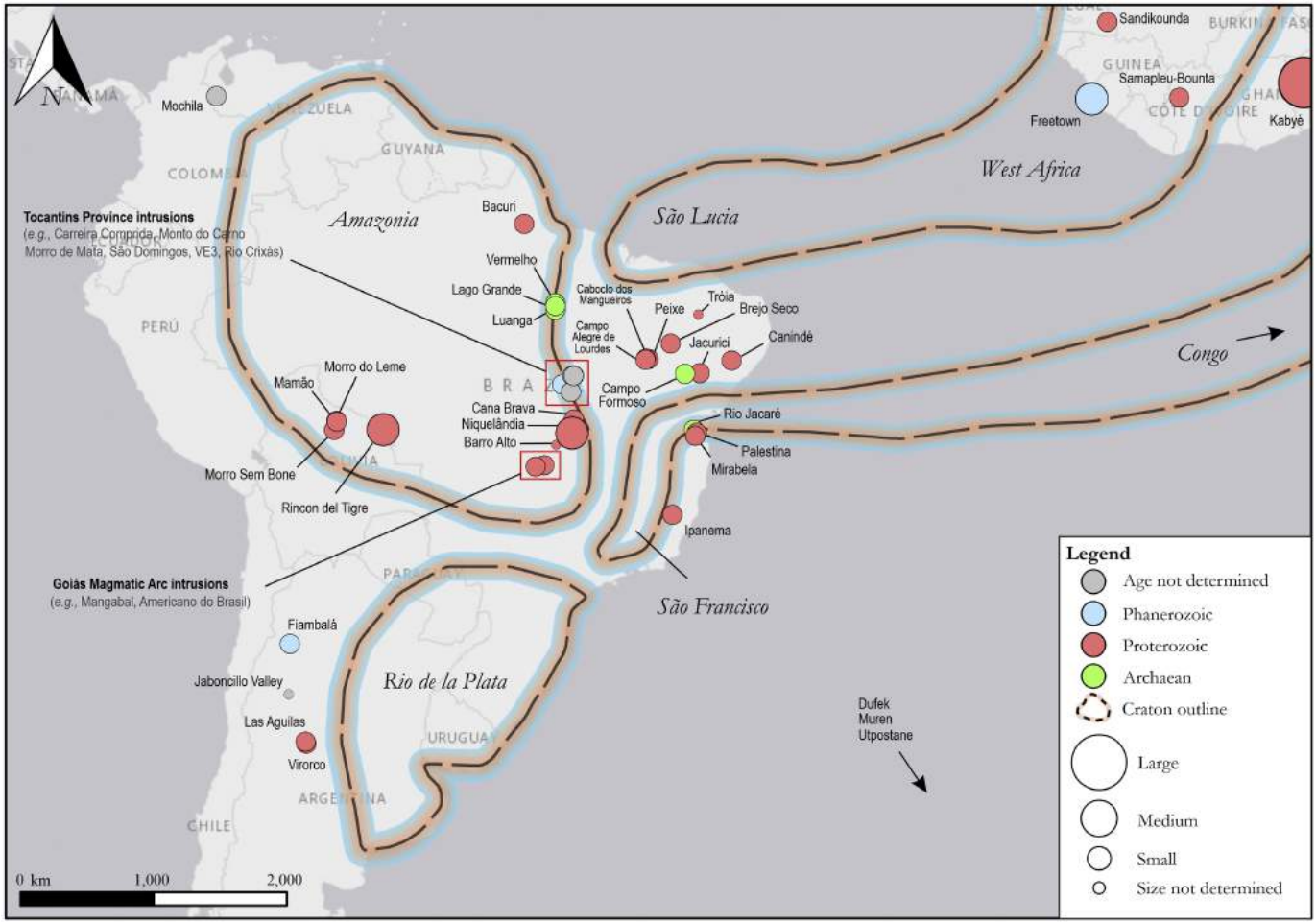
Sandikounda
Samapleu-Bounta
Freetown
Kabyé
Mochila
West Africa
São Lucia
Amazonia
Congo
São Francisco
Rio de la Plata
Tocantins Province intrusions
(e.g., Carreira Comprida, Monto do Carno
Morro de Mata, São Domingos, VE3, Rio Crixás)
Goiás Magmatic Arc intrusions
(e.g., Mangabal, Americano do Brasil)
Bacuri
Vermelho
Lago Grande
Luanga
Cabocio dos Mangueiros
Tróia
Peixe
Brejo Seco
Campo Alegre de Lourdes
Jacurici
Canindé
Campo Formoso
Rio Jacaré
Palestina
Mirabela
Ipanema
Cana Brava
Niquelândia
Barro Alto
Morro do Leme
Mamão
Morro Sem Bone
Rincon del Tigre
Fiambalá
Jaboncillo Valley
Las Aguilas
Virorco
Dufek
Muren
Utpostane
Legend
Age not determined
Phanerozoic
Proterozoic
Archaean
Craton outline
Large
Medium
Small
Size not determined
0 km
1,000
2,000

Figure 8

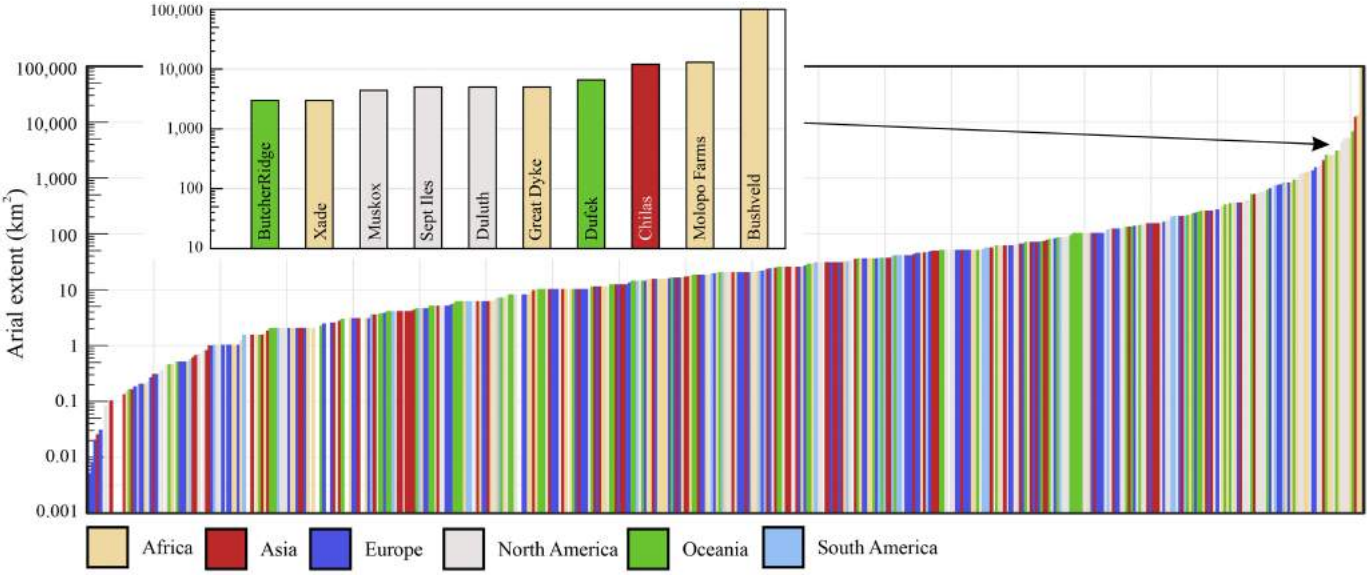
100,000
10,000
1,000
100
10
1
0.1
0.01
0.001
Arial extent (km²)
ButcherRidge
Xade
Muskox
Sept Iles
Duluth
Great Dyke
Dufek
Chilas
Molopo Farms
Bushveld
Africa
Asia
Europe
North America
Oceania
South America

Figure 9

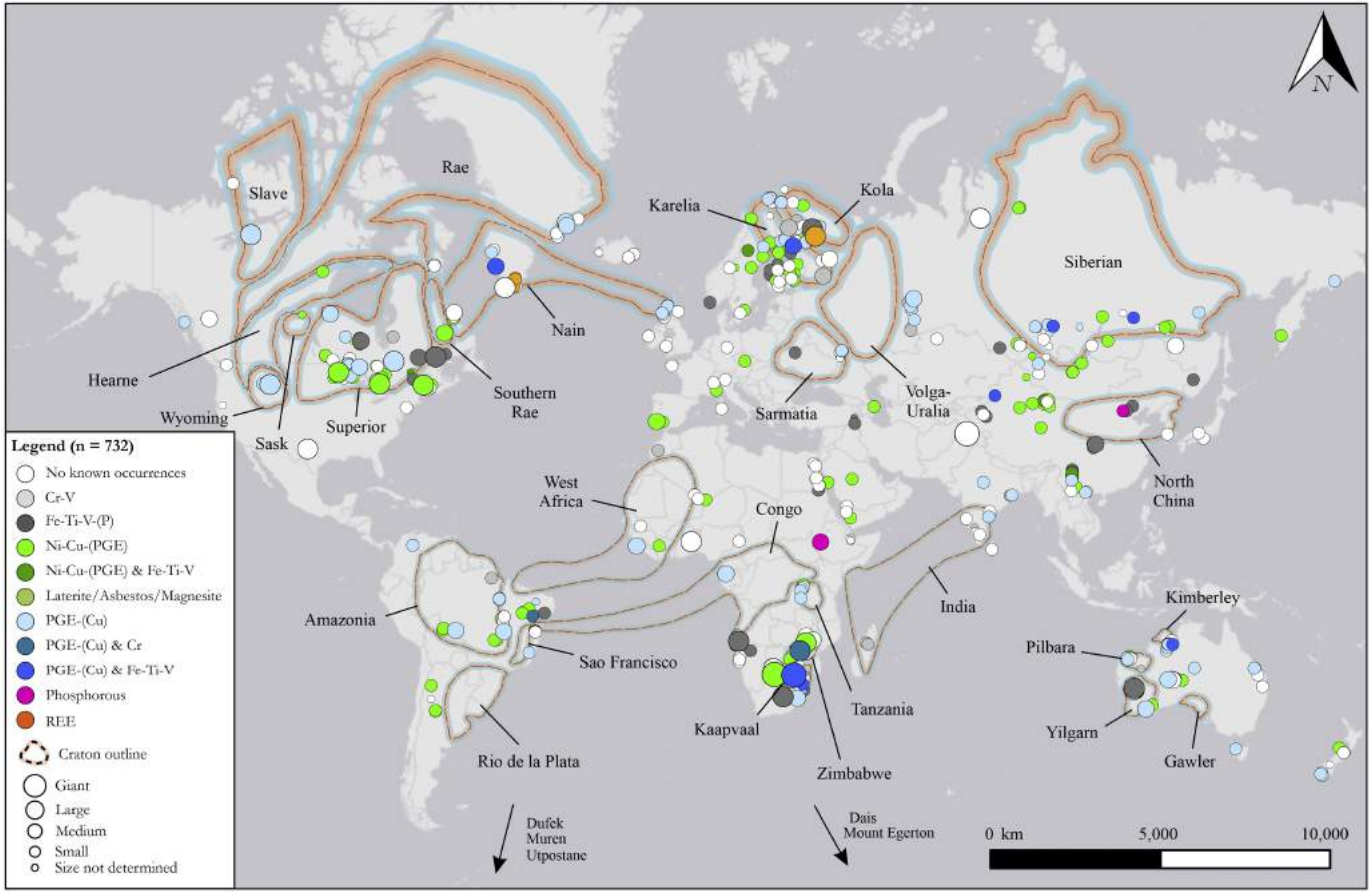
N
Slave
Rae
Karelia
Kola
Siberian
Nain
Hearne
Wyoming
Sask
Superior
Southern
Rae
Sarmatia
Volga-
Uralia
North
China
West
Africa
Congo
India
Amazonia
Sao Francisco
Kimberley
Pilbara
Yilgarn
Gawler
Kaapvaal
Tanzania
Zimbabwe
Rio de la Plata
Dufek
Muren
Utpostane
Dais
Mount Egerton
0 km
5,000
10,000
Legend (n = 732)
No known occurrences
Cr-V
Fe-Ti-V-(P)
Ni-Cu-(PGE)
Ni-Cu-(PGE) & Fe-Ti-V
Laterite/Asbestos/Magnesite
PGE-(Cu)
PGE-(Cu) & Cr
PGE-(Cu) & Fe-Ti-V
Phosphorous
REE
Craton outline
Giant
Large
Medium
Small
Size not determined

Figure 10

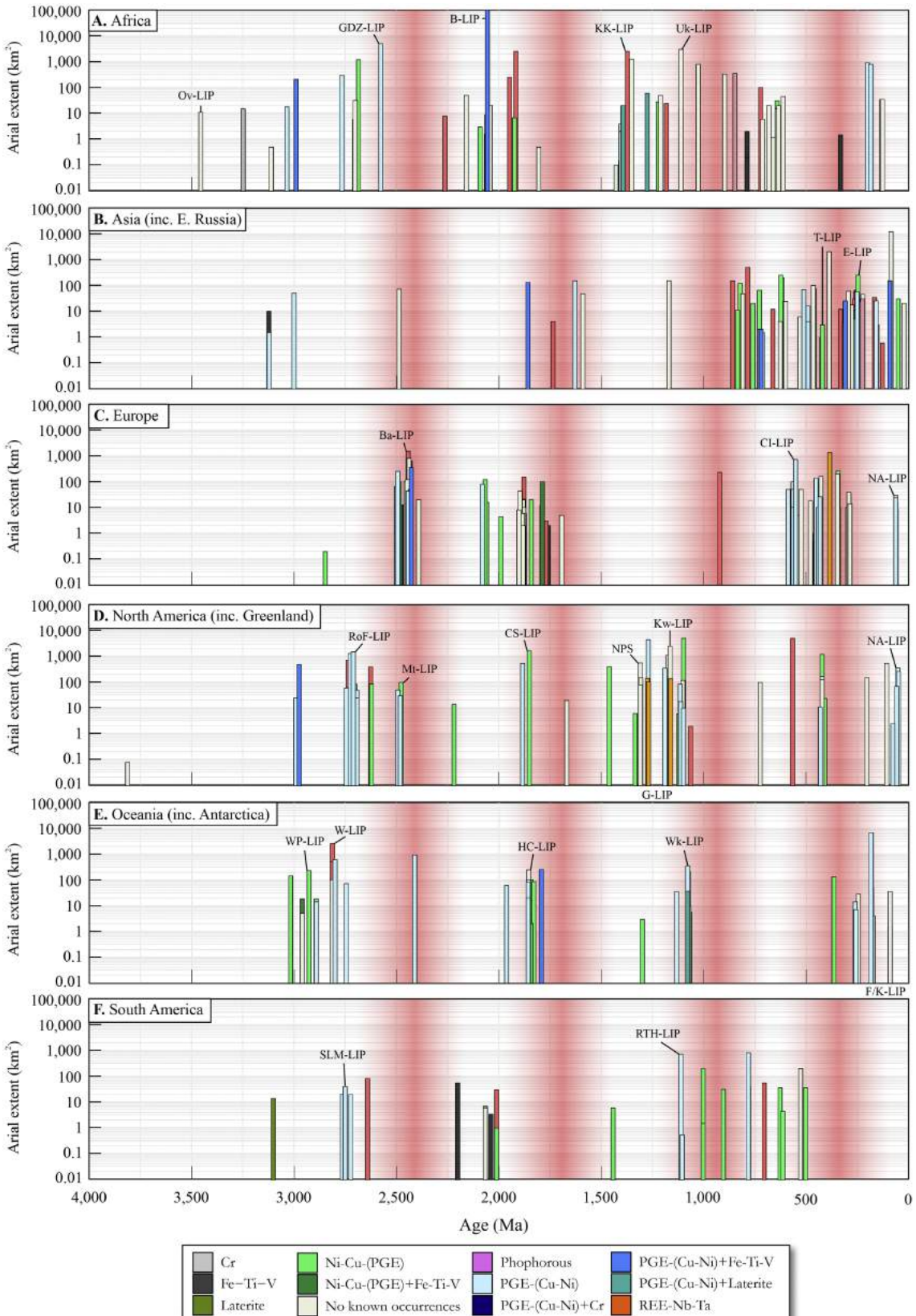
A. Africa
Ov-LIP
GDZ-LIP
B-LIP
KK-LIP
Uk-LIP
B. Asia (inc. E. Russia)
T-LIP
E-LIP
C. Europe
Ba-LIP
Cl-LIP
NA-LIP
D. North America (inc. Greenland)
RoF-LIP
Mt-LIP
CS-LIP
NPS
Kw-LIP
NA-LIP
G-LIP
E. Oceania (inc. Antarctica)
WP-LIP
W-LIP
HC-LIP
Wk-LIP
F/K-LIP
F. South America
SLM-LIP
RTH-LIP
Arial extent (km²)
100,000
10,000
1,000
100
10
1
0.1
0.01
4,000
3,500
3,000
2,500
2,000
1,500
1,000
500
0
Age (Ma)
Cr
Fe–Ti–V
Laterite
Ni-Cu-(PGE)
Ni-Cu-(PGE)+Fe-Ti-V
No known occurrences
Phophorous
PGE-(Cu-Ni)
PGE-(Cu-Ni)+Cr
PGE-(Cu-Ni)+Fe-Ti-V
PGE-(Cu-Ni)+Laterite
REE-Nb-Ta

Figure 11

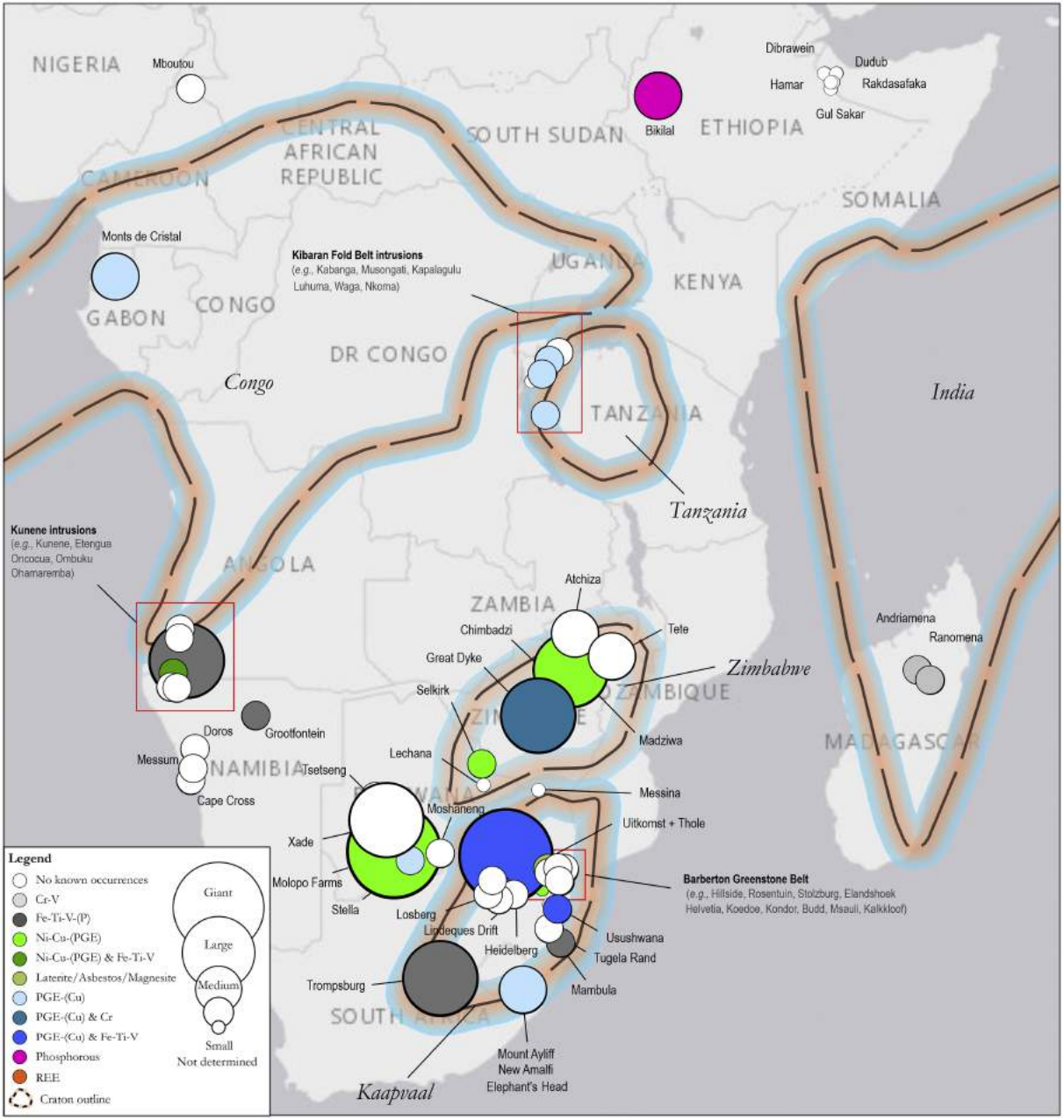
NIGERIA
Mboutou
CENTRAL AFRICAN REPUBLIC
SOUTH SUDAN
Bikilal
ETHIOPIA
Dibrawein
Hamar
Dudub
Rakdasafaka
Gul Sakar
SOMALIA
CAMEROON
Monts de Cristal
GABON
CONGO
Kibaran Fold Belt intrusions
(e.g., Kabanga, Musongati, Kapalagulu Luhuma, Waga, Nkoma)
UGANDA
KENYA
DR CONGO
Congo
India
TANZANIA
Tanzania
Kunene intrusions
(e.g., Kunene, Etengua Oncocua, Ombuku Ohamaremba)
ANGOLA
ZAMBIA
Atchiza
Chimbadzi
Tete
Great Dyke
Zimbabwe
Selkirk
MOZAMBIQUE
Madziwa
Andriamena
Ranomena
MADAGASCAR
Doros
Grootfontein
Messum
NAMIBIA
Tsetseng
Lechana
Cape Cross
Messina
Moshaneng
Uitkomst + Thole
Xade
Molopo Farms
Barberton Greenstone Belt
(e.g., Hillside, Rosentuin, Stolzburg, Elandshoek Helvetia, Koedoe, Kondor, Budd, Msauli, Kalkkloof)
Stella
Losberg
Lindeques Drift
Heidelberg
Usushwana
Tugela Rand
Trompsburg
Mambula
SOUTH AFRICA
Mount Ayliff
New Amalfi
Elephant's Head
Kaapvaal
Legend
No known occurrences
Cr-V
Fe-Ti-V-(P)
Ni-Cu-(PGE)
Ni-Cu-(PGE) & Fe-Ti-V
Laterite/Asbestos/Magnesite
PGE-(Cu)
PGE-(Cu) & Cr
PGE-(Cu) & Fe-Ti-V
Phosphorous
REE
Craton outline
Giant
Large
Medium
Small
Not determined

Figure 12

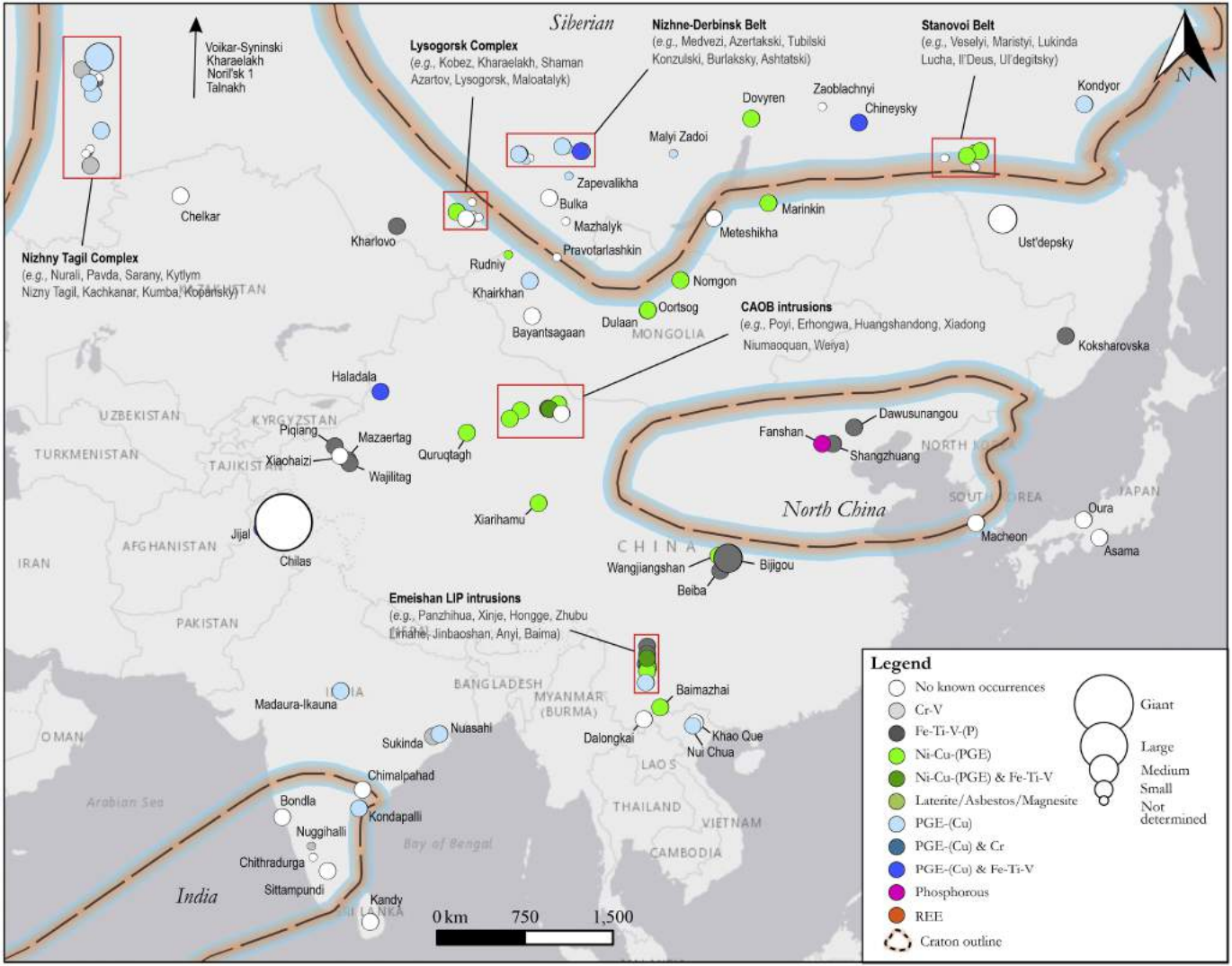
Siberian
Voikar-Syninski
Kharaelakh
Noril'sk 1
Talnakh
Lysogorsk Complex
(e.g., Kobez, Kharaelakh, Shaman
Azartov, Lysogorsk, Maloatalyk)
Nizhne-Derbinsk Belt
(e.g., Medvezi, Azertakski, Tubilski
Konzulski, Burlaksky, Ashtatski)
Stanovoi Belt
(e.g., Veselyi, Maristyi, Lukinda
Lucha, Il'Deus, Ul'degitsky)
Dovyren
Zaoblachnyi
Chineysky
Kondyor
Malyi Zadoi
Zapevalikha
Bulka
Mazhalyk
Pravotarlashkin
Marinkin
Meteshikha
Ust'depsky
Chelkar
Kharlovo
Rudniy
Khairkhan
Bayantsagaan
Dulaan
Oortsog
Nomgon
Nizhny Tagil Complex
(e.g., Nurali, Pavda, Sarany, Kytlym
Nizny Tagil, Kachkanar, Kumba, Kopansky)
CAOB intrusions
(e.g., Poyi, Erhongwa, Huangshandong, Xiadong
Niumaoquan, Weiya)
Koksharovska
Haladala
UZBEKISTAN
KYRGYZSTAN
TURKMENISTAN
TAJIKISTAN
Piqiang
Mazaertag
Xiaohaizi
Wajilitag
Quruqtagh
Dawusunangou
Fanshan
Shangzhuang
North China
Xiarihamu
Jijal
Chilas
AFGHANISTAN
IRAN
CHINA
Wangjiangshan
Bijigou
Beiba
Macheon
Oura
Asama
JAPAN
Emeishan LIP intrusions
(e.g., Panzhihua, Xinje, Hongge, Zhubu
Limahe, Jinbaoshan, Anyi, Baima)
PAKISTAN
Madaura-Ikauna
BANGLADESH
MYANMAR
(BURMA)
Baimazhai
Dalongkai
Khao Que
Nui Chua
Sukinda
Nuasahi
LAOS
THAILAND
VIETNAM
CAMBODIA
OMAN
Arabian Sea
Chimalpahad
Bondla
Kondapalli
Nuggihalli
Chithradurga
Sittampundi
Kandy
Bay of Bengal
India
SRI LANKA
0 km
750
1,500
N
Legend
No known occurrences
Cr-V
Fe-Ti-V-(P)
Ni-Cu-(PGE)
Ni-Cu-(PGE) & Fe-Ti-V
Laterite/Asbestos/Magnesite
PGE-(Cu)
PGE-(Cu) & Cr
PGE-(Cu) & Fe-Ti-V
Phosphorous
REE
Craton outline
Giant
Large
Medium
Small
Not determined

Figure 13

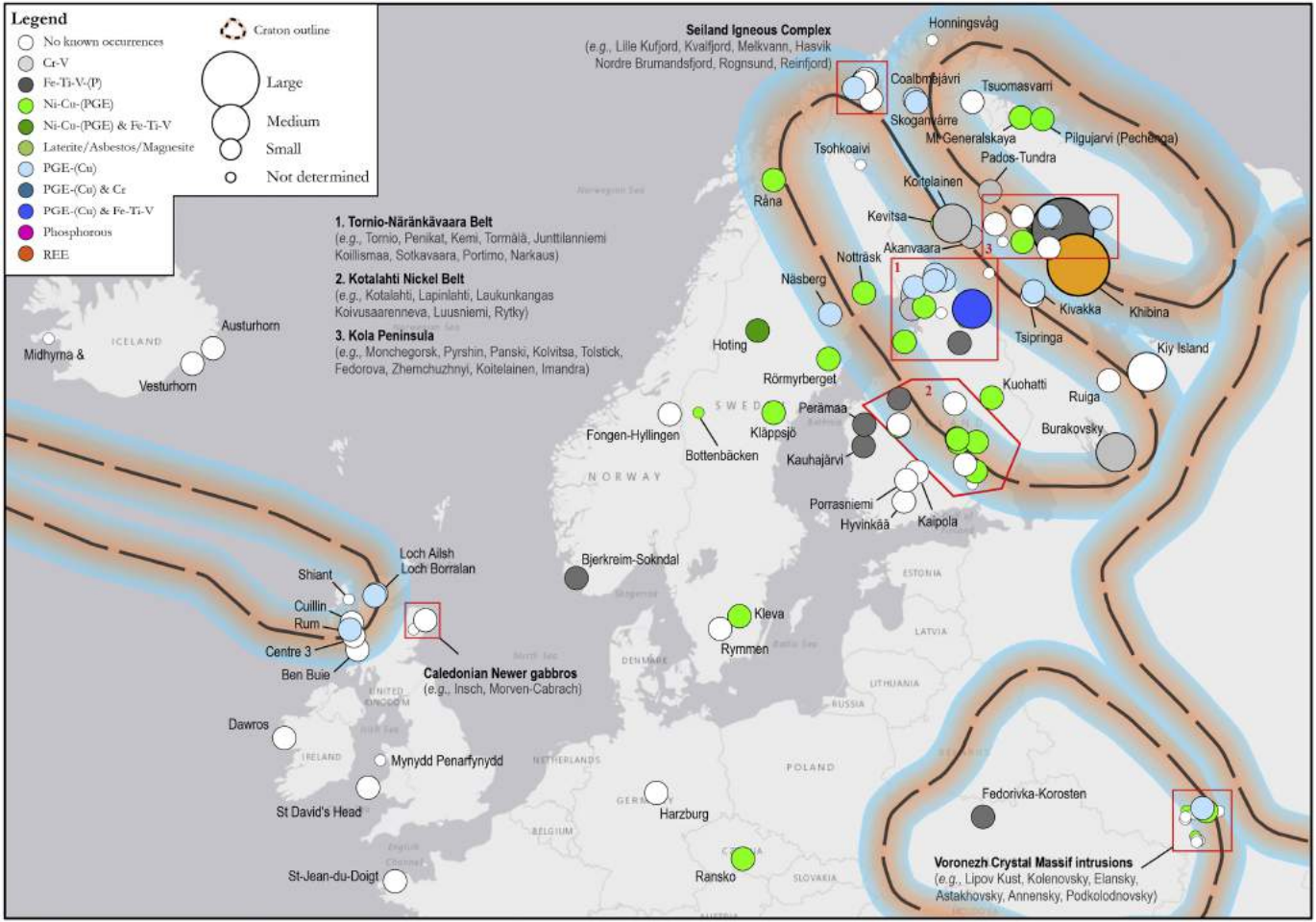
Legend
No known occurrences
Cr-V
Fe-Ti-V-(P)
Ni-Cu-(PGE)
Ni-Cu-(PGE) & Fe-Ti-V
Laterite/Asbestos/Magnesite
PGE-(Cu)
PGE-(Cu) & Cr
PGE-(Cu) & Fe-Ti-V
Phosphorous
REE
Craton outline
Large
Medium
Small
Not determined
1. Tornio-Näränkävaara Belt
(e.g., Tornio, Penikat, Kemi, Tormälä, Junttilanniemi Koillismaa, Sotkavaara, Portimo, Narkaus)
2. Kotalahti Nickel Belt
(e.g., Kotalahti, Lapinlahti, Laukunkangas Koivusaarenneva, Luusniemi, Rytky)
3. Kola Peninsula
(e.g., Monchegorsk, Pyrshin, Panski, Kolvitsa, Tolstick, Fedorova, Zhemchuzhnyi, Koitelainen, Imandra)
Seiland Igneous Complex
(e.g., Lille Kufjord, Kvalfjord, Melkvann, Hasvik Nordre Brumandsfjord, Rognsund, Reinfjord)
Honningsvåg
Coalbmejávri
Tsuomasvarri
Skoganvárre
Mt Generalskaya
Pilgujarvi (Pechenga)
Tsohkoaivi
Pados-Tundra
Koitelainen
Råna
Kevitsa
Akanvaara
Notträsk
Näsberg
Kivakka
Khibina
Tsipringa
Hoting
Rörmyrberget
Kuohatti
Ruiga
Kiy Island
Perämaa
Kläppsjö
Fongen-Hyllingen
Bottenbäcken
Kauhajärvi
Burakovsky
Porrasniemi
Hyvinkää
Kaipola
Midhyrna &
Austurhorn
Vesturhorn
Loch Ailsh
Loch Borralan
Shiant
Cuillin
Rum
Centre 3
Ben Buie
Caledonian Newer gabbros
(e.g., Insch, Morven-Cabrach)
Bjerkreim-Sokndal
Kleva
Rymmen
Dawros
Mynydd Penarfynydd
St David's Head
Harzburg
St-Jean-du-Doigt
Ransko
Fedorivka-Korosten
Voronezh Crystal Massif intrusions
(e.g., Lipov Kust, Kolenovsky, Elansky, Astakhovsky, Annensky, Podkolodnovsky)
NORWAY
SWEDEN
ICELAND
IRELAND
DENMARK
ESTONIA
LATVIA
LITHUANIA
RUSSIA
POLAND
NETHERLANDS
BELGIUM
SLOVAKIA

Figure 14

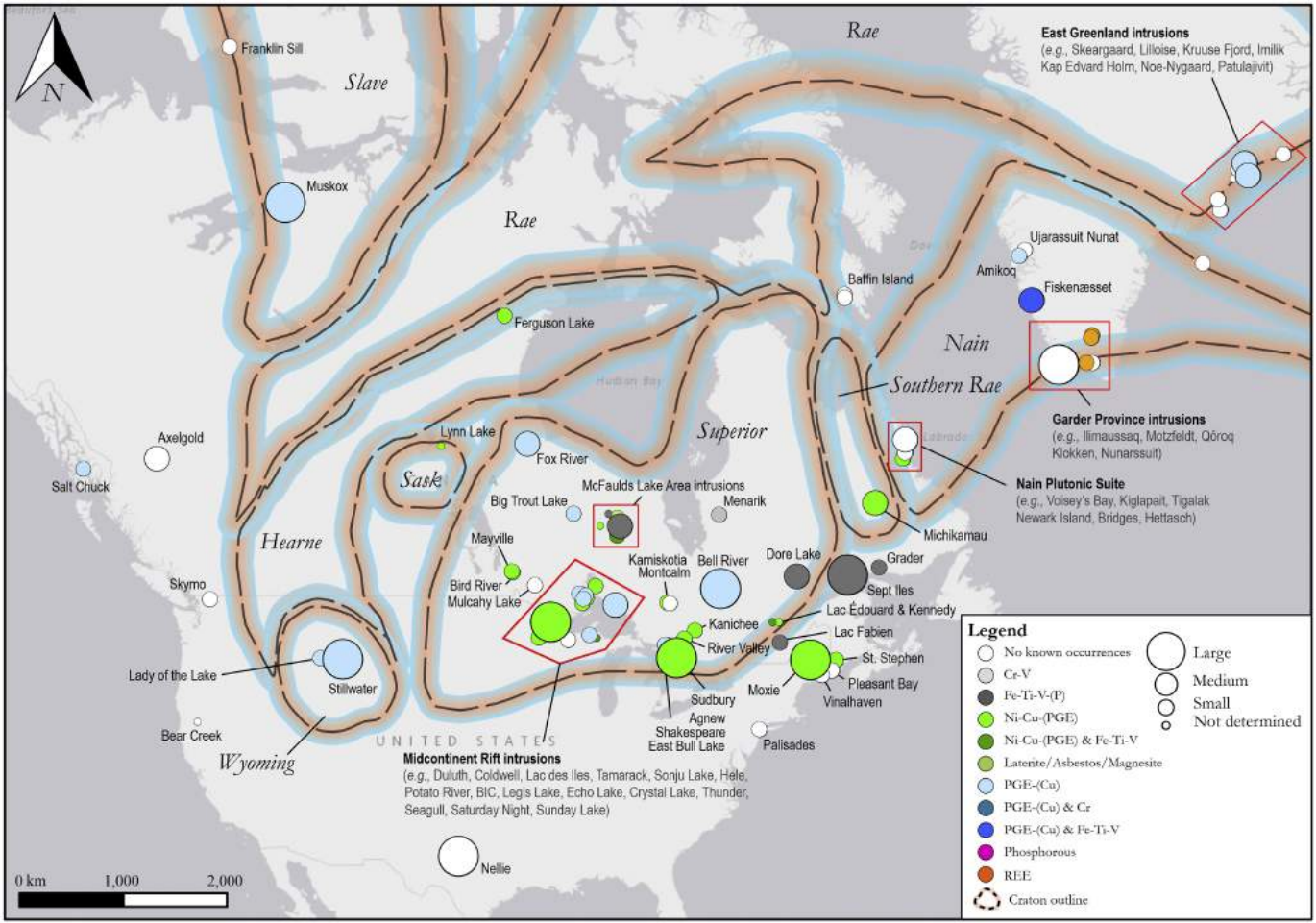
N
Franklin Sill
Slave
Muskox
Rae
Rae
East Greenland intrusions
(e.g., Skeargaard, Lilloise, Kruuse Fjord, Imilik Kap Edvard Holm, Noe-Nygaard, Patulajivit)
Ujarassuit Nunat
Amikoq
Fiskenæsset
Baffin Island
Ferguson Lake
Nain
Southern Rae
Garder Province intrusions
(e.g., Ilimaussaq, Motzfeldt, Qôroq Klokken, Nunarssuit)
Nain Plutonic Suite
(e.g., Voisey's Bay, Kiglapait, Tigalak Newark Island, Bridges, Hettasch)
Michikamau
Axelgold
Salt Chuck
Lynn Lake
Fox River
Superior
Sask
McFaulds Lake Area intrusions
Big Trout Lake
Menarik
Hearne
Mayville
Bird River
Mulcahy Lake
Kamiskotia
Montcalm
Bell River
Dore Lake
Grader
Sept Iles
Lac Édouard & Kennedy
Lac Fabien
Kanichee
River Valley
St. Stephen
Pleasant Bay
Vinalhaven
Moxie
Sudbury
Agnew
Shakespeare
East Bull Lake
Palisades
Skymo
Lady of the Lake
Stillwater
Bear Creek
Wyoming
UNITED STATES
Midcontinent Rift intrusions
(e.g., Duluth, Coldwell, Lac des Iles, Tamarack, Sonju Lake, Hele, Potato River, BIC, Legis Lake, Echo Lake, Crystal Lake, Thunder, Seagull, Saturday Night, Sunday Lake)
Nellie
0 km
1,000
2,000
Legend
No known occurrences
Cr-V
Fe-Ti-V-(P)
Ni-Cu-(PGE)
Ni-Cu-(PGE) & Fe-Ti-V
Latente/Asbestos/Magnesite
PGE-(Cu)
PGE-(Cu) & Cr
PGE-(Cu) & Fe-Ti-V
Phosphorous
REE
Craton outline
Large
Medium
Small
Not determined

Figure 15

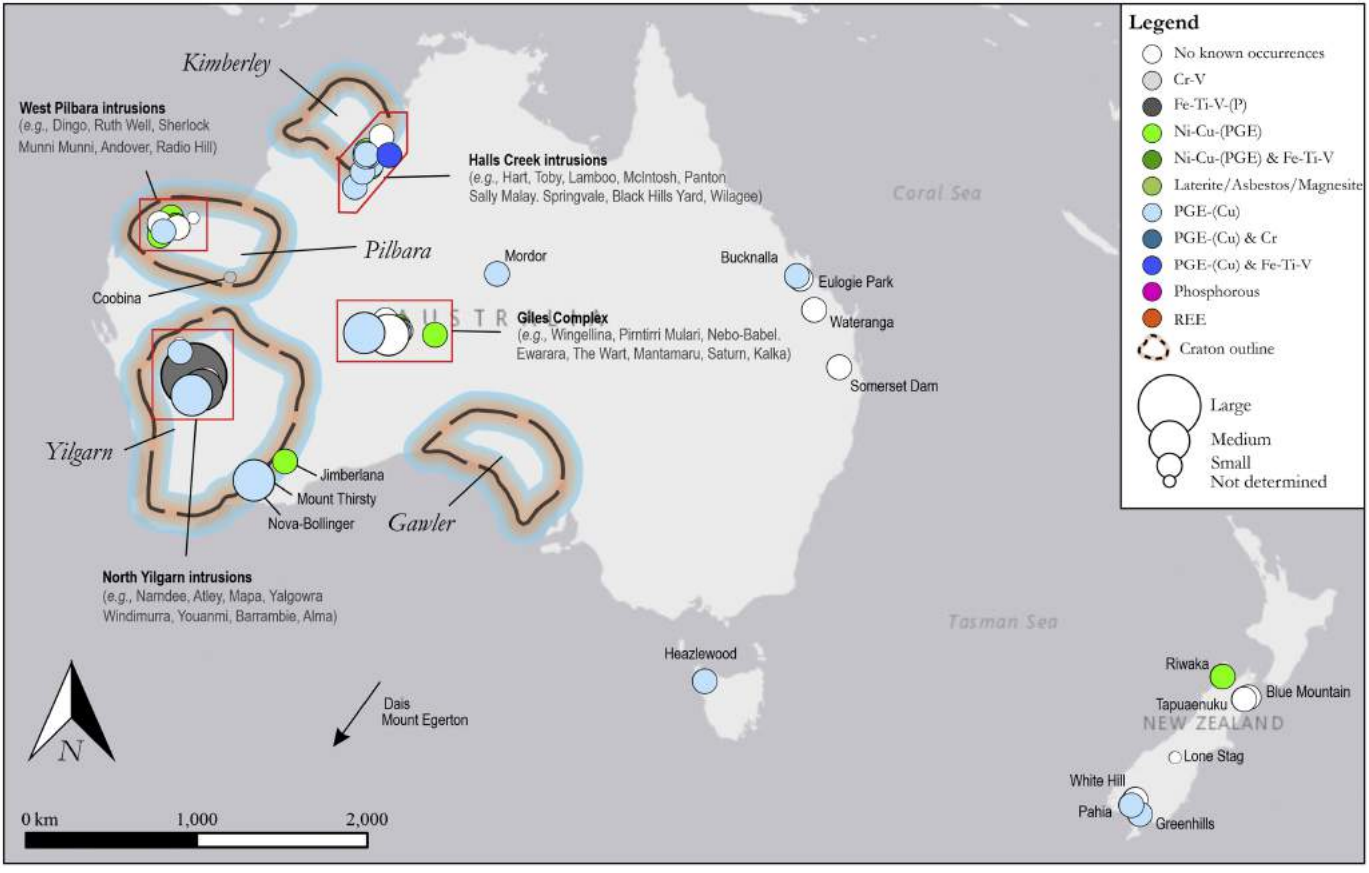
Kimberley
West Pilbara intrusions
(e.g., Dingo, Ruth Well, Sherlock
Munni Munni, Andover, Radio Hill)
Halls Creek intrusions
(e.g., Hart, Toby, Lamboo, McIntosh, Panton,
Sally Malay. Springvale, Black Hills Yard, Wilagee)
Pilbara
Coobina
Mordor
Bucknalla
Eulogie Park
Wateranga
Somerset Dam
Giles Complex
(e.g., Wingellina, Pirntirri Mulari, Nebo-Babel.
Ewarara, The Wart, Mantamaru, Saturn, Kalka)
Yilgarn
Jimberlana
Mount Thirsty
Nova-Bollinger
Gawler
North Yilgarn intrusions
(e.g., Narndee, Atley, Mapa, Yalgowra
Windimurra, Youanmi, Barrambie, Alma)
Coral Sea
Tasman Sea
Heazlewood
Dais
Mount Egerton
Riwaka
Blue Mountain
Tapuaenuku
NEW ZEALAND
Lone Stag
White Hill
Pahia
Greenhills
N
0 km
1,000
2,000
Legend
No known occurrences
Cr-V
Fe-Ti-V-(P)
Ni-Cu-(PGE)
Ni-Cu-(PGE) & Fe-Ti-V
Laterite/Asbestos/Magnesite
PGE-(Cu)
PGE-(Cu) & Cr
PGE-(Cu) & Fe-Ti-V
Phosphorous
REE
Craton outline
Large
Medium
Small
Not determined

Figure 16

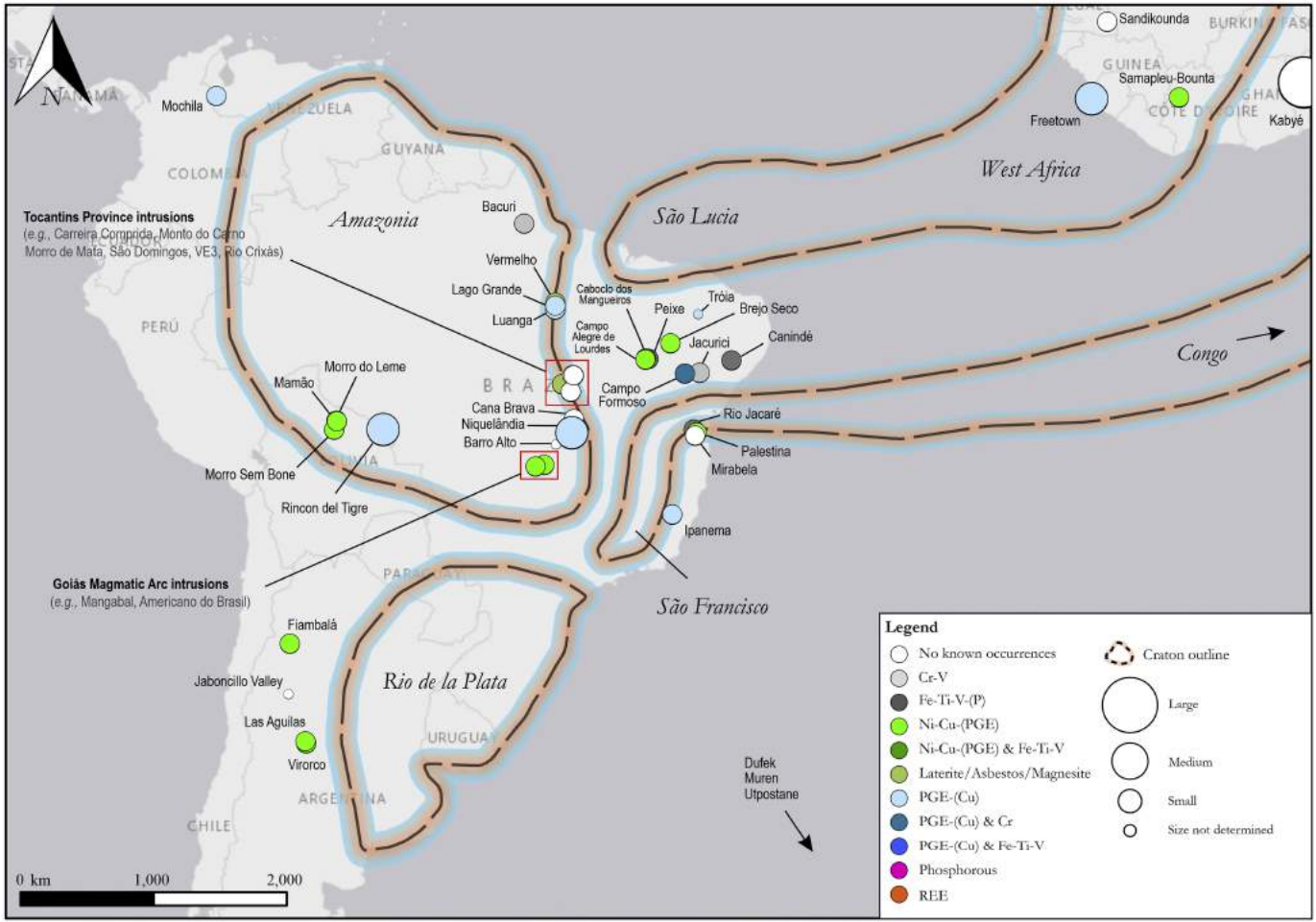
Sandikounda
Samapleu-Bounta
Freetown
Kabyé
West Africa
Mochila
Amazonia
São Lucia
Bacuri
Tocantins Province intrusions
(e.g., Carreira Comprida, Monto do Carno
Morro de Mata, São Domingos, VE3, Rio Crixás)
Vermelho
Lago Grande
Luanga
Caboclo dos Mangueiros
Peixe
Tróia
Brejo Seco
Campo Alegre de Lourdes
Jacurici
Canindé
Congo
Morro do Leme
Mamão
Campo Formoso
Cana Brava
Niquelândia
Barro Alto
Rio Jacaré
Palestina
Mirabela
Morro Sem Bone
Rincon del Tigre
Ipanema
Goiás Magmatic Arc intrusions
(e.g., Mangabal, Americano do Brasil)
São Francisco
Fiambalá
Jaboncillo Valley
Rio de la Plata
Las Aguilas
Virorco
Dufek
Muren
Utpostane
0 km
1,000
2,000
Legend
No known occurrences
Cr-V
Fe-Ti-V-(P)
Ni-Cu-(PGE)
Ni-Cu-(PGE) & Fe-Ti-V
Laterite/Asbestos/Magnesite
PGE-(Cu)
PGE-(Cu) & Cr
PGE-(Cu) & Fe-Ti-V
Phosphorous
REE
Craton outline
Large
Medium
Small
Size not determined

Figure 17